NOAA Technical Memorandum ERL PMEL-90

BEAUFORT SEA MESOSCALE CIRCULATION STUDY – FINAL REPORT

K. Aagaard
C. H. Pease
A. T. Roach
S. A. Salo

Pacific Marine Environmental Laboratory
Seattle, Washington
November 1989

UNITED STATES DEPARTMENT OF COMMERCE

Robert A. Mosbacher
Secretary

NATIONAL OCEANIC AND ATMOSPHERIC ADMINISTRATION

John A. Knauss
Under Secretary for Oceans and Atmosphere/Administrator

Environmental Research Laboratories

Joseph O. Fletcher
Director

NOTICE

Mention of a commercial company or product does not constitute an endorsement by NOAA/ERL. Use of information from this publication concerning proprietary products or the tests of such products for publicity or advertising purposes is not authorized.

Contribution No. 1155 from NOAA/Pacific Marine Environmental Laboratory

For sale by the National Technical Information Service, 5285 Port Royal Road
Springfield, VA 22161

CONTENTS

PAGE

List of Figures iv
List of Tables vi
List of Appendices. vii

Abstract 1

I. INTRODUCTION 2

A. Flow Through Bering Strait 2
B. Flow Through the Chukchi Sea 4
C. Deep Exchange Through Barrow Canyon 4
D. Flow in the Beaufort Sea. 6
E. Nutrient Sources 6
F. Meteorology 7

II. METHODS 8

A. Chukchi Sea 8
B. Barrow Canyon 8
C. Beaufort Sea 13
D. Meteorological Stations 13

III. RESULTS 20

A. Chukchi Sea 20
B. Barrow Canyon 27
C. Beaufort Sea 38
1. Hydrography. 38
2. General Flow Characteristics 40
3. Variability at Very Low Frequencies 44
4. Correlation Analysis. 53
5. Tidal Characteristics. 56
D. Meteorological Results and Correlations 59

IV. SYNOPSIS OF THE REGIONAL CIRCULATION 102

V. SUMMARY OF THE PRINCIPAL CONCLUSIONS. 107

VI. ACKNOWLEDGMENTS 108

VII. REFERENCES 109

LIST OF FIGURES

PAGE

1. Regional map . . . 3
2. Barrow Canyon location and mooring placement . . . 5
3. Barrow Canyon array design . . . 9
4. Beaufort Sea array locations . . . 14
5. Weekly average current vectors at Cape Thompson . . . 21
6. Temperature, salinity, and nutrient structure in the upper 500 m of the Arctic Ocean (from observations by J.H. Swift) . . . 23
7. Near-bottom distributions of salinity and nitrate in the Chukchi, East Siberian and Laptev seas . . . 24
8. Nutrient profiles from ISHTAR . . . 25
9. Nutrient profiles from ISHTAR . . . 26
10. Time series of currents from Barrow Canyon . . . 29
11. Time series of salinity from Barrow Canyon . . . 30
12. Time series of temperature from Barrow Canyon . . . 31
13. Volumetric temperature-salinity and mean velocity plots for Barrow Canyon mooring BC1 . . . 32
14. Same as Figure 13 for BC2 . . . 33
15. Profile of light attenuation at Section C near 144°W . . . 39
16. Low-pass filtered current vectors from Beaufort Sea moorings . . . 41
17. Same as Figure 16 . . . 42
18. Energy-preserving rotary coherence spectra for Beaufort Sea records . . . 45
19. Same as Figure 18 . . . 46
20. Same as Figure 18 . . . 47
21. Same as Figure 18 . . . 48
22. Same as Figure 18 . . . 49
23. Monthly mean velocity from outer shelf moorings . . . 51
24. Monthly mean variance from outer shelf moorings . . . 52
25. Tidal elevation characteristics from mooring MB2B . . . 57
26. Tidal currents from mooring MB2B . . . 58
27. Plots of all parameters from land-based weather stations . . . 62
28. Same as Figure 27 . . . 63
29. Same as Figure 27 . . . 64
30. Same as Figure 27 . . . 65
31. Same as Figure 27 . . . 66
32. Same as Figure 27 . . . 67
33. Same as Figure 27 . . . 68
34. Same as Figure 27 . . . 69
35. Ice drifts for the ARGOS buoys . . . 70
36. Same as Figure 35 . . . 71
37. Time series of ARGOS buoy and METLIB data . . . 72
38. Same as Figure 37 . . . 73
39. Same as Figure 37 . . . 74
40. Same as Figure 37 . . . 75
41. Same as Figure 37 . . . 76
42. Same as Figure 37 . . . 77
43. Same as Figure 37 . . . 78
44. Same as Figure 37 . . . 79
45. Seasonally averaged values for temperature, pressure and wind . . . 88
46. Same as Figure 45 . . . 89
47. Same as Figure 46 . . . 90
48. Same as Figure 46 . . . 91

49. Monthly mean values for land-based stations 92
50 Same as Figure 49 93
51. Same as Figure 49 94
52. Same as Figure 49 95
53. Monthly mean wind variance for land-based stations 96
54. Weather map for selected times and areas 97
55. Same as Figure 54 98
56. Same as Figure 54 99
57. Same as Figure 54 100
58. Same as Figure 54 101
59. Annual Bering Strait transport signal. 104
60. Forty years of annual transport estimates through Bering Strait 105

LIST OF TABLES

PAGE

1. Location, instrumentation, and duration of the Barrow Canyon current meters 10
2. Pressure gauge statistics for Barrow Canyon moorings 12
3. Surface wind statistics for Barrow Canyon analysis 12
4. Location, instrumentation, and duration for Beaufort Sea moorings 15
5. GOES station deployment information 16
6. ARGOS buoy deployment information. 18
7. APL buoy deployment information. 19
8. Record-length current statistics for one-year moorings in the Chukchi Sea 20
9. Current meter statistics for Barrow Canyon 27
10. Record-length statistics for the SeaCat temperature-salinity loggers from Barrow Canyon 34
11. Record-length correlations of Barrow Canyon currents with regional winds and surface pressure gradients 35
12. Turbulent heat and salt flux estimates for Barrow Canyon. 37
13. Record-length statistics for Beaufort Sea current meters. 43
14. Beaufort Sea mean velocity comparison 50
15. Linear correlations of Beaufort Sea current meters. 54
16. Linear correlations of Beaufort Sea currents with regional winds 55
17. Record-length statistics for ARGOS, GOES, climate, and METLIB data 60
18. Sea-level pressure correlations for ARGOS, GOES, climate, and METLIB data . . . 80
19. Air temperature correlations for ARGOS, GOES, climate, and METLIB data 82
20. Wind speed correlations for ARGOS, GOES, climate, and METLIB data 84
21. Correlations among climate stations 85
22. Correlations among METLIB records at climate stations 86
23. Correlations among GOES stations. 87
24. Correlations among METLIB records at GOES stations 87

LIST OF APPENDICES

APPENDIX A. Aagaard, K., C.H. Pease, and S.A. Salo, *Beaufort Sea Mesoscale Circulation Study – Preliminary Results*, NOAA Technical Memorandum ERL PMEL-82, Pacific Marine Environmental Laboratory, Seattle, WA, 171 pp., 1988.

APPENDIX B. Aagaard, K., S. Salo, and K. Krogslund, *Beaufort Sea Mesoscale Circulation Study: Hydrography, USCGC Polar Star Cruise, October 1986*, NOAA Data Report ERL PMEL-19, Pacific Marine Environmental Laboratory, Seattle, WA, 83 pp., 1987.

APPENDIX C. Aagaard, K., S. Salo, and K. Krogslund, *Beaufort Sea Mesoscale Circulation Study: Hydrography, Helicopter Operations, April 1987*, NOAA Data Report ERL PMEL-22, Pacific Marine Environmental Laboratory, Seattle, WA, 25 pp., 1988.

Beaufort Sea Mesoscale Circulation Study – Final Report

K. Aagaard, C.H. Pease, A.T. Roach, and S.A. Salo

ABSTRACT. The Beaufort Sea Mesoscale Project was undertaken to provide a quantitative understanding of the circulation over the Beaufort Sea shelf and of its atmospheric and oceanic forcing. Major emphasis has been placed on providing extensive synoptic oceanographic and meteorological coverage of the Alaskan Beaufort Sea during 1986–88. In addition, supplementary measurements have been made in the southern upstream waters of Bering Strait and the Chukchi Sea. The work has resulted in an unprecedented regional data set for both the ocean and the atmosphere. The principal conclusions are as follows:

1) Below the upper 40–50 m of the ocean, the major circulation feature of the outer shelf and slope is the Beaufort Undercurrent, a strong flow which is directed eastward in the mean, but which is subject to frequent reversals toward the west. The reversals are normally associated with upwelling onto the outer shelf. The undercurrent is very likely part of a basin-scale circulation within the Arctic Ocean.

2) While we find statistically significant wind influence on the subsurface flow in the southern Beaufort Sea, it is generally of secondary importance, accounting for less than 25% of the flow variance below 60 m. An important implication is that at least below the mixed layer, the circulation on the relatively narrow Beaufort shelf is primarily forced by the ocean rather than by the local wind. This oceanic forcing includes shelf waves and eddies. Therefore, to the extent that a localized problem or process study requires consideration of the shelf circulation, such as would be the case for oil-spill trajectory modeling, a larger-scale framework must be provided, within which the more local problem may be nested.

3) There were large changes in wind variance with season, with the largest variances occurring in the late summer/early autumn and again in January because of blocking ridges in the North Pacific shifting the storm track westward over the west coast of Alaska and across the North Slope.

4) Despite the seasonally varying wind field, as well as the large seasonal differences in the upper-ocean temperature and salinity fields, we find no evidence for a seasonal variability in the subsurface circulation in the Beaufort Sea. This situation contrasts with that in Bering Strait and probably in the Chukchi Sea, where a seasonal cycle in the transport is apparent. Therefore, while the northward flow of water from the Pacific is of major significance to the structure and chemistry of the upper ocean in the Arctic (including the Beaufort Sea), as well as its ice cover and biota, the dynamic significance of that flow to the Beaufort Sea appears small.

5) In contrast to the lack of a seasonal oceanographic signal at depth, the interannual variability in the flow characteristics can be considerable. For example, during the period fall 1986–spring 1987, the Beaufort Undercurrent appears to have been deeper by 30–40 m compared with both earlier and ensuing measurements. The consequences of such anomalies for the upper-ocean velocity structure and transport are likely significant.

6) During much of the experiment, the meteorological conditions were milder than normal, consistent with less coastal ice in the summer and autumn, the passage of more storms up the west coast of Alaska and across the North Slope, and generally higher air temperatures along the North Slope. These climatological near-minimum ice years were followed in 1988 by the heaviest summer ice along the Chukchi coast since 1975.

7) The atmospheric sea-level pressure field was well represented by the METLIB products from the FNOC surface analysis if the 12-hour lag of the FNOC pressures was taken into account. However, the FNOC surface air temperature field does not accurately represent either the land-based stations or the drifting ice buoys. The errors in the FNOC temperature field showed a systematic over-prediction during winter and spring of 10–20°C, leading to an annual over-prediction of air temperature by 3–13°C at all sites. Gradient winds from FNOC are therefore well suited for modeling purposes if they are calculated from the time-shifted surface analysis, but the FNOC surface temperature analysis should not be used for any model calculations, except perhaps as an upper boundary condition for a rather complete planetary boundary layer model.

I. INTRODUCTION

The Beaufort Sea Mesoscale Circulation Study was initiated in 1986 to develop a quantitative and dynamically founded understanding of the circulation over the Beaufort Sea shelf (Fig. 1) and its atmospheric and oceanic forcing. The study was conducted within the overall context of a regional environmental assessment related to petroleum exploration and development.

Earlier work in the Beaufort Sea either concentrated on limited near-shore areas, or did not provide a sufficiently broad spatial and temporal coverage to define the shelf circulation on appropriately large scales. A further serious limitation of previous work was the inadequate determination of the atmospheric forcing on a regional scale. These deficiencies are particularly troublesome when constructing and validating numerical models of the shelf circulation. Finally, the earlier hydrographic sampling on the shelf (which included nutrients and dissolved oxygen) was restricted to a brief period during the summer, yielding no information on conditions during other seasons. To substantially remedy these shortcomings, the present study was designed to provide broad spatial and temporal coverage of the circulation, hydrography and synoptic winds over the continental shelf. The field work began in autumn 1986 and continued through spring 1988, resulting in an unprecedented regional data set for both the ocean and the atmosphere.

This report is divided into five major sections: Introduction (including a brief background), Methods, Results and Discussion, Synopsis of the Regional Circulation, and Summary of the Principal Conclusions. In addition, there is a secondary organization on the basis of geography and discipline: the southern upstream sources for shelf waters in the Beaufort Sea, specifically the flow through Bering Strait and in the Chukchi Sea; the circulation in the Beaufort Sea itself, primarily seaward of the 50-m isobath; and the meteorology and climatology of the Beaufort Sea, including pertinent aspects of sea ice kinematics and dynamics in the region.

A. Flow Through Bering Strait

The strong northward flow through Bering Strait, which connects the Pacific and Arctic oceans, has major consequences for much of the Arctic Ocean (see Coachman and Barnes, 1961; Codispoti, 1979; Killworth and Smith, 1984; Yeats, 1988; and Walsh *et al.*, in press, for examples). The flow also has a major impact on conditions in the Beaufort Sea, as was first pointed out by Johnson (1956) and has since been elaborated by a number of investigators (see Aagaard, 1984, for a review). Conditions in the strait have been the subject of numerous investigations (see Coachman *et al.*, 1975, and Aagaard *et al.*, 1985b for reviews), but it is only relatively recently that the very large variability of the flow through the strait has become evident (Coachman and Aagaard, 1981). Much of this variability appears to be wind-driven and has been the subject of several recent investigations, both experimental and theoretical (Aagaard

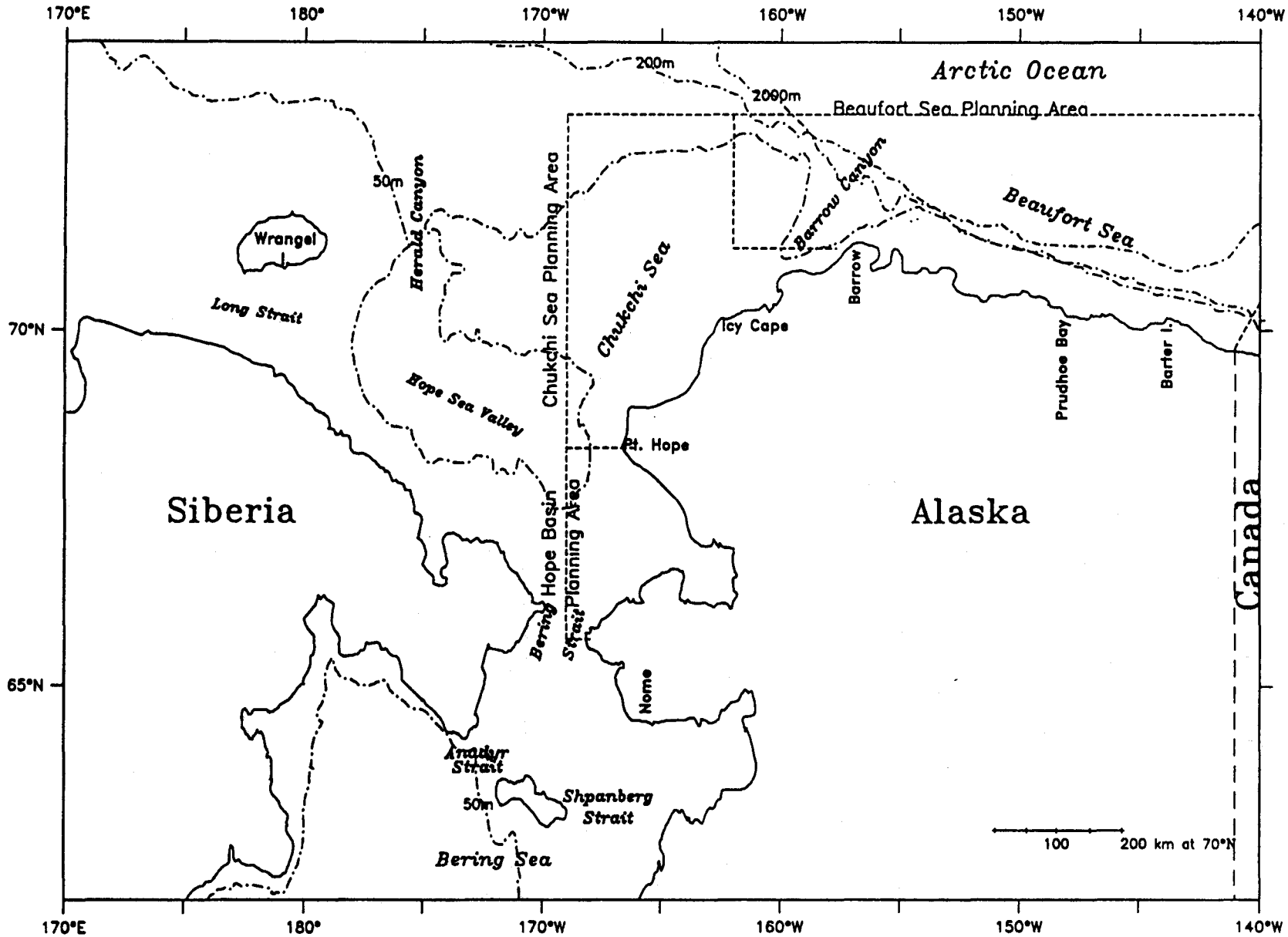

Figure 1. Location figure showing study areas and place names.

et al., 1985b; Overland and Roach, 1987; and Spaulding *et al.*, 1987). We have reassessed this situation in light of the recent study of transport by Coachman and Aagaard (1988).

B. Flow Through the Chukchi Sea

The generally northward movement of water through the Chukchi Sea represents the flow of Pacific water from the Bering Sea towards the Arctic Ocean; it has considerable spatial and temporal structure (Coachman *et al.*, 1975; Coachman and Aagaard, 1981). From the earlier work of Coachman *et al.* (1975), we know that in the vicinity of Bering Strait, the relatively saline water which flows northward across the western Bering shelf (termed Anadyr Water) mixes with the central water mass of the Bering Sea and enters the Chukchi Sea, where it is referred to as Bering Sea Water. This water mass remains distinct from the Alaskan Coastal Water to the east, which is characterized by lower salinity. The latter water follows the Alaskan coast northward and enters the Arctic Ocean and the Beaufort Sea immediately west of Pt. Barrow.

The course of the Bering Sea Water, on the other hand, is not well documented, but appears to occupy most of the western Chukchi Sea, and likely follows the Hope Sea Valley northwestward before entering the Arctic Ocean east of Wrangel Island. In addition to the inflow through Bering Strait, there is exchange with the East Siberian Sea through Long Strait (Coachman and Rankin, 1968) and with the Arctic Ocean across the northern shelf break (see Mountain *et al.*, 1976, for an example). There is also large temporal variability, including prolonged flow reversals, much of which appears to be wind-driven (Aagaard, 1988).

C. Deep Exchange Through Barrow Canyon

The most immediate connection between the Beaufort and the Chukchi seas is via Barrow Canyon. During 1986–87 we deployed two densely instrumented arrays in the canyon, primarily under NSF sponsorship. The measurements are of major interest to issues of Beaufort Sea circulation and we have therefore included their analysis in the present study.

Barrow Canyon is a 250-km long depression crossing the northeastern-most Chukchi Sea. It runs parallel to the coast and comes within 10 km of it off Point Barrow (Fig. 2). The canyon steepens both at its shelf and its mid-slope terminations, but over its intermediate course, where the depth is between 100–200 m, the along-canyon gradient is small, about 10^{-3}. The characteristic width is about 30 km. Earlier flow measurements in the canyon by Mountain *et al.* (1976) and Aagaard (1988) have shown a long-term mean velocity directed down-canyon at 15–20 cm s^{-1} or more, but with instantaneous speeds frequently attaining 100 cm s^{-1}. Flow reversals are common and may last up to several weeks, during which the daily mean up-canyon speeds commonly reach 40 cm s^{-1}. Much of the variability has appeared to be atmospherically

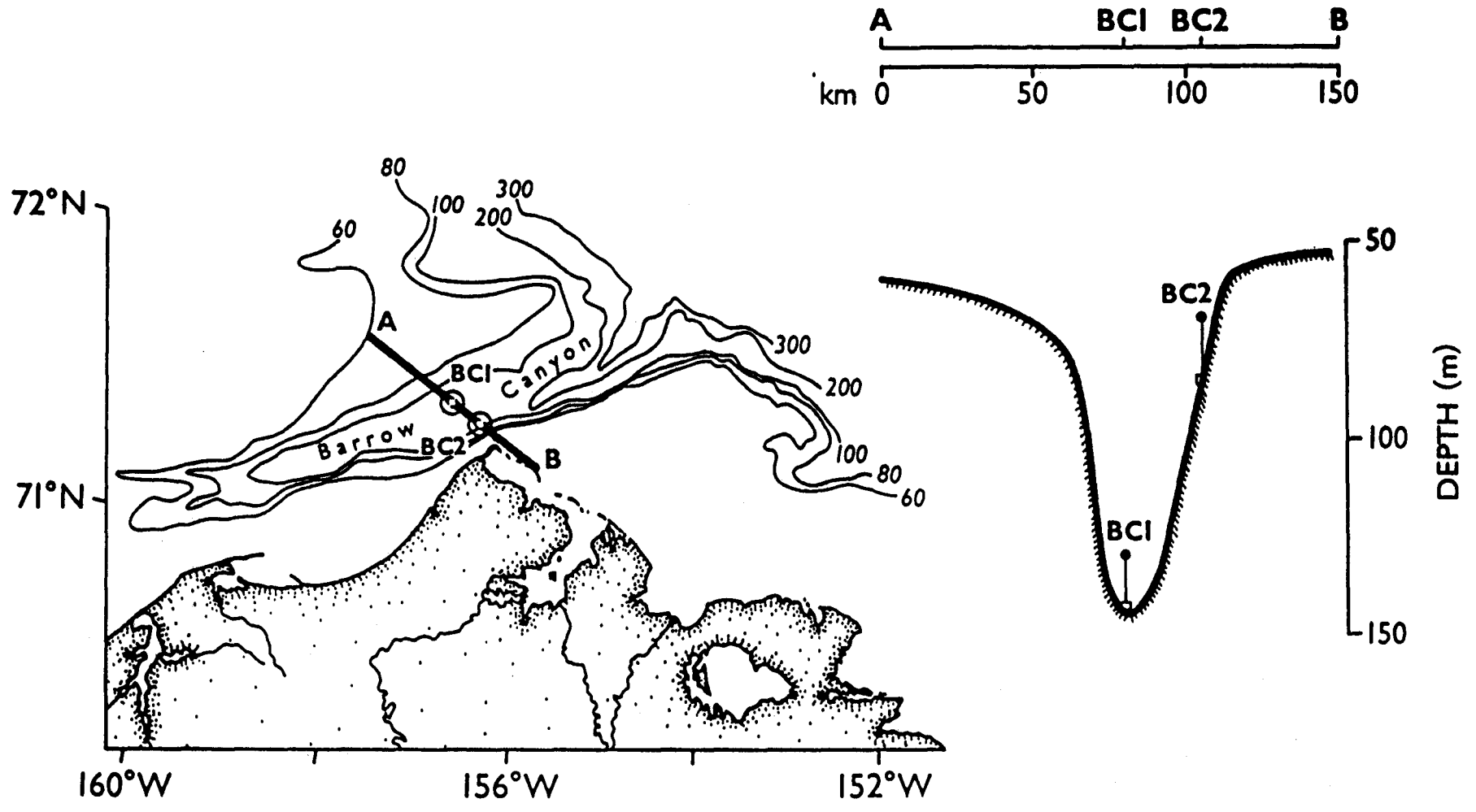

Figure 2. Location and local bathymetry of Barrow Canyon, indicating placement of moorings BC1 and BC2. A plan view along the transect labeled AB showing placement of moorings within the canyon is to the right of the figure.

driven, either by the longshore pressure gradient (Mountain *et al.*, 1976) or by the wind (Aagaard, 1988).

The interaction between the Arctic Ocean and its adjacent shelf seas is of considerable current interest because much of both the hydrographic structure (Aagaard *et al.*, 1981; Melling and Lewis, 1982; Moore *et al.*, 1983; Aagaard *et al.*, 1985a; Jones and Anderson, 1986; Wallace *et al.*, 1987) and the velocity field (Hart and Killworth, 1976; Manley and Hunkins, 1985; D'Asaro, 1988) of the interior ocean appears to originate over certain of the shelves. In the western Arctic, the Chukchi Sea is probably the most important region in this regard (Aagaard *et al.*, 1981), and in particular Barrow Canyon has been suggested by a number of investigators (Coachman *et al.*, 1975; Garrison and Becker, 1976; Mountain *et al.*, 1976; Garrison and Paquette, 1982; Aagaard *et al.*, 1985a; D'Asaro, 1988) as a likely avenue of exchange between the shelf and the deep ocean.

D. Flow in the Beaufort Sea

The relatively narrow (50–100 km) Alaskan Beaufort Sea shelf extends about 600 km from Point Barrow to the Canadian border. Aagaard (1984) has pointed out that there are two substantially different circulation regimes on this shelf. Landward of about the 50-m isobath (the inner shelf), the circulation has a large wind-driven component, particularly in summer. In winter, the flow over the inner shelf is much less energetic, but still shows a wind influence. Farther seaward (the outer shelf), the dominant subsurface circulation feature is the Beaufort Undercurrent, which in the mean state is directed eastward along the entire outer shelf and slope. It underlies a very shallow flow regime in which the ice and uppermost ocean in the mean moves westward, representing the southern limb of the clockwise Beaufort gyre. The Beaufort Undercurrent is characterized by large low-frequency variability, including frequent current reversals toward the west. It is probably a part of the large-scale circulation of the Arctic Ocean, which appears to be characterized by relatively strong topographically trapped boundary currents (Aagaard, 1989). While the Beaufort shelf is strongly influenced by the Arctic Ocean, it also shows a clear connection with the Pacific via the flow through Bering Strait and the Chukchi Sea, which results not only in seasonally distinctive water properties, but also in the introduction of Pacific life forms (cf. Johnson, 1956 for a seminal example).

E. Nutrient Sources

Almost 30 years ago, Coachman and Barnes (1961) pointed out that the temperature structure of the sub-surface layer of much of the Arctic Ocean originates in the flow of water from the south through Bering Strait, which has mixed with resident shelf waters in the Chukchi Sea before moving into the Arctic Ocean. In particular, they argued that the temperature maximum near 75 m represents summer flow through the strait, and that the temperature minimum

between 150–200 m represents winter inflow. The argument was reconsidered by Coachman *et al.* (1975), who concluded that the subsurface temperature maximum in the Arctic Ocean in fact is contributed entirely by the northeast branch (Alaskan Coastal Water) of the Bering Strait inflow and its mixtures. They looked in vain for an Arctic Ocean temperature maximum originating in the northwest branch (Bering Sea Water).

Detailed vertical profiles of nutrient distributions in the Arctic Ocean were obtained by Kinney *et al.* (1970), who showed the pronounced nutrient maximum between 150–200 m. Their analysis supported a Bering Sea origin of the temperature-minimum water, as well as of the temperature-maximum water (which had much lower nutrient concentrations). Moore (1981) and Yeats (1988) found trace metal maxima coincident with the nutrient maximum, and they argued that the data were consistent with a Bering Sea origin. However, Moore *et al.* (1983), Jones and Anderson (1986), and Moore and Smith (1986) have stressed that the various geochemical profiles in the Arctic Ocean, including those of nutrients, reflect the importance of modification on the shelf, particularly due to sediment interaction.

A new perspective on these issues is provided by recent observations from the Bering and Chukchi seas under the ISHTAR program, which show that nutrient-rich water carried northwestward in the Bering Sea with the Bering Slope Current moves onto the southwestern Bering shelf and thence northward through Anadyr Strait into the northern Bering and southern Chukchi seas, where it supports one of the world's most productive marine ecosystems (Walsh *et al.*, 1989).

F. Meteorology

The topography of the land adjacent to the Beaufort and Chukchi seas can be described as low plains, except for three important features: the Brooks Range which foots at the Chukchi coast near Cape Lisburne and at the Beaufort coast from between Barter and Herschel Islands, Cape Mountain and associated high bluffs near Cape Prince of Wales at the tip of the Seward Peninsula, and several similar low mountains and bluffs along the Siberian Peninsula. These topographic features have localized effects on wind speed and direction for some orientations of atmospheric pressure gradient (Dickey, 1961; Kozo, 1980), especially considering the strong capping inversion present in the atmosphere much of the year (Sverdrup, 1933; Overland, 1985).

The Chukchi and northern Bering seas span the transition between polar oceanic climate typical of the central Bering Sea and high-contrast polar climate typical of the Beaufort Sea. A polar region is a geographic region with a mean monthly air temperature for the warmest month of less than 10°C (Overland, 1981). The polar oceanic climate has the additional constraint of high annual precipitation (>0.3 m) that is fairly uniformly distributed through the seasons. A high-contrast polar climate like the Beaufort Sea region, has lower total precipitation and larger seasonal variability in temperature and precipitation (Overland, 1981).

A major influence on the general circulation in the area is a region of high pressure normally located over the Beaufort Sea. The region is centered at about 79°N, 170°W in winter and drives easterly winds across the North Slope and northeasterly winds offshore at Icy Cape (Pease, 1987; Aagaard *et al.*, 1988). At Cape Lisburne there are mountain effects, and the vector mean winter wind is southeasterly. The Siberian high pressure system is southwest of the Beaufort high; the two occasionally form a saddle over the central and western Chukchi Sea in winter, resulting in light winds. In summer there is often a low pressure system occupying the same spot over the Beaufort or shifted more symmetrically over the pole. There is considerably more variability in the monthly synoptic conditions than in the interannual pattern (Pease, 1987).

In autumn, as the solar input wanes, the Beaufort and Chukchi seas are culled by net upward longwave radiation, turbulent (sensible) heat flux to the atmosphere, and melting sea ice advected from the north. Coastally ice-free waters typically reach their freezing point in late September or early October along the North Slope and by early December in Bering Strait. There is enormous interannual variability in the timing of the onset of freezing, especially southwest of Barrow (Campbell *et al.*, 1976, 1980; Carsey and Holt, 1987; Mysak and Manak, 1989). This variability depends on the regional atmospheric temperature anomalies (Rogers, 1978), the transport of heat by the barotropic currents through Bering Strait (Hufford, 1973; Paquette and Bourke, 1974; Aagaard *et al.*, 1985b; Coachman and Aagaard, 1988), and the variability in occurrence of northwesterly winds which push the high-Arctic pack ice against the North Slope and enhance the oceanic cooling in the coastal zone by melting ice (Aagaard *et al.*, 1988; Mysak and Manak, 1989). The latter occurred rather dramatically in the late summer and autumn of 1988, following the completion of this study.

II. METHODS

A. Chukchi Sea

During 1986–87, we had a mooring deployed in the eastern Chukchi Sea south of Cape Thompson at 67° 39′N, 165° 39′W in water 43 m deep. The site lies within the Alaskan Coastal Current, which carries water northward through the eastern Bering and Chukchi seas. A current meter was located at 33 m, and the year-long record extended from 25 August 1986 to 25 August 1987.

B. Barrow Canyon

We moored two 14-m long arrays in Barrow Canyon from October 1986 to August 1987 (Fig. 3). The array BC1 was near the axis of the canyon at a depth of 145 m, while array BC2 was on the shoreward wall of the canyon at about 90 m (Fig. 2, Table 1). These taut-wire moorings were each instrumented with three Aanderaa RCM-4 current meters, four Sea-Bird SeaCat conductivity-temperature data loggers, and one Aanderaa TG-3A pressure gauge. All

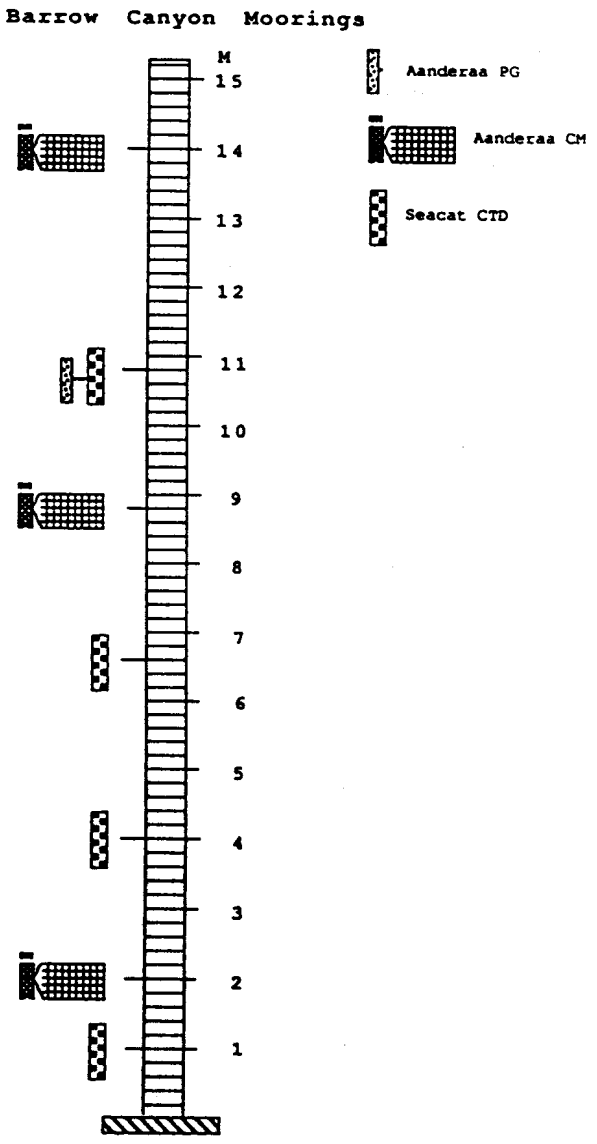

Figure 3. Vertical arrangement of instruments on each Barrow Canyon mooring. Each mooring had three Aanderaa RCM-4 current meters interspersed with four SeaBird SeaCat data loggers with one Aanderaa TG3A pressure gauge attached to the topmost SeaCat.

TABLE 1. Location, instrumentation and duration of the Barrow Canyon current meter moorings and sites for regional wind calculations. The instrument types are; CM = Aanderaa current meter, SC = Sea-Bird SeaCat temperature-salinity data logger and PG = Aanderaa pressure gauge.

Series	Latitude N	Longitude W
Oceanographic moorings:		
BC1	71° 27.48′	156° 52.87′
BC2	71° 26.16′	156° 40.10′
Winds:		
Barrow	71° 24.00′	157° 00.00′
Shelf break	74° 00.00′	156° 00.00′
Pt. Lay	70° 24.00′	165° 00.00′
Kuparuk R.	70° 48.00′	149° 00.00′

Mooring	Depth m	Inst. type	Height m	Record start GMT	Record end GMT
BC1	129.0	CM	14.0	0000 05 Oct 86	0000 11 Dec 86
	132.2	SC	10.8	0000 05 Oct 86	2100 08 Aug 87
	132.2	PG	10.8	0000 05 Oct 86	2100 08 Aug 87
	134.0	CM	9.0	0000 05 Oct 86	2100 08 Aug 87
	136.4	SC	6.6	0000 05 Oct 86	2100 08 Aug 87
	139.0	SC	4.0	0000 05 Oct 86	2100 08 Aug 87
	141.0	CM	2.0	0000 05 Oct 86	2100 08 Aug 87
	142.0	SC	1.0	0000 05 Oct 86	2100 08 Aug 87
BC2	76.0	CM	14.0	0000 05 Oct 86	0000 15 Nov 86
	79.2	SC	10.8	0000 05 Oct 86	2100 08 Aug 87
	79.2	PG	10.8	0000 05 Oct 86	0200 27 Nov 86
	81.0	CM	9.0	0000 05 Oct 86	2100 08 Aug 87
	82.4	SC	6.6	0000 05 Oct 86	2100 08 Aug 87
	86.0	SC	4.0	0000 05 Oct 86	2100 08 Aug 87
	88.0	CM	2.0	0000 05 Oct 86	2100 08 Aug 87
	89.0	SC	1.0	0000 05 Oct 86	2100 08 Aug 87

instruments, except the top current meter on each array and the pressure gauge on the shallower mooring, recorded data of good quality throughout the deployment period (Table 1). The pressure gauges monitored the vertical motion of the moorings, so that pressure variations could be accounted for in the salinity calculations (tidal heights are of order 10 cm and can be ignored for these purposes). The maximum mooring excursions proved to be only 225 and 175 mb at BC1 and BC2, respectively, corresponding to maximum salinity errors of 0.011 and 0.008 psu, which are well within the salinity error bands due to conductivity uncertainties. The standard deviation of the pressure was considerably less, about 35–40 mb (Table 2), with a corresponding reduction of the standard error in salinity associated with pressure variations. We have therefore ignored the effects of mooring motion in calculating salinity.

Comparison of the pre- and post-deployment calibrations for the SeaCats suggests that the temperatures were stable over the year to within 0.005°C. Unfortunately, the pre-deployment calibration of conductivity was invalidated by a glycol leak into the calibration tank. An accumulation of silt in the conductivity cell apparently degraded the signal further during the course of the deployment. The silting of the cell occurred because we had mounted it horizontally in an effort to improve flushing. However, the combination of this particular cell geometry and a heavy suspended load in the boundary layer made this an unfortunate choice. Nonetheless, we were able to calibrate the conductivity cells *in situ* by comparing the observed temperature-salinity (T-S) correlations during periods of upwelling of warm intermediate waters into the canyon with a canonical T-S correlation derived from a large number of regional CTD casts. The latter correlation is quite tight, so that in effect an *in situ* calibration bath was advected past the instruments during each upwelling episode. Assuming an accurate temperature measurement, the offset in salinity between the SeaCats and the canonical correlation provided a time history of the conductivity degradation by month. A linear least squares fit to these offsets was computed for each instrument over the deployment period to provide a time-dependent salinity correction. The offsets were largest for the instruments nearest the bottom, where the suspended load presumably was greatest, and they increased with time at all instruments. We estimate that the final salinities are accurate to within 0.06 psu.

The current data were low-pass filtered using a cosine-squared Lanczos filter with a half-power point of 35 hr. We also calculated year-long time series of 6-hr surface winds by reducing (by 36%) and rotating (27° CCW) the geostrophic wind at selected locations. The reduction and rotation were derived by a comparison with measured winds (Table 3). Finally, a surface pressure difference series was created by subtracting the demeaned and detrended surface atmospheric pressure series at Nome from that at Barrow. In the correlation analysis between these various data series, a positive lag indicates that the column data lead the row data, while a negative lag implies the row leads the column. A positive correlation coefficient means that as one parameter increases, so does the other, while a negative coefficient implies that as one

TABLE 2. Pressure gauge statistics for Barrow Canyon.

Mooring	Depth (m)	Mean Pressure (mb)	Standard Deviation (mb)
BC1	132.2	13901.0	34.7
BC2	79.2	8755.4	39.7

TABLE 3. Surface wind statistics.

Site	Mean velocity (m/s)	Direction (°T)	Standard Deviation (m/s)
Barrow	3.2	242.0	5.8
Shelf Break	1.8	246.4	5.5
Pt. Lay	3.8	218.9	6.2
Kuparuk R.	2.7	255.5	5.6

parameter increases, the other decreases. If two data sets are related by a correlation coefficient r, the amount of variance that can be explained in one data set by the variance in the other is r^2.

C. Beaufort Sea

The 1986–87 hydrography and moored measurements, together with the concurrent meteorological and sea-ice investigations, are described in NOAA Technical Memorandum ERL-PMEL 82 and in NOAA Data Reports ERL PMEL-19 and ERL PMEL-22. These are presented in Appendices A, B, and C.

During 1987–88 we had six moored instrument arrays deployed in the Beaufort Sea between Pt. Barrow and Barter Island. Two of the arrays were sited in the mid-shelf region, near the 50 m isobath; three were close to the shelf break, near the 200 m isobath; and one was located over the slope, at about 1000 m depth. The locations are shown in Fig. 4, and the mooring particulars are given in Table 4.

D. Meteorological Stations

Extensive meteorological and ice drift data were obtained throughout the experiment, using a combination of drifting and land-based stations transmitting through the ARGOS and GOES satellite telemetry systems. Three GOES stations were installed in September 1986 to fill gaps in the primary National Weather Service (NWS) coastal observing network. Stations were established at Resolution Island in Prudhoe Bay, at the Lonely Dewline site near Pitt Point east of Barrow, and at Icy Cape southwest of Barrow. A fourth GOES station, funded by the Office of Naval Research (ONR), was placed at the Cape Prince of Wales navigation daymarker along Bering Strait in September 1987. Each station in the GOES network measured air pressure, ventilated air temperature, and wind components hourly, and transmitted the meteorological observations every three hours to the GOES-West satellite. These data were then rebroadcast to the GOES receiving station at Wallops Island, VA, which maintains a computer database which our laboratory computer interrogated daily. Data gaps shorter than a day were linearly interpolated. Gaps longer than a day, but less than a week were bridged using Joseph's scheme (Anderson, 1974). One gap in the temperature data at Resolution Island lasted from 6 October to 18 November 1987, and was not satisfactorily bridged. Deployment information is given in Table 5. The GOES stations at Lonely and Resolution Island were recovered in April 1988.

Further climate data were obtained for the primary NWS stations at Barter Island, Barrow, Kotzebue, and Nome from the National Climatic Data Center, Asheville, NC. These data included hourly sea-level pressure, air temperature, and wind components for the entire experiment period at standard levels for each station. The use of climate and GOES stations gave a nominal 150 km spacing for the land-based meteorological network.

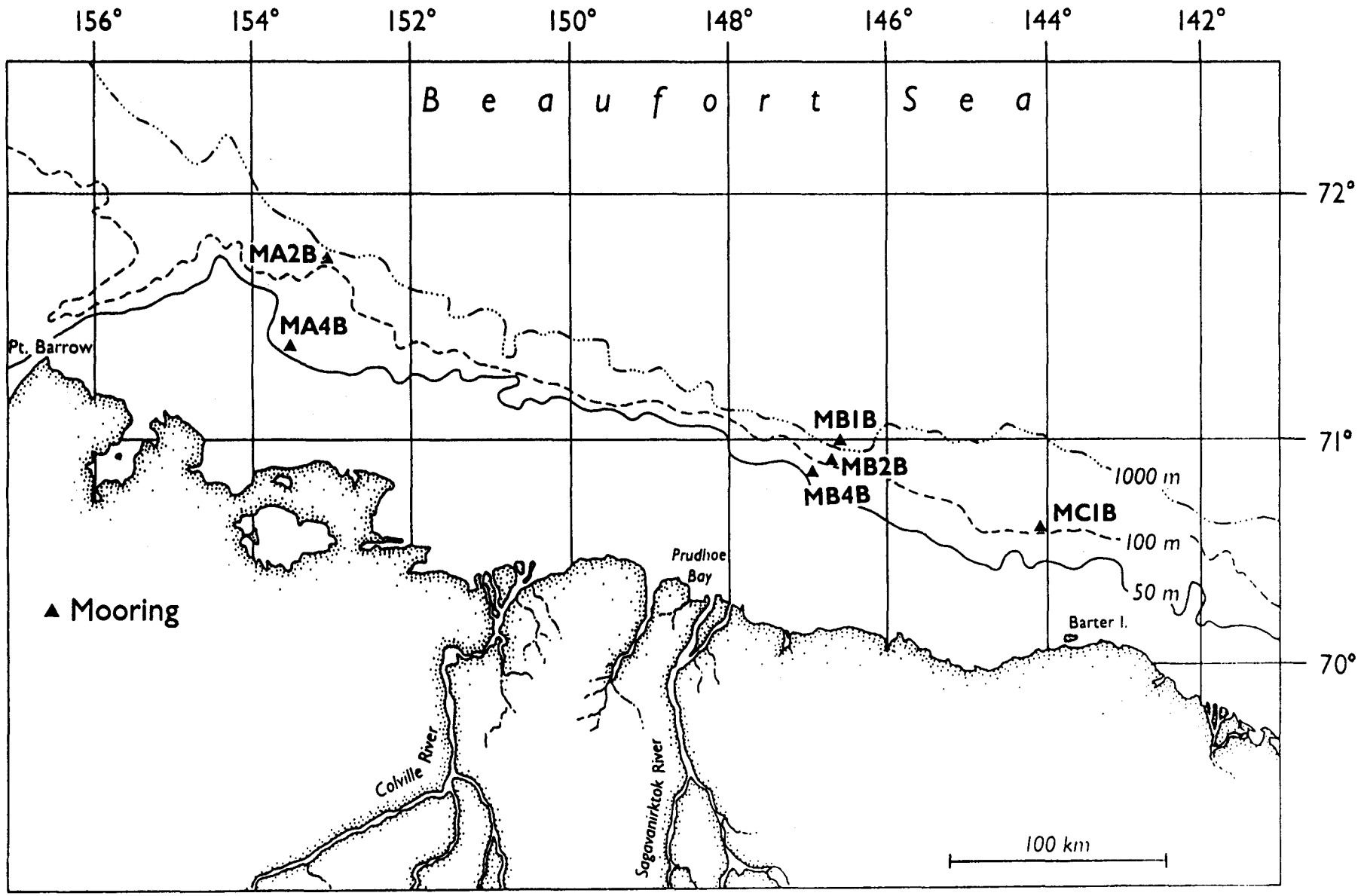

Figure 4. Beaufort Sea mooring locations, 1987–88.

TABLE 4. Beaufort Sea Moored Instruments, 1987-88.

Mooring	Latitude N	Longitude W	Depth m	Instrument depths, m		Dates GMT
MA2B	71°43.5′	153°04.4′	187	CM:	79	18-Apr-87
					112*	to
					162	17-Apr-88
				PG:	185	
MA4B	71°22.6′	153°28.7′	53	CM:	45	28-Mar-87
						to
						27-Apr-88
MB1B	70°59.4′	146°38.2′	1022	CM:	64	26-Apr-87
					97	to
					162	6-Apr-88
					994	
MB2B	70°55.1′	146°45.8′	185	CM:	72	5-Apr-87
					105	to
					155	4-Apr-88
				PG:	183	
MB4B	70°52.6′	146°57.3′	60	CM:	52	3-Apr-87
				PG:	58	to
						30-Mar-88
MC1B	70°36.9′	144°08.1′	216	CM:	108	11-Apr-87
					141	to
					191	9-Apr-88
				PG:	214	

* Note that record MA2B, 112 m, lasted only 39 days.

TABLE 5. Coastal meteorological station summary information. See Table 4 of Aagaard, Pease and Salo (1988) for information on gaps in the GOES data.

	Type	Start time			End Time			Position	
Barter I.	NWS-10	0000	1 Sep	1986	2300	31 Jul	1988	70.125°N	143.667°W
Resolution I.	GOES-6	1800	26 Sep	1986	1200	29 Mar	1988	70.370°N	148.047°W
Lonely	GOES-6	2300	25 Sep	1986	1800	29 Mar	1988	70.917°N	153.253°W
Barrow	NWS-10	0000	1 Sep	1986	2300	31 Jul	1988	71.300°N	156.733°W
Icy Cape	GOES-3	2100	22 Mar	1987	1800	31 Dec	1988	70.325°N	161.867°W
Kotzebue	NWS-10	0000	1 Sep	1986	2300	31 Jul	1988	66.883°N	162.625°W
Wales	GOES-10	1300	14 Sep	1987	1800	31 Dec	1988	65.633°N	168.117°W
Nome	NWS-10	0000	1 Sep	1986	2300	31 Jul	1988	64.517°N	165.433°W

Pressure and temperature fields at 6- and 12-hour intervals, respectively, were obtained from the Fleet Numerical Oceanography Center (FNOC), Monterey, CA. From these fields, we generated time series of sea-level pressure, surface air temperature, and winds at each of the above stations, at each current meter mooring site, and along the track of each ARGOS buoy, using the METLIB programs (Overland *et al.*, 1980; Macklin *et al.*, 1984). Temperature time series were resampled with a cubic spline to give 6-hourly data.

Time series of the surface winds were first obtained by rotating the gradient wind 30° toward low pressure and reducing the magnitude by a factor of 0.8. To verify this turning angle and reduction factor, we calculated the coherence of the northward component of the Climate or GOES winds with the component of the METLIB wind ranging from 350° to 010°T. We also calculated the complex correlation coefficient between these two types of winds at each meteorological station. The direction comparisons were hindered by the fact that NWS wind directions are reported only to the nearest 10°. However, results from the two most stable stations, Barrow and Resolution Island, suggested that appropriate rotation and reduction for the recalculation of the METLIB winds were 23° and 0.64, respectively. These turning and reduction values are consistent with the seasonal mean wind statistics from the 1975–76 AIDJEX Experiment, which found a range of reduction ratios of 0.55 to 0.60 and turning angles of 24° to 30° (Albright, 1980). Ratios of surface to geostrophic wind seem to vary from 0.75–0.80 in the subarctic Bering Sea to 0.55–0.60 in the high Arctic, with the North Slope values lying between these estimates.

Additional meteorological coverage was provided by deployments of ARGOS buoys and land stations by helicopter onto sea ice floes along the Beaufort and Chukchi coasts. Eleven ARGOS buoys and three ARGOS stations were deployed over 18 months in support of this study. In addition, four ARGOS buoys were deployed for the ONR Freeze experiment in the Chukchi Sea. Deployment information for the above buoys is summarized in Table 6. An example of one of the drifting meteorological stations is given in Fig. 97 of Appendix A. ARGOS buoys were not recovered from the ice, but were left to drift until failure, which was typically caused by the buoys melting out of the ice and sinking.

Three additional ARGOS buoys were deployed from Prudhoe Bay in cooperation with the Polar Science Center, Applied Physics Laboratory (APL) at the University of Washington. They shared the data from 16 additional buoys, which were part of the Arctic Buoy Program. The APL buoy deployments are summarized in Table 7.

ARGOS buoys transmit surface pressure and ventilated air temperature data to the NOAA polar-orbiting satellites when the satellite is overhead and the satellites later rebroadcast to the Service ARGOS receiving stations in Toulouse, France, and/or Suitland, MD. Positions are calculated by Service ARGOS from the Doppler shift of the transmissions, and the calculated positions and the sensor data are then available in preliminary form for daily computer

TABLE 6. ARGOS Buoy deployment information. All ARGOS buoys had ventilated air temperature and surface air pressure sensors. In addition, buoys 7420a, 7420b, and 7429 had 3-m vector-averaged anemometers and 6-m vector-averaged current meters. All times are GMT.

Buoy	Start time			Deployment Position		End Time			Last Position		Hours	Type[1]
7424[3]	1855	9 Oct	1986	71.528°N	145.239°W	0213	18 Dec	1986	71.034°N	164.889°W	1662	E B
7420a	1707	14 Oct	1986	70.660°N	141.282°W	0252	26 Oct	1986	70.526°N	144.314°W	268	C S
7428a	1730	17 Oct	1986	71.919°N	152.146°W	0314	4 Nov	1986	72.136°N	154.557°W	416	E B
7421[2]	0214	2 Mar	1987	65.899°N	168.469°W	0719	20 Mar	1987	66.886°N	167.909°W	436	P B
7422[2,3]	2121	1 Mar	1987	64.737°N	167.570°W	1545	12 Jun	1987	63.312°N	165.720°W	2464	P B
7423[2]	0500	8 Mar	1987	71.843°N	151.910°W	1958	12 Apr	1987	71.078°N	160.621°W	854	E B
7425[2]	1105	8 Mar	1987	72.018°N	154.984°W	2232	16 Mar	1987	72.025°N	154.860°W	205	E B
7426[2]	0313	13 Mar	1987	71.338°N	149.020°W	1731	2 Jun	1987	71.961°N	160.118°W	1956	E B
7427[2]	2017	13 Mar	1987	71.041°N	145.915°W	0709	30 Mar	1987	71.236°N	147.738°W	394	E B
7420b	1332	29 Apr	1987	71.336°N	144.554°W	0253	14 Jun	1987	71.644°N	159.344°W	1092	C S
7013[2,7,9]	2218	3 Sep	1987	71.936°N	158.086°W		8		73.951°N	178.440°E	9429	C T
7429[2,5,9]	2213	5 Sep	1987	72.001°N	160.765°W	0849	21 Sep	1987	71.637°N	156.134°W	369	C S
7014[2,7,9]	0653	8 Sep	1987	72.359°N	164.810°W		8		71.244°N	178.066°E	9325	C T
7015[2,9]	2308	9 Sep	1987	72.810°N	168.930°W	0236	7 Dec	1987	71.694°N	177.297°W	2114	C T
7430[7]	1900	17 Nov	1987	71.662°N	148.643°W	0751	30 Jun	1988	71.879°N	177.028°W	5408	C T
7432[7]	2100	17 Nov	1987	71.454°N	145.466°W	0912	24 Jul	1988	73.095°N	175.412°W	5971	C T
7431	0000	18 Nov	1987	71.893°N	151.744°W		8		71.317°N	150.983°W	7627	C T
7428b	2342	16 Apr	1988	71.594°N	159.043°W	1915	27 May	1988	71.721°N	165.534°W	955	E B

1. Buoy types are: EB = ESI box, CS = Coastal Climate Company Station, PB = PMEL/Synergetics box, CT = Coastal Climate Company short tube.
2. Time of first transmission.
3. Buoy 7424 had poor transmissions; stable positions were rare.
4. Buoy 7422 had a data gap 21–25 May 1987.
5. Buoy 7429 had a data gap 1–5 Sep 1987.
6. Buoy 7428 had a data gap 5–13 Apr 1988.
7. Buoys 7013, 7014, 7428, 7430, and 7432 had a data gap 29–31 Apr 1988.
8. Buoy was still transmitting on 1 Oct. 1988. Last transmission processed was 30 Sep 1988.
9. ONR funded deployment.

TABLE 7. APL buoy deployment information. Data for the following buoys, from the Applied Physics Laboratory of the University of Washington were used to fill in gaps in our ARGOS buoy array. All start times are times of the first ARGOS transmissions. All times are GMT.

Buoy	Start time			Deployment Position		End Time			Last Position		Hours
3161	0304	1 Aug	1986	70.281°N	145.458°W	2114	20 Sep	1986	70.646°N	145.610°W	1217
3164[6,7]	0304	1 Aug	1986	75.892°N	157.802°W	0439	22 Nov	1987	80.243°N	150.224°W	11472
3165	0122	1 Aug	1986	72.447°N	173.619°W	1825	12 Sep	1986	72.744°N	168.297°W	1024
3848[5]	0140	1 Aug	1986	76.724°N	163.814°E	0855	18 Aug	1986	74.349°N	165.704°E	3342
3849[3,4]	0123	1 Aug	1986	76.578°N	134.065°W	0120	3 Nov	1986	76.517°N	128.183°W	2255
3880	0122	1 Aug	1986	73.332°N	157.428°W	0736	1 Jun	1987	73.027°N	174.152°W	7301
7012	0122	1 Aug	1986	76.975°N	172.230°W	0305	8 Sep	1986	77.538°N	174.109°W	913
7021[6]	0317	1 Aug	1986	74.361°N	142.797°W	0317	9 Aug	1987	75.776°N	166.470°W	8951
7022[6]	0307	1 Aug	1986	77.165°N	154.610°W	1700	15 Oct	1987	81.234°N	144.497°W	10573
7002[6,9]	1125	12 Aug	1986	79.998°N	165.542°E	2222	19 Mar	1988	85.656°N	176.578°E	15802
7011	2259	19 Mar	1987	71.796°N	145.459°W	1658	10 Apr	1987	72.001°N	148.432°W	521
7047[6]	0535	3 Apr	1987	72.005°N	148.360°W	1441	23 Nov	1987	73.106°N	179.630°W	5624
2380	0050	12 Apr	1987	71.288°N	161.371°W	0215	20 Jul	1988	71.660°N	156.454°W	457
3160[6,8]	0040	12 Apr	1987	70.200°N	148.468°W	0142	29 Jan	1988	72.704°N	175.199°E	7008
7024	2351	27 Apr	1987	70.198°N	148.466°W	0043	20 Jun	1987	71.767°N	158.176°W	1272
7027[6]	0112	14 Jun	1987	73.992°N	130.137°W	2114	31 Dec	1987	72.220°N	165.180°W	4819
3831[9]	2114	31 Oct	1987	73.352°N	131.028°W	2227	31 May	1988	72.340°N	166.261°W	(1*)
7026[6,9]	1837	1 Nov	1987	74.016°N	130.776°W	2232	31 Dec	1987	72.272°N	141.321°W	(2*)
7054	1147	15 Aug	1988	70.260°N	141.545°W	2009	31 Oct	1988	69.400°N	137.115°W	1856

1*. Buoy 3831 was missing data from 1–31 July 1988. Its record was divided into two sections, one spanning 5112 hrs, the other 2954 hrs.

2*. Buoy 7026 lacked data from 1–31 Jan 1988. Its file was divided into records 1443 hrs and 2903 hrs long. Other data gaps were:

3. 21–27 Oct 1986.
4. 31 Oct–2 Nov 1986.
5. 4–17 Dec 1986.
6. 25–27 July 1987.
7. 18–20 Nov 1987.
8. 18–23 Jan 1988, and
9. 28 Apr–1 May 1988.

interrogation and through fortnightly distribution by magnetic tape. Because the satellite passes were irregularly distributed in time, positions and data points were irregularly spaced. Therefore, we resampled the time series with a cubic spline to obtain data with a spacing of 60 minutes. The resampled position data was used to calculate the velocity and acceleration of the ice by central differencing.

III. RESULTS

A. Chukchi Sea

The current meter array deployed in the Chukchi Sea during 1986–87 is at essentially the same location as one deployed from 6 September 1981 to 17 August 1982 (Aagaard, 1988). The statistics of the two records are compared in Table 8.

We see that, on an annual mean basis, the flow was essentially identical in the two years, but that the extreme speed recorded was 30% greater during 1981–82. Figure 5, comparing the weekly mean currents, shows that although the annual mean statistics were very similar for the two years, there are important differences in the the low-frequency flow. Compared to 1986–87, the 1981–82 record shows: 1) more extreme currents both northward and southward, 2) flow reversals extending much longer into the spring, and 3) stronger flow during most of the summer. On the other hand, there are points of similarity, with a highly variable flow (including reversals) occurring during the fall and early winter of both years and a period of weaker currents followed by an increasing flow in the spring which reaches a maximum in mid-summer. This sequence is consonant with the normal seasonal cycle in the inflow through Bering Strait (Coachman and Aagaard, 1988).

Our numerous nutrient sections in the Beaufort Sea show the Arctic Ocean nutrient maximum to be present above the continental slope and at times to extend onto the shelf (see Appendix A). The origin and maintenance of the nutrient-rich layer in the Arctic Ocean is therefore of considerable importance to conditions on and adjacent to the Beaufort shelf (see also Aagaard, 1984, and Hufford, 1974).

TABLE 8. Record-length current statistics for one-year moorings in the Chukchi Sea near 67° 39′N, 165° 38′W.

Year	Max. speed	Mean velocity		Principal axis	
	cm s^{-1}	cm s^{-1}	°T	°T	Variance %
1981–82	74	5.9	345	318	85
1986–87	57	5.6	336	325	87

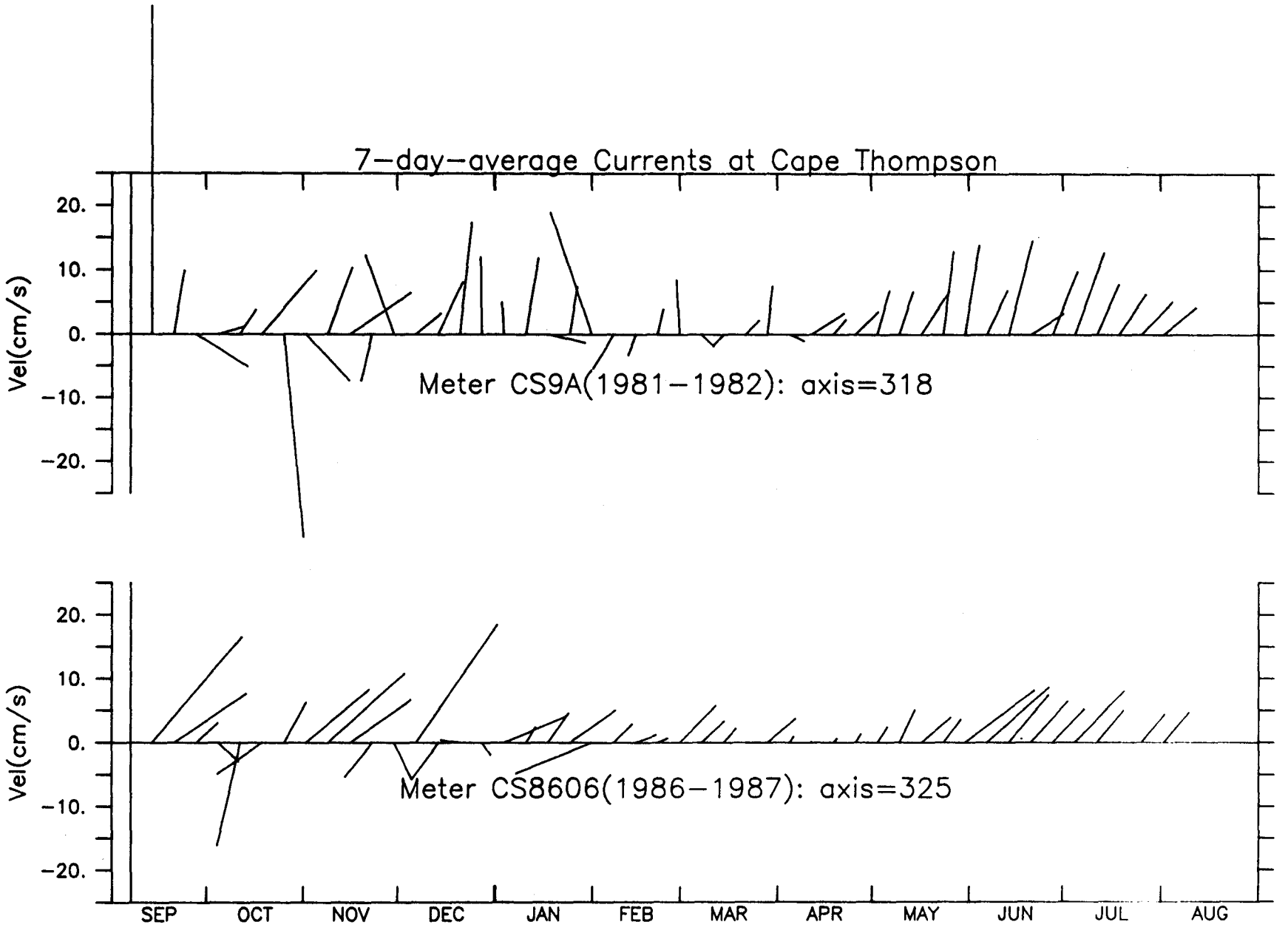

Figure 5. Weekly averaged current vectors at Cape Thompson for years 1981–82 (top) and 1986–87 (bottom) resolved on their respective axes of greatest variance.

Figure 6 shows the temperature, salinity, and nutrient structure in the upper 500 m of the Arctic Ocean about 400 km north of the Alaskan coast; the data were made available by J.H. Swift. The temperature maximum at 75 m occurs near the salinity 32.0 and is associated with relatively low nutrient values. In contrast, the temperature minimum centered near 180 m and corresponding to a salinity near 33.1, coincides with the nutrient maximum. Values for the latter exceed 15 for nitrate and 1.8 for phosphate, and are near 40 for silicate (all values in micromoles per liter). The various distributions are fully consistent with earlier Arctic Ocean profiles and can therefore be considered typical of at least the Canadian Basin.

To address the origin of these waters, consider the near-bottom distributions of salinity and nitrate in the Chukchi, East Siberian and Laptev seas (Fig. 7) depicted by Codispoti and Richards (1968). Note that only in the western Chukchi Sea, are waters both saline enough and have sufficiently high nitrate concentrations to account for the properties of the nutrient-maximum layer in the Arctic Ocean. The same conclusion can be drawn from the near-bottom phosphate and silicate distributions (not shown). Now, from where does this water derive?

The essential element in this portrayal is the coincidence of high salinities (~33) and high nutrient levels in the western water mass and the contrasting lower salinities and nutrient levels of the Alaskan Coastal Water. This situation is seen in the recent sections by Tripp (1987) which spanned across Shpanberg and Anadyr straits in the northern Bering Sea and extended west from Point Hope into the central Chukchi Sea. In Anadyr Strait, the deep shelf waters at the time of the 1987 cruise were near 33 in salinity and had a nutrient content even higher than the maximum Arctic Ocean values, while in Shpanberg Strait the salinity was close to 32 and the nutrient values were very low (Fig. 8). A similar situation occurred in the Chukchi Sea (Fig. 9), where saline high-nutrient water was found at the western stations (although apparently the section did not extend far enough west to observe the water with the highest nutrient values), while the deep water in the eastern part of the section was similar to that observed in Shpanberg Strait.

The implication of these various data is that it is the nutrient-rich Anadyr Water which ultimately is responsible for the high subsurface nutrient levels in the Arctic Ocean. The corresponding Arctic Ocean temperature minimum is therefore not a temporal signal (from a winter shelf source), but a spatial one (from a western shelf source with a lower mean annual temperature than the eastern source) (Coachman *et al.*, 1975). This saline high-nutrient western source water moves onto the shelf in the southwestern Bering Sea and then northward via the westward-intensified Bering Sea circulation (Kinder *et al.*, 1986) and into the western Chukchi Sea, eventually to supply the Arctic Ocean from east of Wrangel Island.

The salinity and nutrient distributions observed northwest of Pt. Barrow in October 1986 (Appendix A, Figs. 8 and 11–15) are consistent with such a scheme. The saline, high-nutrient water was found over the slope (with some suggestion of upwelling at the time of the observations), where it participated in the net eastward flow of the Beaufort Undercurrent, and

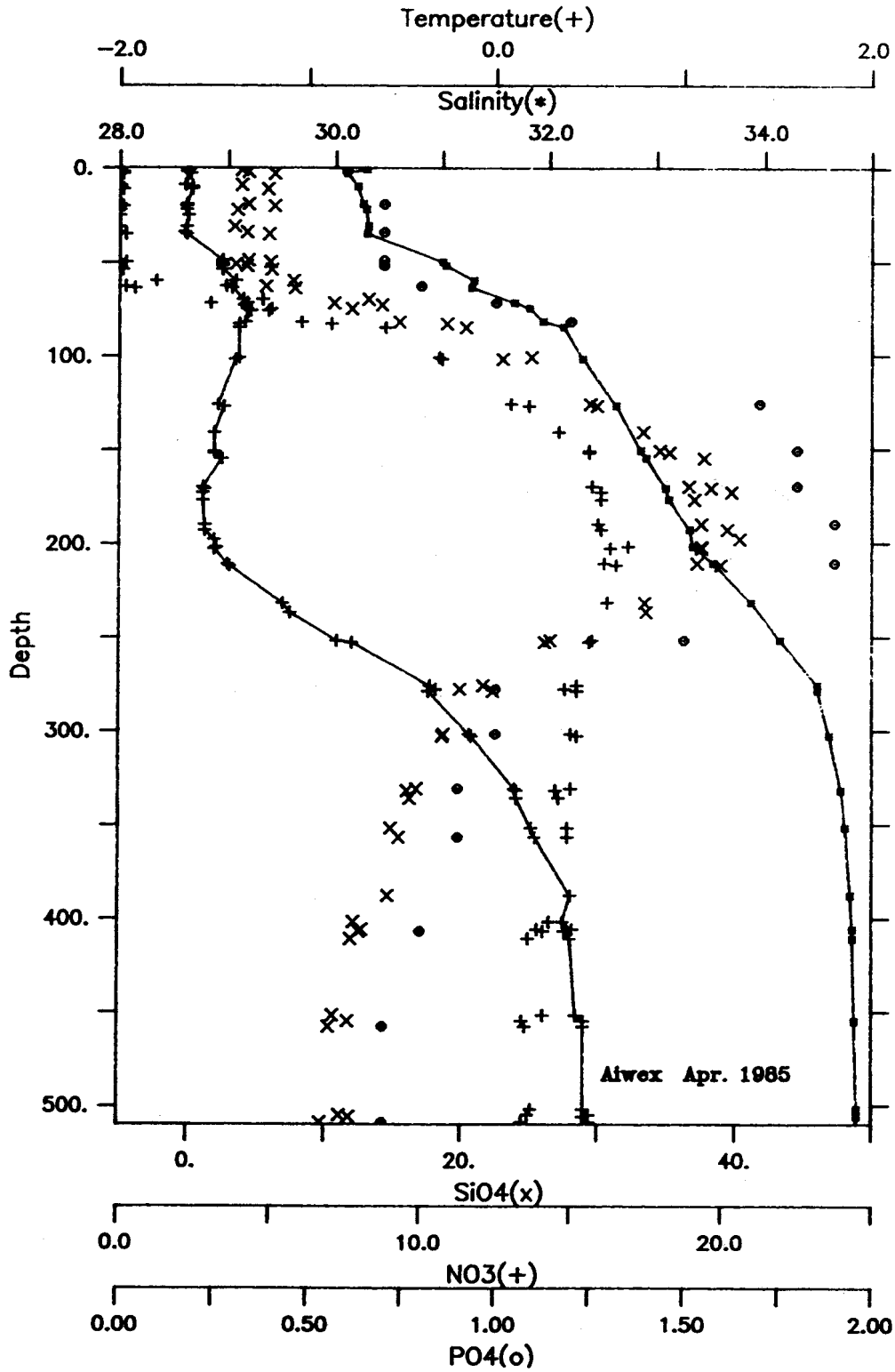

Figure 6. Profiles of temperature and salinity (symbols connected by solid lines) with scatter plots of nutrients composited from AIWEX (Arctic Internal Wave Experiment) conducted in April 1985 near 74°N and 144°W.

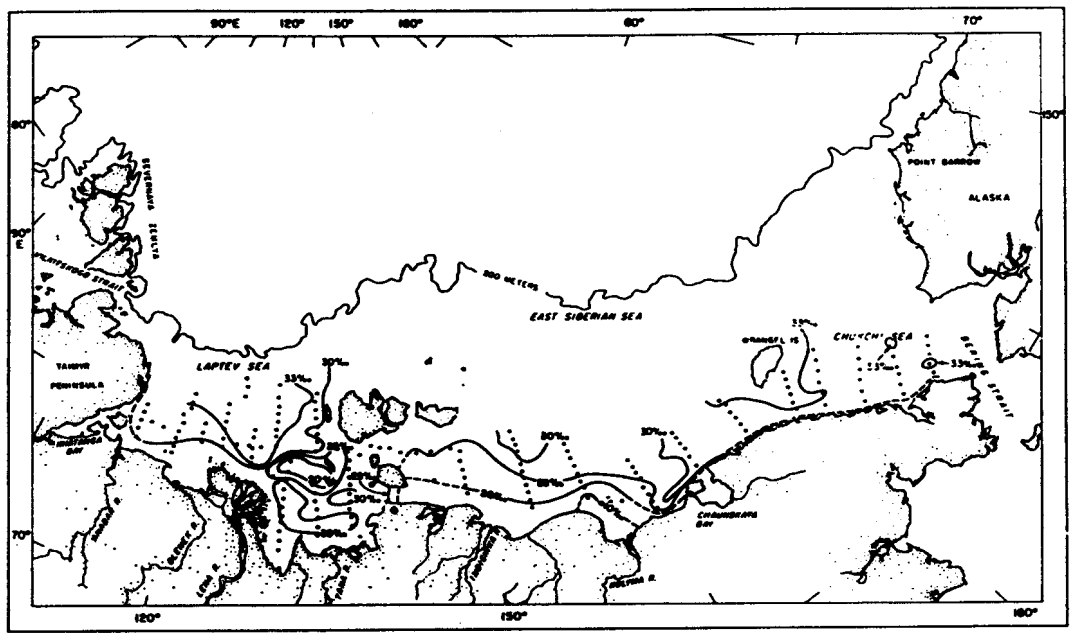

Figure 7a. Horizontal distribution of salinity, in psu, in the bottom waters (from Codispoti *et al.*, 1969).

Figure 7b. Horizontal distribution of nitrate, in micro-grams-at/liter, in the bottom waters (from Codispoti *et al.*, 1969).

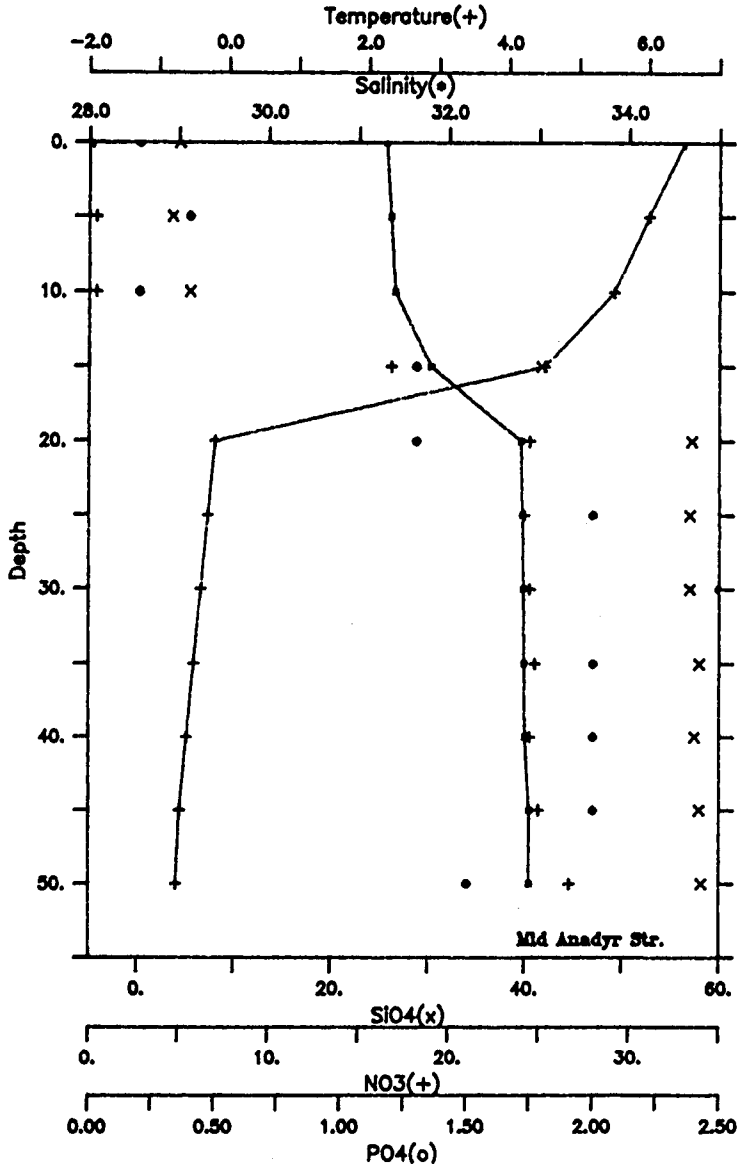

Figure 8a. As in Figure 6, at Anadyr Strait ISHTAR (Inner SHelf Transport and Resources) station.

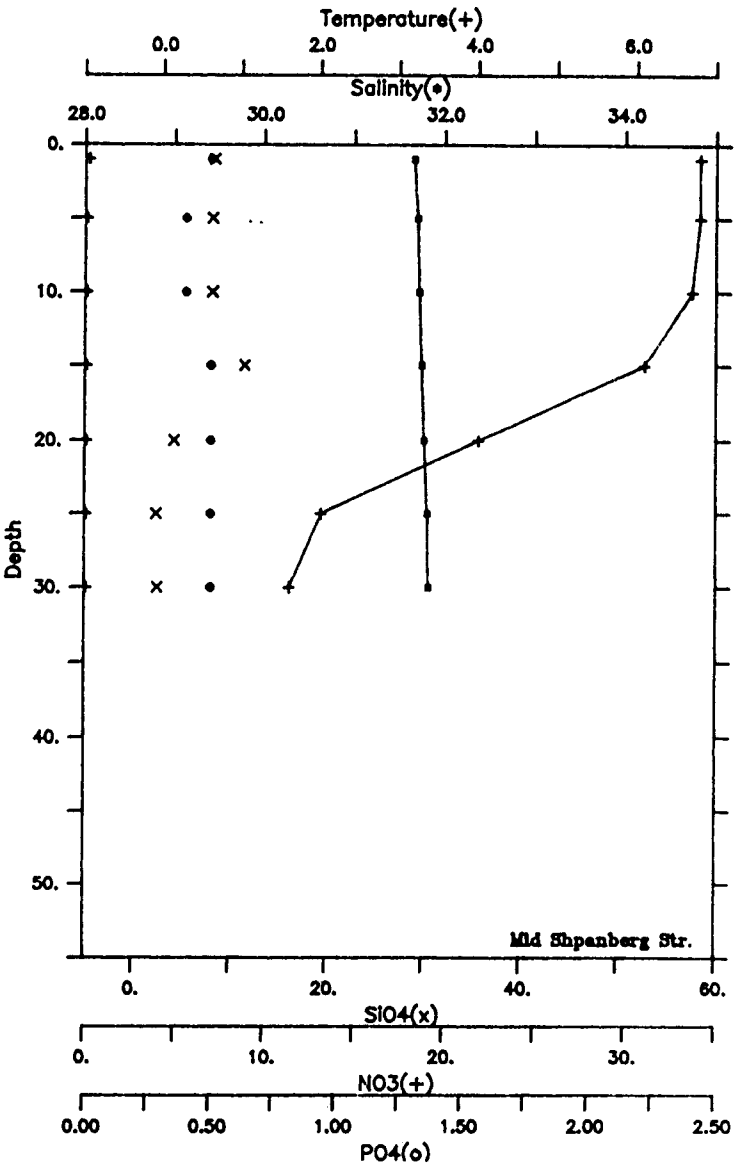

Figure 8b. As in Figure 6, at Shpanberg Strait ISHTAR station.

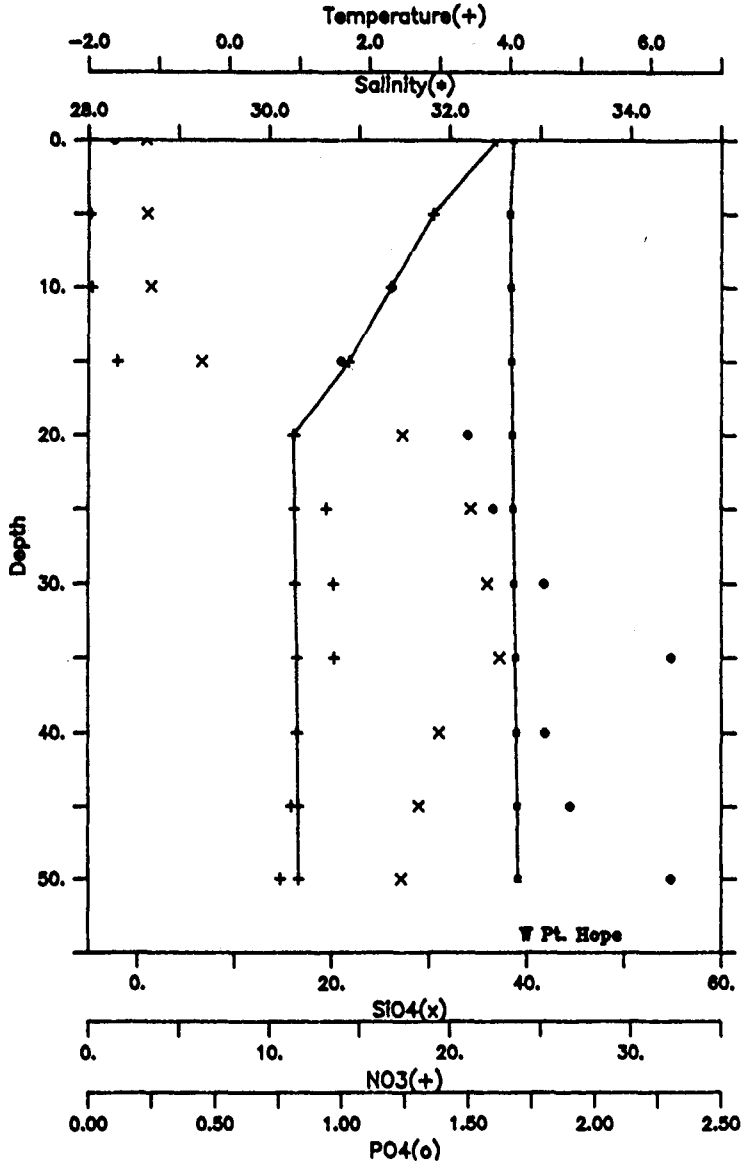

Figure 9a. As in Figure 6, at an ISHTAR station approximately 120 km off of Pt. Hope.

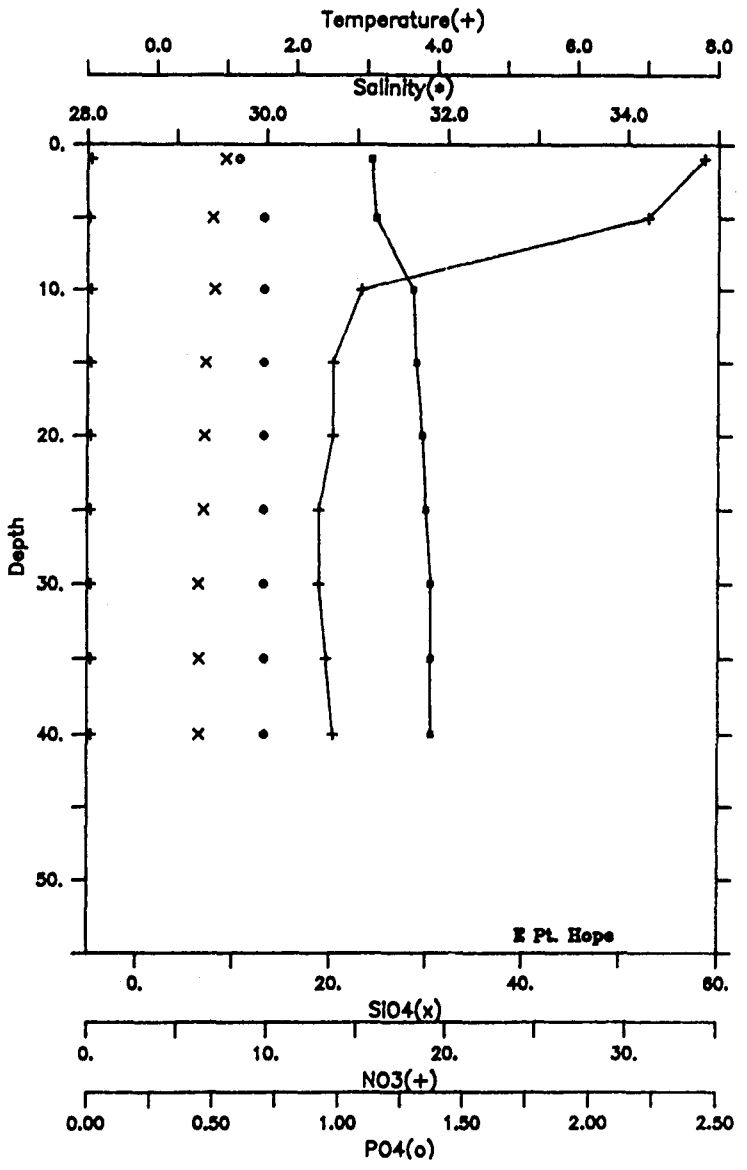

Figure 9b. As in Figure 6, at an ISHTAR station approximately 20 km off of Pt. Hope.

apparently followed the isobaths to enter Barrow Canyon from the northeast. In contrast, the water in the canyon immediately adjacent to the Alaskan coast was of lower salinity and greatly reduced nutrient content. Note particularly the high ammonia content (Appendix A, Fig. 14) of the water with Bering Sea characteristics below 140 m at station W3. Although the applicable nitrogen regeneration rate is uncertain, it's unlikely that significant ammonia concentrations would persist over more than a few months. These concentrations therefore suggest a relatively recent shelf origin for the high-nutrient water, such as Herald Canyon, immediately east of Wrangel Island.

B. Barrow Canyon

The record-length mean flow through Barrow Canyon was directed northeast throughout the bottom layer (Table 9). Mean speeds were 13–16 cm s^{-1} near the axis of the canyon, with somewhat stronger flow of 17–23 cm s^{-1} on the shoreward wall of the canyon at BC2. The mean shear between the bottom two instruments, which were in each case separated by 5 m, was 1–3 cm s^{-1}. Both moorings measured peak outflow speeds in excess of 90 cm s^{-1} and the flow was generally closely aligned with the canyon axis: nearly 98% of the current variance was contained within the sector 45–60°T. The direction of the axis of greatest variance was slightly more variable vertically at BC2 than at BC1, but even the former record contains no significant rotational energy. The flow through the canyon is therefore essentially rectilinear.

TABLE 9. Current meter statistics for Barrow Canyon. Instrument designated by mooring and elevation above sea floor (m).

Instrument	Mean velocity		Principal axis	
	cm s^{-1}	°T	°T	% of variance
BC1/14.0	14.8	54.4	225	97.5
/ 9.0	15.9	59.8	226	97.2
/ 2.0	12.8	59.7	223	97.7
BC2/14.0	22.7	53.4	229	98.0
/ 9.0	18.0	45.8	223	94.0
/ 2.0	16.9	48.0	222	97.8

There is, however, a suggestion of eastward rotation of the velocity component at BC1 following flow reversals. The latter are a prominent feature of the records and represent water being moved up-canyon toward the southwest (Fig. 10). Each flow reversal typically lasted from two to six days, with southwestward flow as rapid as 60 cm s^{-1}. Mooring BC1 generally showed reversals first, leading by 12–13 hr, whereas BC2 reverted to normal down-canyon outflow first, leading by 1–2 hr. While a clear seasonal signal is not evident in the current speeds, the number and intensity of reversal events declined throughout the winter and into the spring. The SeaCat records show that during the reversals, warm and saline water from the Atlantic layer (Arctic Intermediate Water [AIW]) in water mass terminology [cf. Aagaard *et al.*, 1985]) moved up-canyon into the Chukchi Sea (compare Figs. 10–12), although in a number of instances the clear presence of upwelled water could only be detected at BC1, where the water was about 50 m deeper than at BC2. Such upwelling events in the canyon have previously been described by Mountain *et al.* (1976), and they have also been inferred by Garrison and Paquette (1982) who hypothesized mixing of upwelled water with ambient shelf waters. While our records do not contain obvious evidence of extensive mixing, the advection of AIW onto the shelf was frequent and often vigorous.

Overall, the temperature-salinity structure observed at the two moorings exhibited two volumetric modes; the largest being of low temperature and salinity and denoting the resident winter water of the Chukchi Sea, while the secondary mode represents upwelled AIW (Figs. 13, 14). There were differences between the two moorings, however, both in the mean state and the property range (Table 10, Figs. 13, 14). The water passing BC2 was in the mean fresher (by about 0.4) and warmer (by about 0.2°C) than at BC1; and the salinity and temperature over the canyon wall at BC2 varied by 3.8 and 5.5°C, respectively, while at BC1 they varied by only 2.4 and 3.1°C. Another point of difference was the seasonal temperature cycle. Neglecting upwelling events (shown by the elevated salinities in Fig. 11), Fig. 12 points to a fall cooling at BC2 from 2–3°C in early October to near-freezing temperatures by mid-November. The latter persisted until early July, when a rapid increase temporarily elevated temperatures back to near 3°C , announcing the arrival of summer water from the Bering Sea. Overall, the temperature record from BC1 shows a seasonal response about three weeks delayed and a magnitude perhaps one-third as great as that at BC2. All these differences are consonant with the two moorings being sited at different depths near the interface between the strongly stratified Arctic Ocean and the highly variable and shallow Chukchi Sea.

Note in Fig. 13 that no water was seen corresponding to the cold and saline corner of the T-S plane, i.e., that there were no plumes carrying cold brines down the canyon. The search for such outflow had provided the original motivation for the study, and their absence from this data set will be considered below.

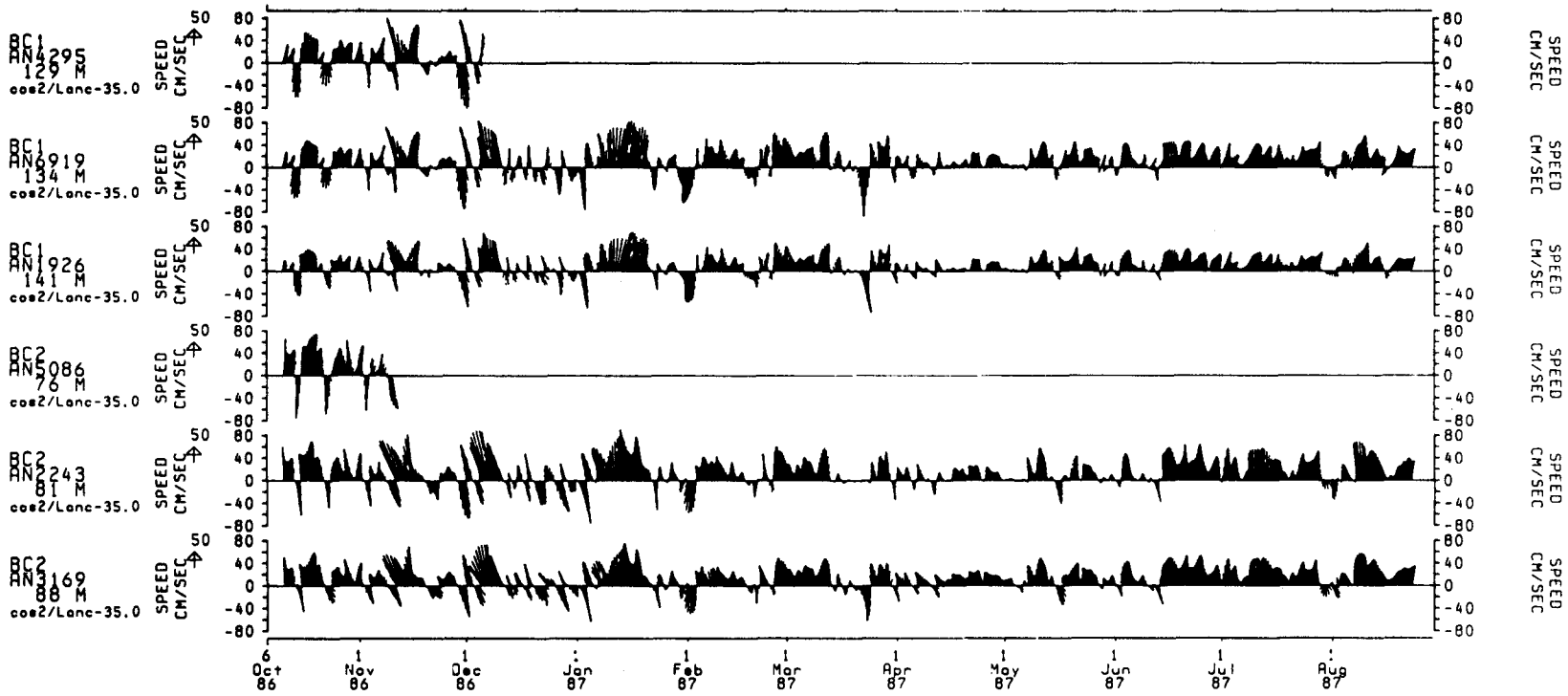

Figure 10. Six hourly, low pass filtered current velocity records from the Barrow Canyon current meters. All records were resolved on 50°T; the canyon's major axis. The topmost current meters at each location failed in the early winter.

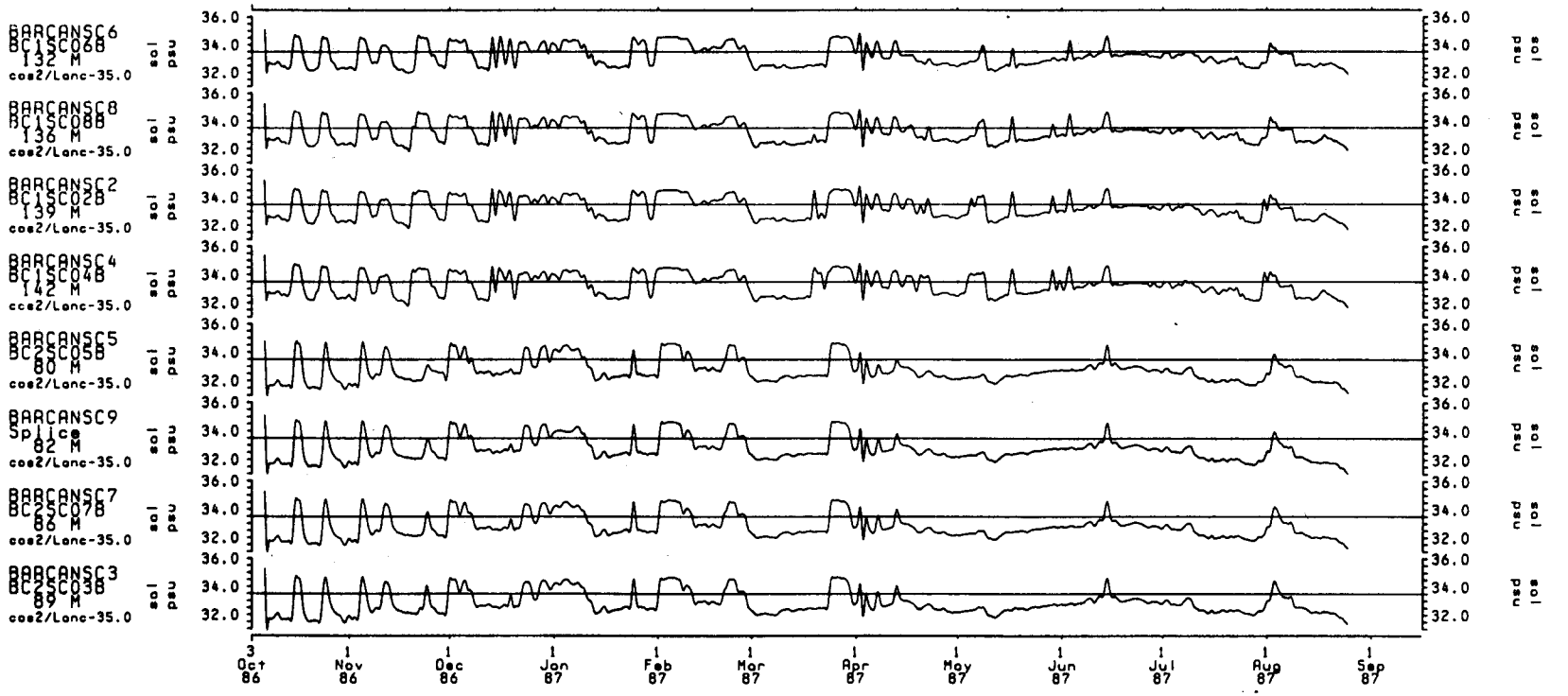

Figure 11. Six hourly, low pass filtered salinity records from the eight Seacats deployed. They are presented BC1, top instrument to bottom; BC2 top to bottom. The vertical scale is 31.0 to 36.0 psu.

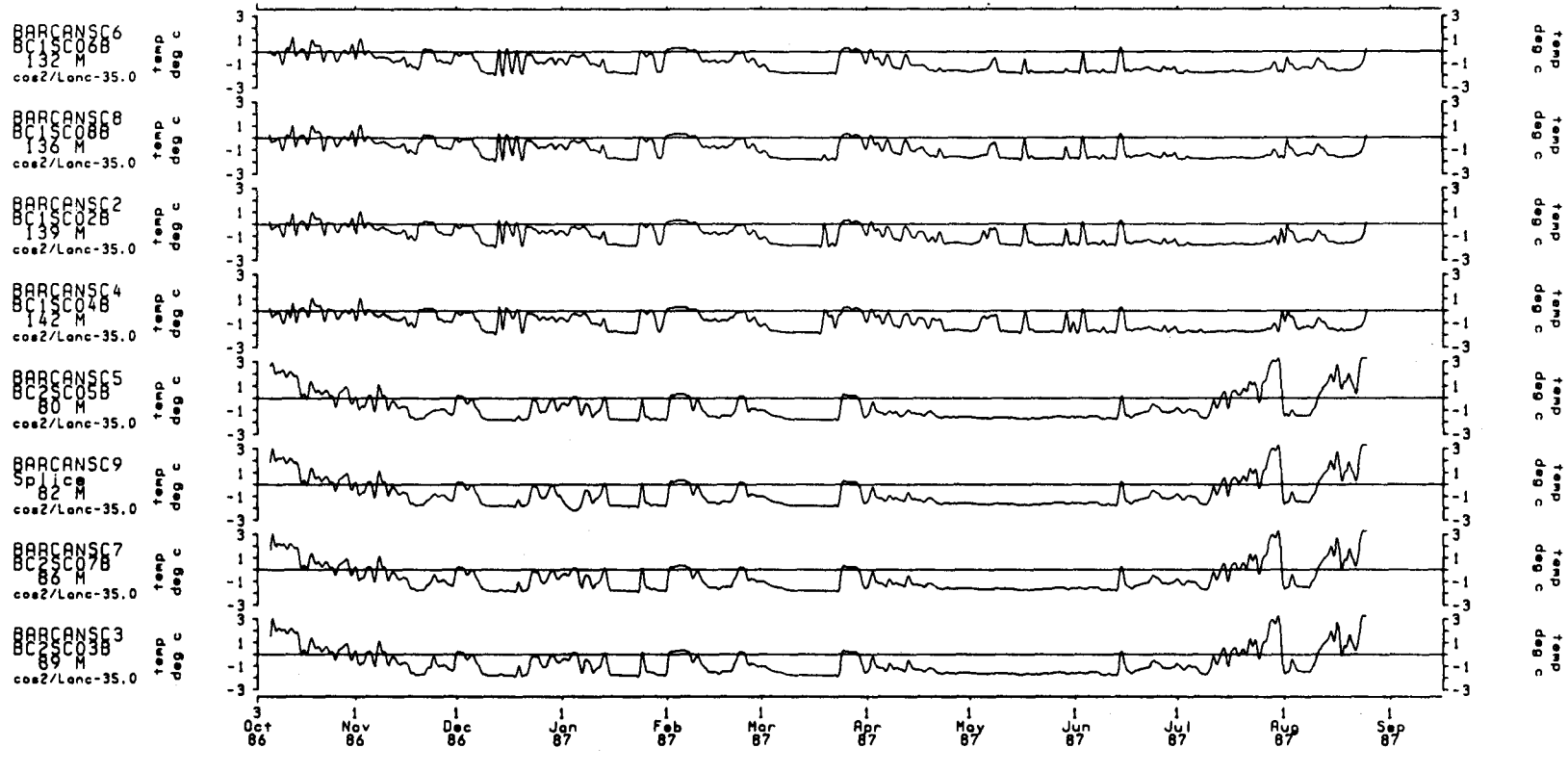

Figure 12. As in C4, except for temperature from –3.0 to 3.0 °C.

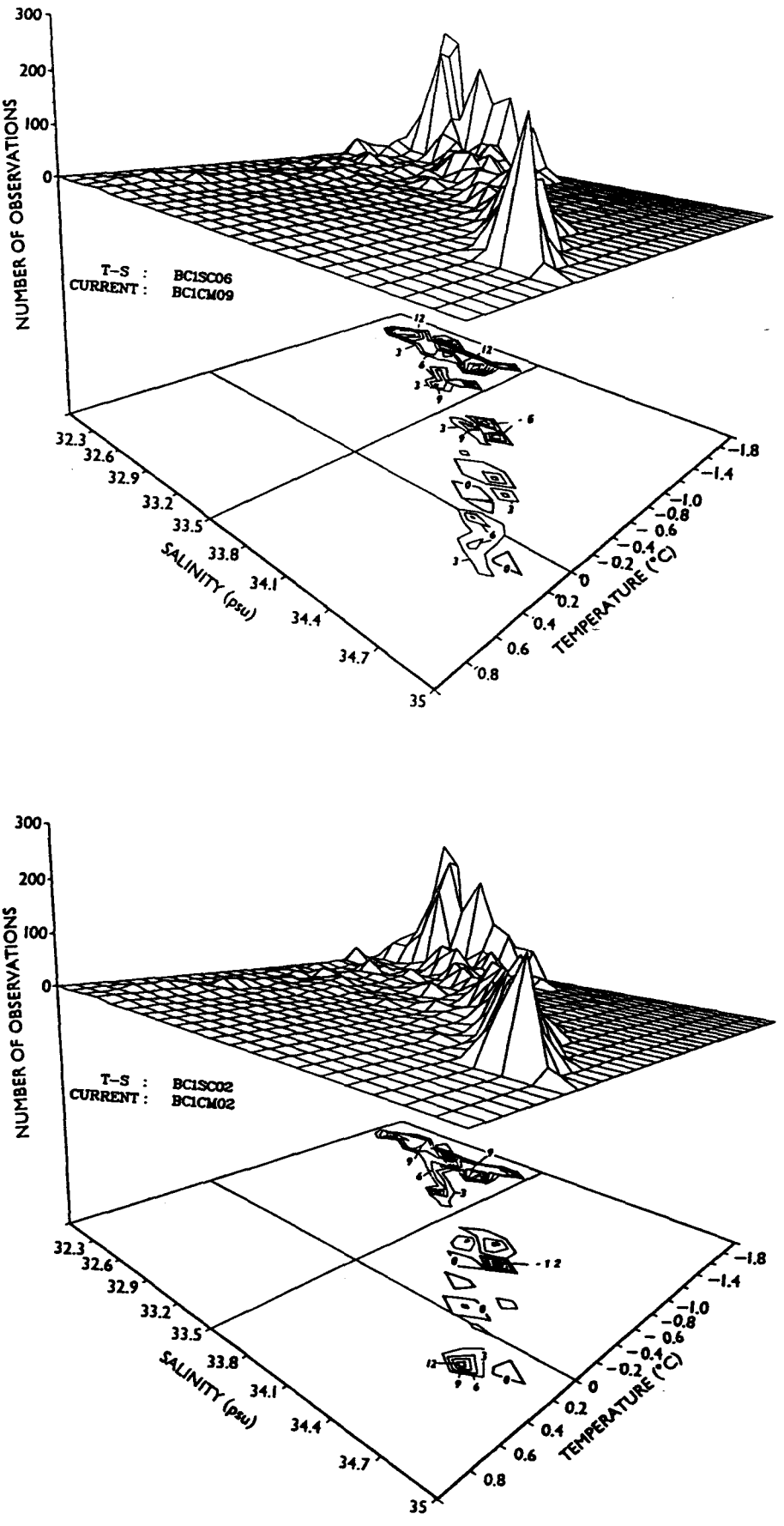

Figure 13. Frequency – mean velocity plot for Seacat and current meter pairs from BC1. The upper mesh plot represents the number of hourly observations of a particular temperature-salinity envelope, while the lower contour plot shows the corresponding net velocity along 50 °T in contours of 3 cm s^{-1}. The pairs chosen are the uppermost Seacat with the current meter directly below it and the lowest current meter with the Seacat directly above it. Areas of negative velocity are centered near – 0.6°C and 33.8–34.1.

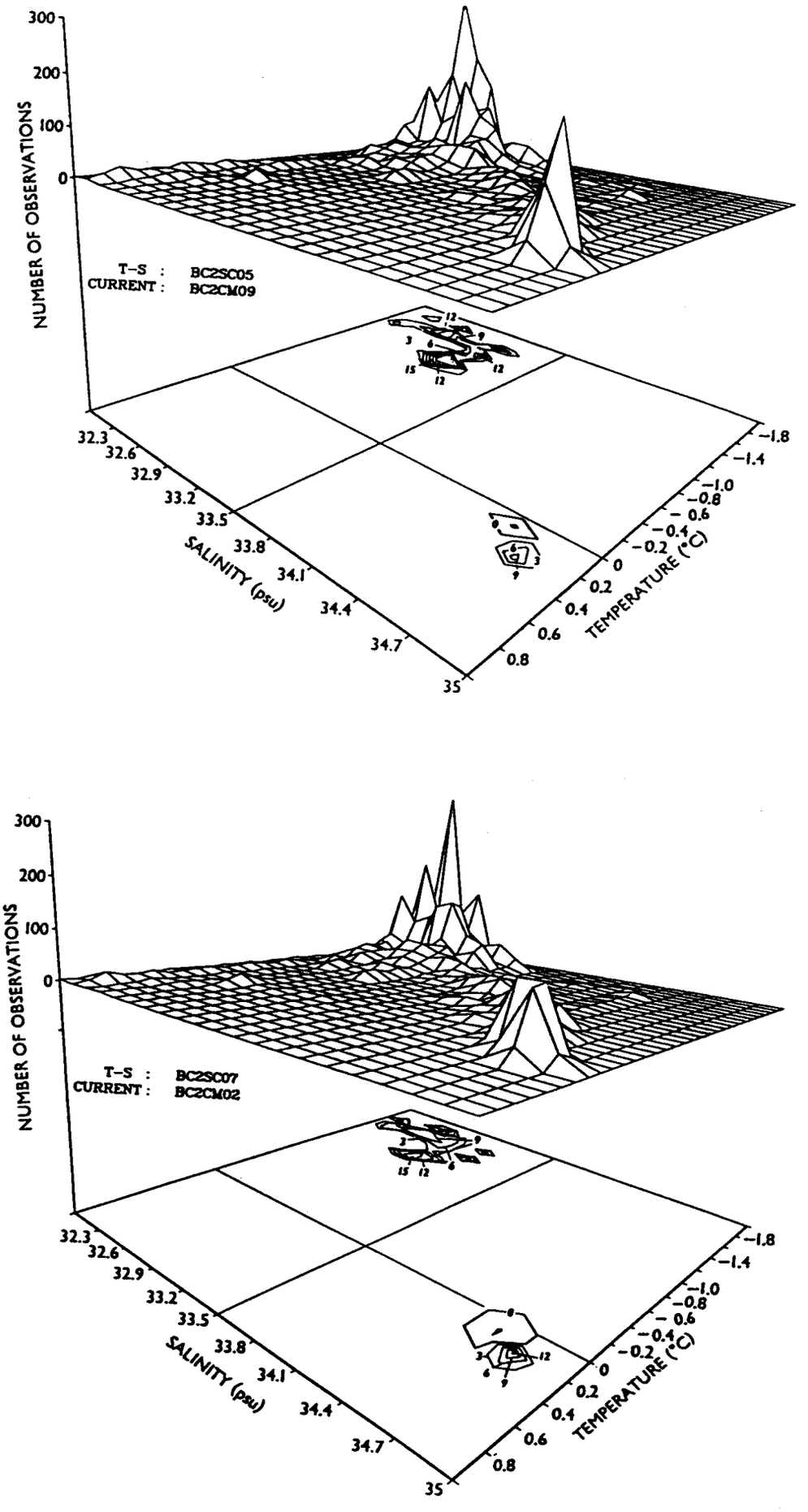

Figure 14. As in Figure 13, but for BC2.

TABLE 10. Seacat statistics.

Mooring	Depth m	Mean Sal.	Sal. RMS	Max. Sal.	Min. Sal.
BC1					
SC 6	132.2	33.199	0.093	34.849	31.839
SC 8	136.4	33.244	0.091	34.848	31.843
SC 2	139.0	33.260	0.093	34.848	31.689
SC 4	142.0	33.300	0.093	34.850	31.649
BC2					
SC 5	79.2	32.754	0.106	34.803	31.161
SC 9	82.4	32.789	0.110	34.831	30.997
SC 7	86.0	32.828	0.110	34.844	31.247
SC 3	89.0	32.869	0.105	34.785	31.357

Mooring	Depth m	Mean Temp. Deg C	RMS	Max. Temp. Deg C	Min. Temp. Deg C
BC1					
SC 6	132.2	–1.012	0.182	1.287	–1.940
SC 8	136.4	–0.985	0.180	1.105	–1.942
SC 2	139.0	–0.952	0.179	1.070	–1.944
SC 4	142.0	–0.920	0.178	1.076	–1.940
BC2					
SC 5	79.2	–0.762	0.230	3.587	–1.904
SC 9	82.4	–0.791	0.203	3.512	–1.915
SC 7	86.0	–0.759	0.237	3.334	–1.919
SC 3	89.0	–0.755	0.237	3.230	–1.912

For periods exceeding three days, comparable velocity records from each mooring were well correlated ($r = 0.85$, which is significant at the 95% confidence level). For example, during the first four inflow events in October-November 1986 (Fig. 10), the moorings showed a nearly uniform behavior, with the current recorded by each instrument leading the one above it by 2–3 hr (presumably a frictional effect) and maintaining a vertical velocity shear of 3–9 cm s^{-1} over the instrument separation. On the other hand, because of the depth differences between the two moorings, the temperature and salinity records were only sporadically similar (Figs. 11, 12). For example, during the same first four inflow events, the variation in water properties recorded by the eight SeaCats was nearly identical. In contrast, during the weaker inflow events in May and early June, only the BC1 instruments showed significantly elevated temperature and salinity. There were also intermediate cases, e.g., in late January, in which the duration of elevated properties was much shorter along the canyon wall than near the floor. These observations are of course consistent with an inflow of AIW into the canyon, which only on occasion introduced a sufficiently thick layer to allow its observation at mid-depth. The frequently very limited thickness of the warm and saline intrusions was perhaps most obvious at the individual moorings. For example, during the mid-December property elevation at BC2 (Figs. 11, 12), the temperature and salinity 1 m above the bottom increased by nearly 1°C and 1 psu, respectively, but the increases were less than one-half that only 10 m higher in the water column.

About 25% of the total low-frequency current variance can be accounted for by estimates of the wind variability near the north coast of Alaska ($r \sim 0.5$, significant at the 95% level), with the wind leading by 6–12 hr (Table 11). The Nome wind was equally well correlated with the flow, but with a greater lead, showing the regional coherence of the wind field. (The latter is also seen in the direct comparison between the Nome and Barrow winds, with a correlation exceeding 0.6 and the former series leading by about a day.) We also found about the same correlation between the surface atmospheric pressure difference between Barrow and Nome and the

TABLE 11. Record length correlations of Barrow Canyon currents to regional winds and surface pressure gradients using 6 hourly data (lag in hours); positive lag means column leads.

	Barrow	Barter Is.	Nome	Barrow-Nome Del P
BC1 134 m	0.45 (6)	0.49 (6)	0.52 (18)	–0.53 (24)
BC1 141 m	0.45 (6)	0.48 (6)	0.52 (24)	–0.51 (24)
BC2 81 m	0.46 (6)	0.55 (6)	0.50 (24)	–0.55 (24)
BC2 88 m	0.46 (6)	0.53 (12)	0.50 (24)	–0.57 (24)

along-channel flow as with the wind and the flow. Note, however, that the portion of the current variance which can be accounted for by this pressure difference (29%) is significantly less than the 55% found by Mountain *et al.* (1976). We do not know the reason for this. We have checked the possible effect of seasonality by calculating the correlation between the flow and the Barrow-Nome pressure difference for 1987 during the same four-month period used by Mountain *et al.* (1976) for 1973, but we find that this correlation does not differ significantly from that for the full year 1986–87. The difference between our results and the earlier ones therefore remain unexplained, although we should expect the earlier results to be less representative because of the much shorter period of measurements.

Finally, we have calculated the turbulent fluxes of salt and heat from the combined current and SeaCat records (Table 12). The estimates are for two levels, approximately 2 and 10 m above the bottom, and the fluxes are referenced to the principal-axis coordinate system. Note that whereas the heat flux at BC2 is directed down-canyon (because ot the surge of warm outflow from the shelf in summer), the salt and heat fluxes at BC1 are all directed up-canyon. These fluxes represent the effect of upwelling events in driving a net onshore turbulent transport of salt and sensible heat near the bottom of the canyon. If we assume a layer 20 m thick and 25 km wide, the up-canyon heat flux will be about 6.8×10^{11}W and that of salt 2.5×10^{8} gm s^{-1}; the latter corresponds to an annual flux of 7.9×10^{15} gm. The surface area over the canyon deeper than 100 m and lying inshore of the measurements is about 1200 km^2. If the deep heat flux were all discharged through this surface area, it would represent an annual average flux of 189 W m^{-2}. Assuming the entire dissipated amount were discharged through the sea surface, that heat flux could melt 31 cm of ice in an intense upwelling period, such as the one lasting about 105 hr in late January 1987. Intermittent upwelling into the canyon could therefore conceivably be locally significant in instances of efficient vertical mixing. The turbulent up-canyon salt flux is also small on an annual basis, but can on occasion approach the offshore fluxes associated with brine drainage. For example, using the 1985 estimate by Aagaard *et al.* of brine discharge through Barrow Canyon during the winter of 1982, and referencing it to the annual mean salinity observed at the BC1 instruments, shows that a salt excess of about 3.8×10^{8} gm s^{-1} was discharged down the canyon during the last week of February 1982. This can be compared with the 2.5×10^{8} gm s^{-1} flux during the upwelling calculated above, less than one-half of which appeared to be removed on the ensuing outflow, suggesting a net onshore flux of, perhaps, 1.4×10^{8} gm s^{-1}.

Also shown in Table 12 are the turbulent fluxes calculated for 1986–87 and 1987–88 at the two moorings MA2 and MB2, located near the shelf break farther east at 153°W and 147°W respectively. The temperature and salinity series were derived from Aanderaa sensors mounted on the current meters. Particularly notable is the absence of indications of net onshore sensible

TABLE 12. Estimates of salt and heat flux. Instruments from Barrow Canyon are referred by depth above the bottom for the current meters and by the SeaCat number using principal axes of 50°T (U) and 140°T (V). The Beaufort Sea current meters are referred to by their depth in meters with 300°T (U) and 30°T (V).

Instrument	Salt Flux (cm psu s^{-1})				Temperature Flux (cm °C s^{-1})			
	U'S'	V'S'	R	Theta	U'T'	V'T'	R	Theta
BC1								
CM9 SC6	–0.22	–1.18	1.20	309	–0.33	–0.05	0.33	239
CM2 SC2	–1.60	–1.08	1.93	264	–1.07	–0.39	1.14	250
BC2								
CM9 SC5	0.14	–1.29	1.30	326	6.21	0.45	6.23	054
CM2 SC7	–0.73	–1.63	1.79	296	4.53	0.01	4.53	050
MA2								
CM 60	–1.06	0.11	1.07	114	4.83	–0.39	4.85	295
CM 93	–0.41	0.03	0.41	116	0.85	0.01	0.85	301
CM 143	1.89	0.36	1.92	311	1.09	0.34	1.14	317
MA2B								
CM 79	1.59	0.13	1.60	305	–7.84	0.47	7.85	116
CM 162*	2.85	–0.46	2.89	291	2.56	0.19	2.57	304
MB2								
CM 62	–0.28	0.06	0.29	108	–1.63	0.56	1.72	101
CM 95	–0.05	–0.18	0.19	195	–0.78	0.72	1.06	077
CM 145	1.17	–0.43	1.25	280	0.33	–0.10	0.34	283
MB2B								
CM 72	–0.42	0.02	0.42	117	–0.06	0.42	0.42	038
CM 105	0.11	–0.26	0.28	232	0.07	0.25	0.26	014
CM 155	1.50	–0.43	1.56	284	0.73	–0.10	0.74	292

* MA2B at 162m was computed from two segments: 18 Apr 87–3 Oct 87 and 25 Oct 87–15 Apr 88.

heat and salt fluxes associated with the frequent upwelling which has been observed along this shelf. The potential for at least locally significant fluxes of heat and salt onto the shelf through upwelling therefore appears to be restricted to major topographic breaks in the shelf, such as Barrow Canyon.

Our original interest in making these measurements was directed toward the outflow of cold brines from the shelf, such as we had found earlier both in Barrow Canyon (Aagaard *et al.*, 1985) and farther south in the Chukchi Sea (Aagaard *et al.*, 1981). The year 1986–87, however, proved to be one which either had insufficient brine production to give measurable signals in the canyon or the brine produced was not exported through the canyon. We do not know the reason for this failure to observe brines, for while the autumn of 1986 was abnormally warm, with an unusually large number of lows propagating northward along the Chukchi coast, the ensuing winter was markedly abnormal in neither air temperature nor wind regime. Furthermore, inspection of the AVHRR imagery for January and February shows the frequent and prolonged occurrence of open water or thin ice along the coast, as much as in any other year. Nevertheless, it is clear that whatever the long-term contribution to the Arctic Ocean of saline outflows from the Chukchi Sea proves to be, there are years in which at least the outflow through Barrow Canyon makes no contribution whatsoever to the shelf-derived brine flux which on longer time scales appears so important to the structure of the Arctic Ocean.

C. Beaufort Sea

1. Beaufort Sea Hydrography

The hydrography of the Beaufort Sea is discussed and portrayed in detail in Appendix A. Note that the hydrographic data of Appendix B also includes profiles of light attenuation during the October 1986 cruise. These profiles were measured to complement the listed discrete measurements of suspended particulate matter (SPM). Figure 15 shows the light attenuation in Section C, near 144°W; it can be considered characteristic of the fall sections. Section C contains an attenuation maximum over the inner shelf and extending seaward over the middle shelf in the lower half of the water column. The maximum measured attenuation exceeded 3 m^{-1}. There is a strong optical front at the surface seaward of the 25 m isobath. Farther offshore, attenuation was quite low, generally less than 0.8 m^{-1}, even over the shelf break. Within the region of maximum attenuation, SPM values exceeded 6 mg l^{-1}. Comparison with Figs. 43–51 in Appendix A shows no coincidence of attenuation with other properties, other than some correlation with the density structure over the shallower portions of the shelf. The implication of these various observations is that the increased water turbidity over the shallower portions of the shelf is primarily due to resuspension of fine sediment. It therefore depends both on water velocity and on the sedimentary nature of the bottom. We note that in general there is little, if any, connection between light attenuation and the principal water masses.

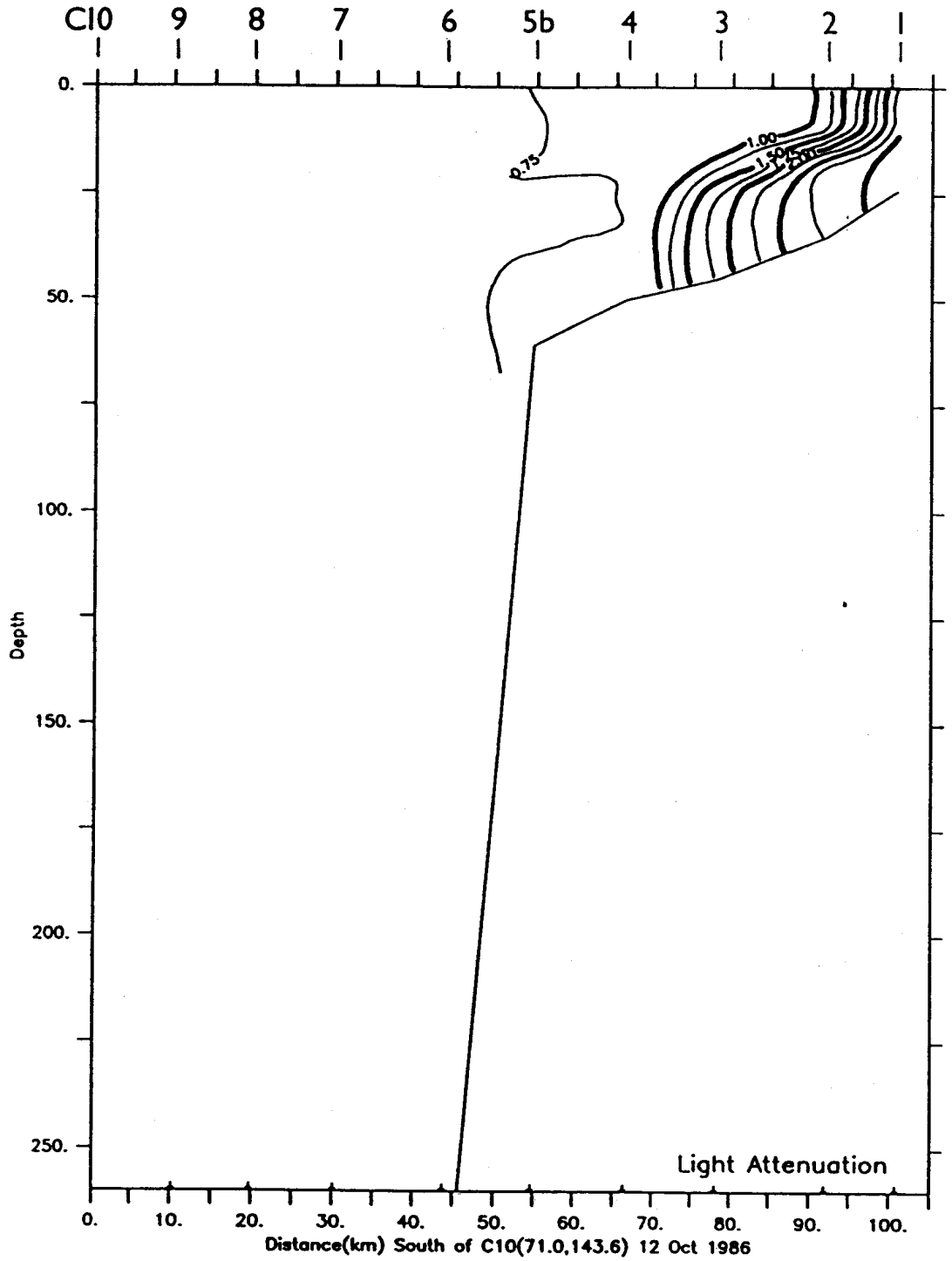

Figure 15. Profile of light attenuation at Section C near 114°W.

Appendices B and C also show that discrete sampling was done for several transient tracers, including tritium, carbon-14, freons, and radioactive isotopes of cesium, radium, and strontium. These were all add-on measurements, with analysis being done by other investigators and laboratories. The analytical procedures and schedules are such that to date, only the tritium and carbon-14 analyses have been completed. These have been released by Prof. Ostlund of the University of Miami as Tritium Laboratory Data Release #88–01. They demonstrate that all the water above 1600 m shows some degree of ventilation within the past 30 years, with values above 1 tritium unit (normalized to 1981).

2. *Beaufort Sea Flow Characteristics*

Table 13 shows the record-length current statistics for the various instruments at the six moorings deployed during 1987–88. Maximum low-pass filtered speeds in the upper 200 m generally ranged from 30–100 cm s^{-1}, with the most rapid flow occurring in the upper part of the water column near the shelf break and over the slope. The mean velocity was also greater in this outer region than over the middle shelf. In contrast to the high-speed flow events, however, the mean motion registered by the uppermost instruments was generally less than at intermediate depths, although the variance was sufficiently large that the error bars at the various levels overlap. At two locations (MA2B, 79 m; and MA4B, 45 m) the mean flow was statistically indistinguishable from zero. Note that the former instrument recorded the fastest short-duration flow of any during the year. Except for the very deep instrument at MB1B (994 m), all statistically significant mean flow was nominally towards the east, manifesting the Beaufort Undercurrent, which sets eastward following the outer shelf and slope over the entire Alaskan and Canadian Beaufort Sea (Aagaard, 1984).

There was considerable low-frequency variation in this flow, but this variability was largely restricted to the mean flow axis, and comparison with local isobath trends suggests strong topographic steering of the flow (compare Aagaard, 1984). Table 13 shows the principal axis (the axis of greatest variance) for each current record, as well as the fraction of the total variance occurring along that axis, and it is clear that at least below the upper 40–50 m the flow is highly two-dimensional, with the principal axis nearly coincident with the mean flow and containing the vast majority of the variance. Interestingly, it is over the continental slope, where the bottom slope is the largest and one might expect the strongest topographic steering, that the variance along the principal axis is the least, indicating the greater relative importance of cross-isobath flow there (although the principal-axis variance is still 86% or more of the total).

Figures 16 and 17 show the 35-hr low-passed velocity vectors recorded at the 15 current meters. Each record has been resampled at 12 hr intervals, and the vertical direction in each display represents the principal axis for that record (see Table 13). Note the differences in the speed scales on the vertical axes. The prevailing downward orientation of the vectors represents

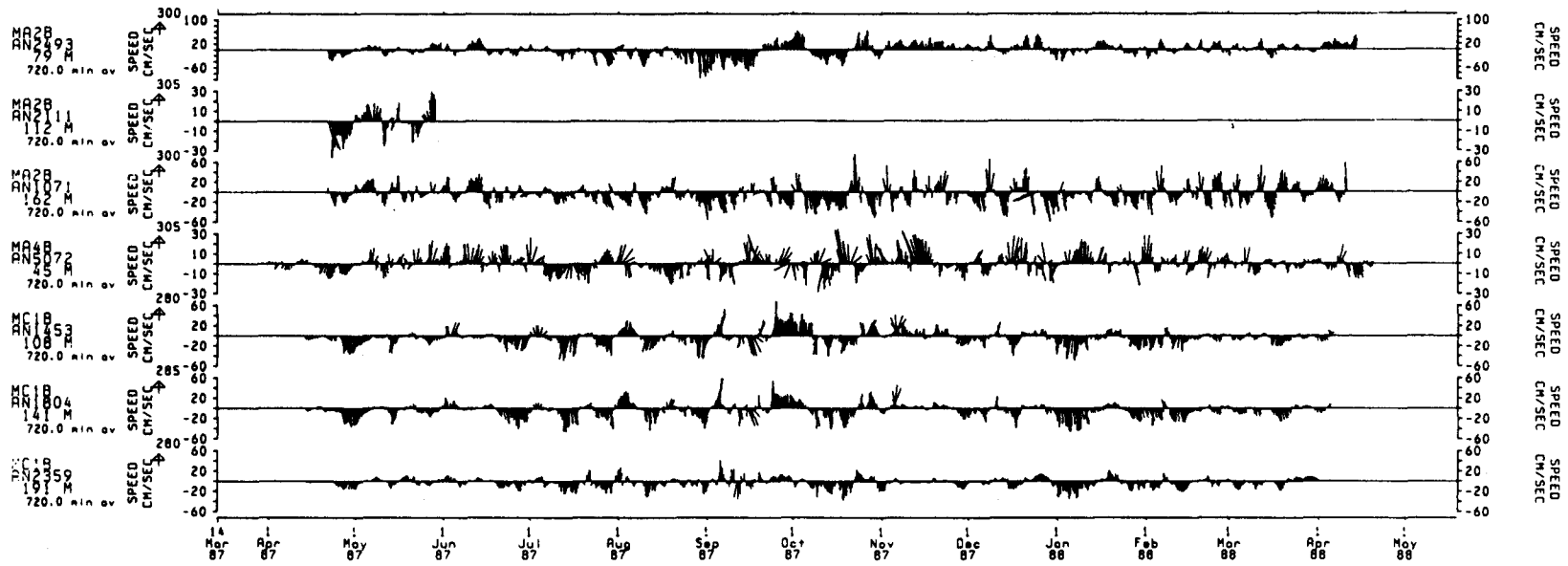

Figure 16. Low-passed velocity records at MA2B, MA4B, and MC1B. The vertical axis is parallel with the principal axis for each record; up is nominally westward.

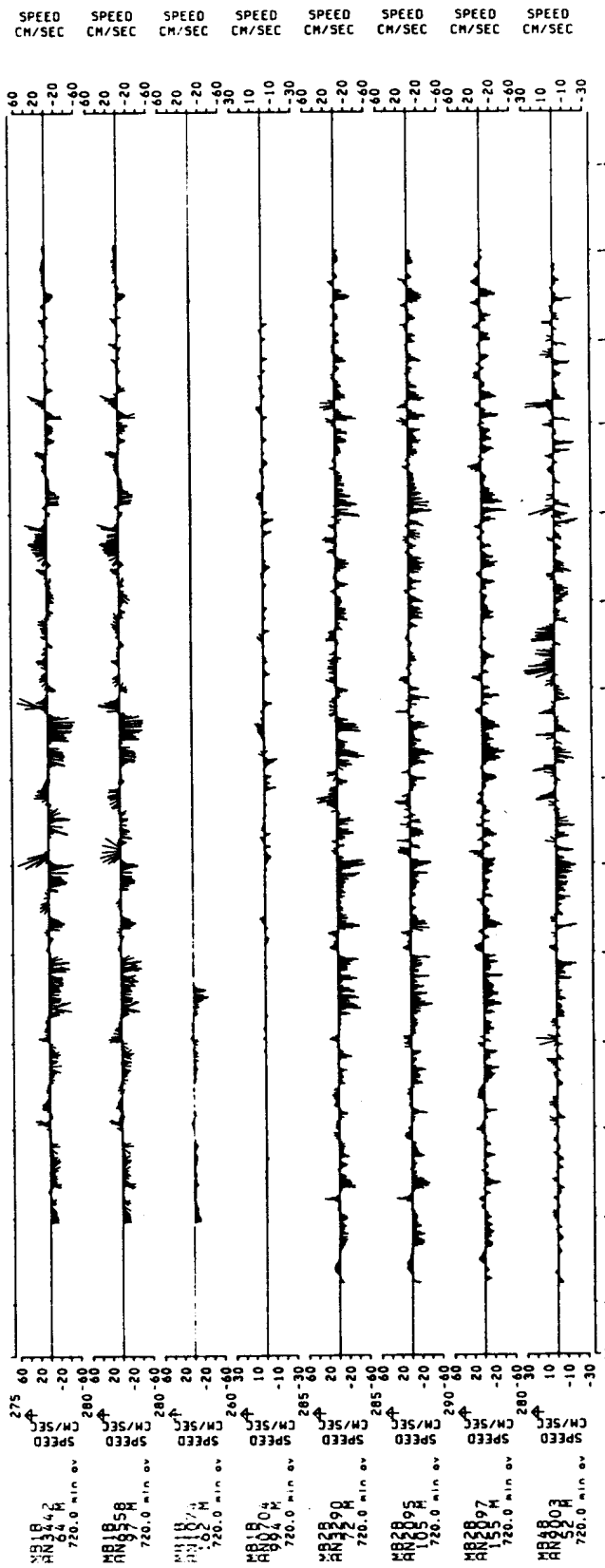

Figure 17. As in Figure 16 for low-passed currents from MB1B, MB2B, and MB4B.

TABLE 13. Beaufort Sea Record-Length Current Statistics, 1987-88. Maximum speed calculated from 35-hour low-passed velocity. The rms error along the principal axis is given in parentheses. Record MA2B, 112 m, lasted only 39 days.

Mooring	Depth m	Maximum speed cm s^{-1}	Mean velocity cm s^{-1}	°T	Principal axis °T	%Variance
MA2B	79	99.4	1.6 (3.8)	102	120	96
	112	38.8	3.3 (5.0)	130	124	97
	162	78.0	5.6 (2.0)	113	117	96
MA4B	45	39.2	1.1 (1.1)	321	125	91
MB1B	64	67.2	3.8 (2.3)	107	095	87
	97	47.7	3.7 (2.2)	106	100	86
	162	31.2	1.1 (0.5)	097	098	92
	994	13.6	0.8 (0.2)	023	082	86
MB2B	72	57.1	5.9 (1.7)	113	106	95
	105	48.5	7.6 (1.2)	110	105	96
	155	51.1	6.6 (1.1)	109	108	99
MB4B	52	30.9	1.4 (0.8)	118	100	94
MC1B	108	72.7	5.1 (2.5)	111	105	93
	141	63.6	5.7 (2.2)	105	103	96
	191	45.0	3.6 (1.1)	103	099	97

the nominally eastward Beaufort Undercurrent. The considerable coherence between many of the records, both vertically and horizontally, is obvious in the figures; we return to this issue later.

In addition to the largely reciprocating motion, in which the velocity switches along the principal axis, corresponding to a local reversal of the undercurrent, there are instances in which the current vector appears to rotate, yielding either an open or a closed pattern. For example, at the two upper current meters at MC1B (Fig. 16), early July shows an open vector pattern, and early November a closed one. Comparison with Fig. 6 in Foldvik *et al.* (1988), suggests that these represent the passage of clockwise (anticyclonic) and counterclockwise (cyclonic) eddies, respectively. Figures 16 and 17 suggest the clockwise eddies to be the more common. We note that the predominance of clockwise eddies is also a feature of the deep Canadian Basin, where baroclinic eddies embedded in the pycnocline are an extremely important feature of the circulation (Manley and Hunkins, 1985). For a typical rotation time scale of 3 days and an advection

velocity of the eddies past the current meter of 10–20 cm s^{-1}, the eddy diameter would be in the range 25–50 km. Such a reconstruction corresponds rather well with the warm eddies suggested in Fig. 2 of Aagaard (1984).

Figures 18–22 show the energy-preserving rotary coherence spectra for the various Beaufort Sea current meter records. Note that the spectral shapes and amplitudes vary considerably. The lack of a low-frequency roll-off at the uppermost instrument on MA2B is particularly noticeable. This is probably due to the relatively brief period of high speeds (particularly toward the west) during late summer and early fall of 1987 (Fig. 16), which contrasts with the more uniform distribution of current speeds recorded by the other instruments. Such non-steady statistics alias the spectral estimates, folding the energy into lower frequencies. Among the other spectral peaks in Figs. 18–22, a consistent peak corresponding to about a 4.5-day period is found at the shelf break moorings, i.e., at MA2B, MB2B, and MC1B, particularly at the deepest meters. This may represent the frequent eastward propagation of a shelf wave, as also suggested by the coherent phased upwelling events extending along the entire Alaskan Beaufort Sea shelf (see Section III.C4). In the suggested eddy frequency band, the spectra generally show more energy in the clockwise mode (e.g., Fig. 18, record MA4B), in agreement with the visual impression from Figs. 16 and 17.

3. *Beaufort Sea Variability at Very Low Frequencies*

At mooring sites MA2, MB1, and MB2 the current meter records were essentially continuous for 18 months and thereby provide evidence of variability on at least seasonal time scales. Table 14 shows the record-length mean currents at comparable locations for nominally the first six and the last twelve months of the joint records. Perhaps the most striking difference between the record segments is in the upper ocean, where during the first period the uppermost current meters recorded either westerly flow (albeit with large rms error estimates) or very weak flow. During the final period the motion was easterly and slower at the two shelf-edge moorings than deeper in the water column. The suggestion is that during the first period the Beaufort Undercurrent did not extend as close to the surface, in the mean, as it did during the second period. This is in agreement with our conclusion in Appendix A, pp. 3–4 that compared to earlier measurements, the undercurrent was anomalously deep during the October 1986-March 1987 period.

Figure 23 shows the monthly mean velocity recorded at the upper- and lowermost current meters at the outer shelf moorings (MA2 and MB2), together with the corresponding estimated wind vector at Barrow. The seasonal cycle in the wind, with maxima in the fall and spring has no obvious reflection in the current records. (On the other hand, the difference in the mean depth of the undercurrent between the first 6 months and the last 12 is clear in the figure.)

Figure 24 shows the mean monthly variance in the current at the same sites as in Fig. 23. The anomalously large variance in the MA2, 150 m record during December 1986 is due to the

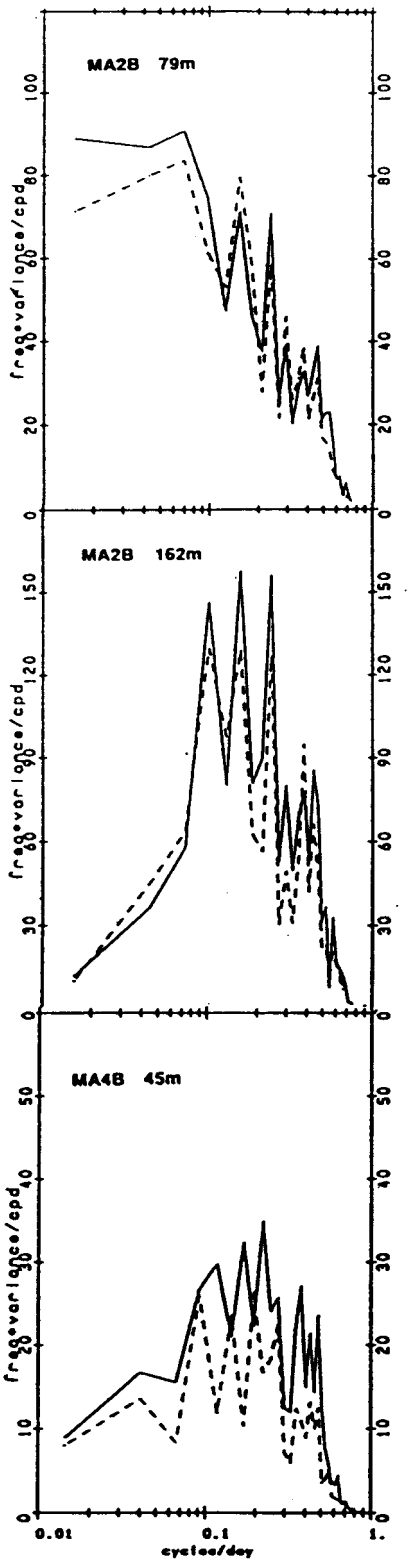

Figure 18. Energy-preserving rotary spectra for moorings MA2B and MA4B. The solid lines represent clockwise rotation and the dashed lines counterclockwise.

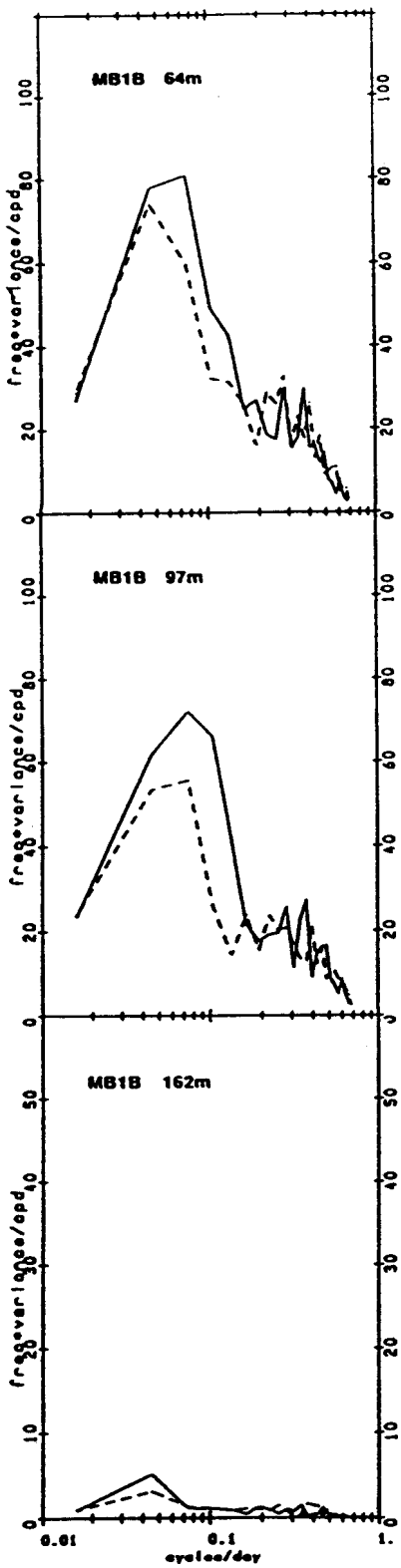

Figure 19. As in Figure 18, for mooring MB1B.

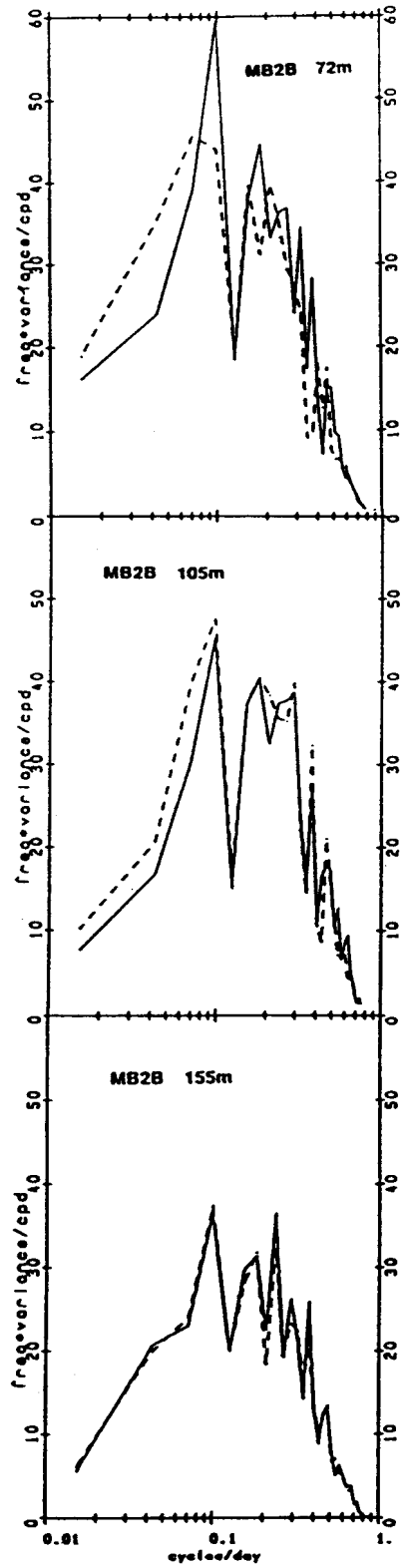

Figure 20. As in Figure 18, for mooring MB2B.

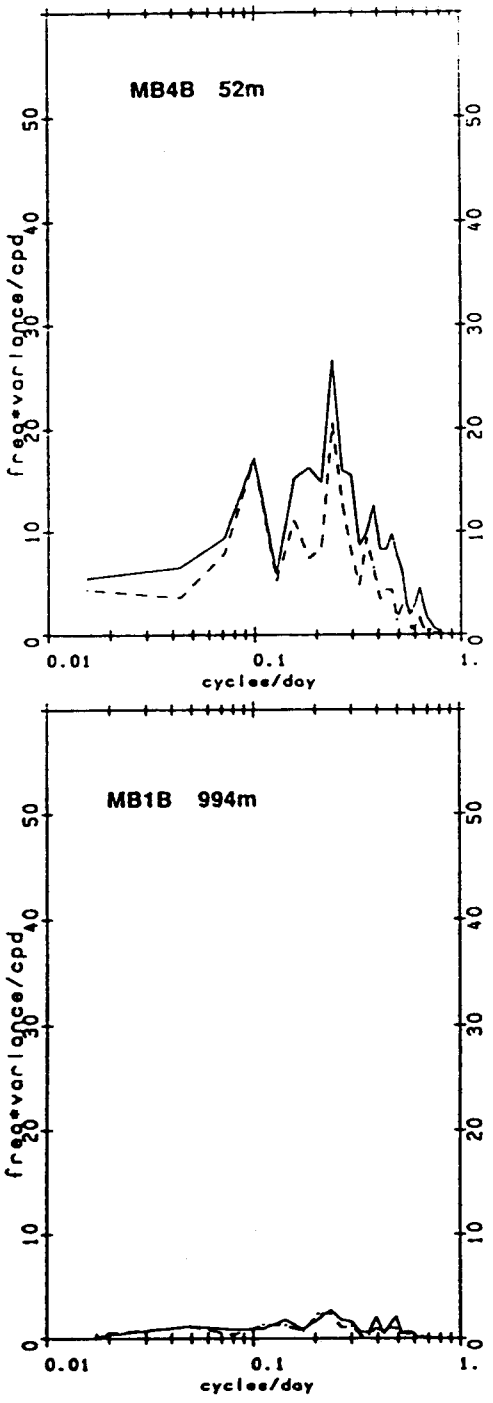

Figure 21. As in Figure 18, for moorings MB4B and MB1B (994 m).

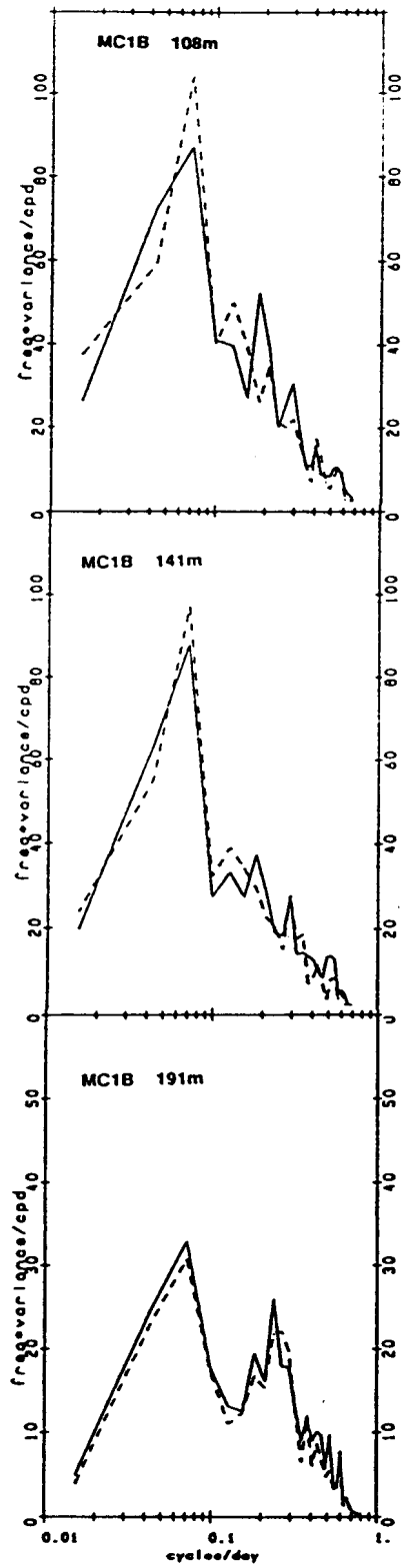

Figure 22. As in Figure 18, for moorings MC1B.

TABLE 14. Beaufort Sea Mean Velocity Comparison: October 1986-March 1987 and April 1987-April 1988.

Mooring site	Approximate depth m	Mean velocity 1986–87 cm s^{-1} (RMS)	°T	1987–88 cm s^{-1} (RMS)	°T
MA2	70	3.5 (4.1)	291	1.6 (3.8)	102
	100	0.1 (0.5)	219	3.3*(5.0)	130
	150	7.8 (4.7)	119	5.6 (2.0)	113
MB1	80	1.5 (1.4)	168	3.8 (2.0)	106
	155	6.9 (3.0)	097	1.1 (0.5)	097
	985	0.0 (0.0)		0.8 (0.2)	023
MB2	65	0.3 (0.5)	181	5.9 (1.6)	113
	100	5.0 (2.0)	112	7.6 (1.2)	110
	150	8.0 (1.8)	103	6.6 (1.1)	109

* Record MA2B at 112 m lasted only 39 days.

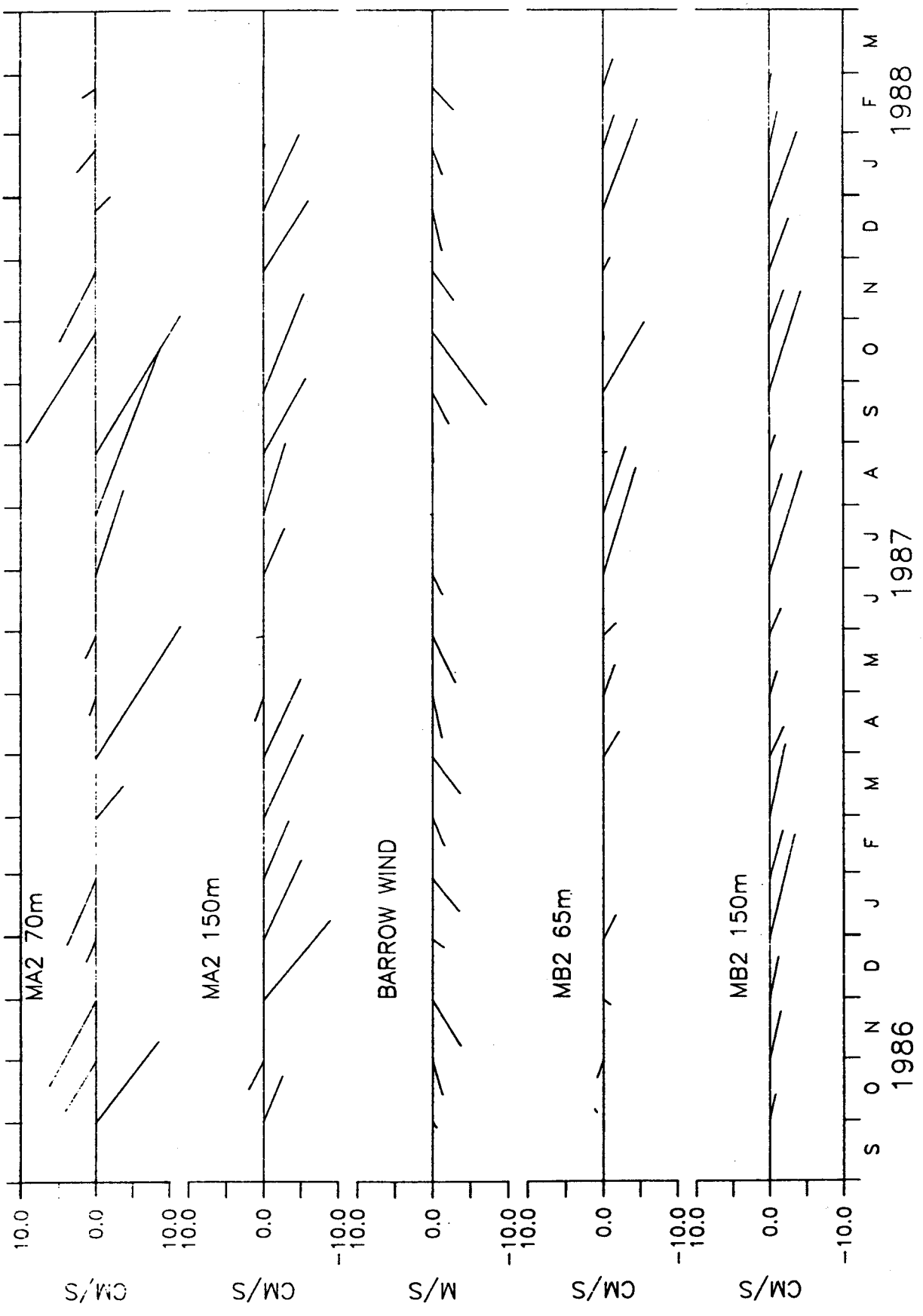

Figure 23. Monthly mean currents at sites MA2 and MB2 during 1986–88, together with the monthly mean wind at Barrow. Up is north.

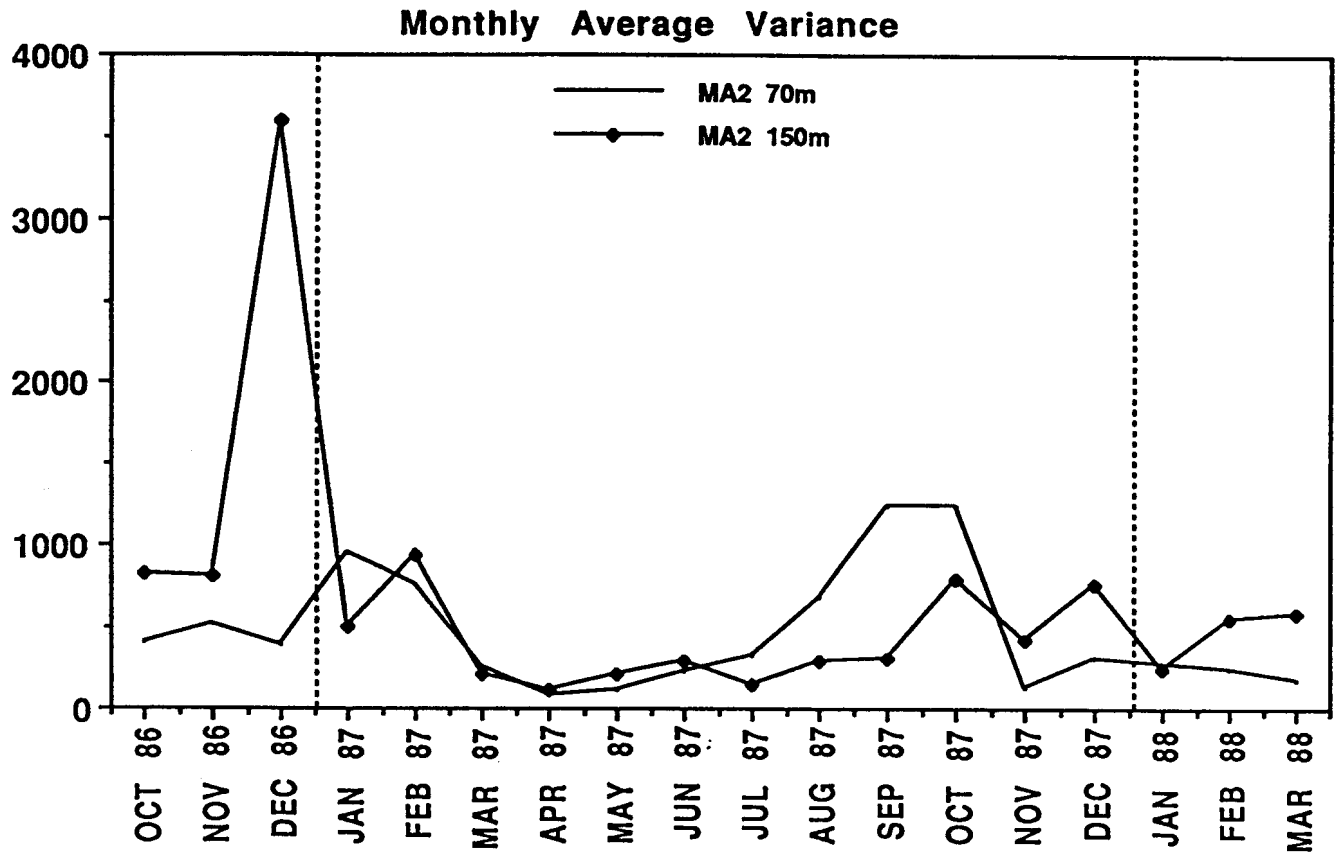

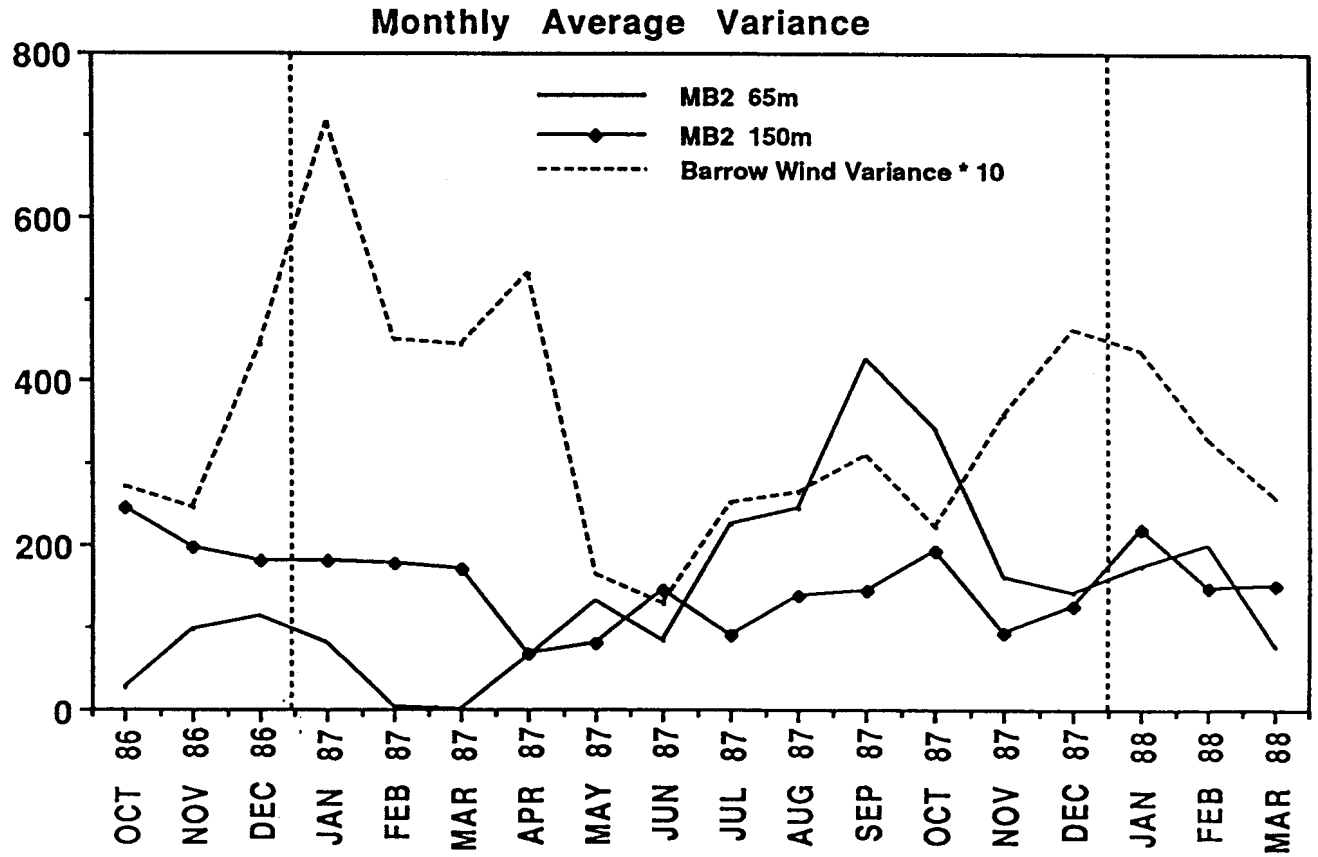

Figure 24. Monthly mean variance in the current at sites MA2 and MB2 during 1986–88. Note the difference in scale (vertical axis) between the two sites.

extremely rapid flow recorded during that period (see Appendix A, p. 3): up to 166 cm s^{-1} in the 35-hour low-passed series, which is well over twice that previously recorded for the Beaufort Undercurrent. Inspection of the filtered time series (Appendix A, Fig. 4) suggests that the event may represent passage of two intense counterrotating baroclinic eddies, the first one counterclockwise and the second clockwise (compare Fig. 6 in Foldvik *et al.*, 1988). While the variance in the wind portrayed in Fig. 24 has a clear seasonal cycle, with a maximum in mid-winter and a minimum in mid-summer, the current variance shows neither a seasonal cycle, nor is the month-to-month variability in the individual records similar. The lack of a seasonal signal in the flow was pointed out earlier by Aagaard (1984), as were the significant differences in the flow to be expected from year to year.

4. Beaufort Sea Correlation Analysis

Table 15 shows the correlation matrix for the 1987-88 current records. The lag in hours for maximum correlation is in parentheses; where no lag is shown, it is zero. A positive lag represents the record listed at the beginning of each row leading the record listed in the corresponding column. All listed correlations are significant at the 95% confidence level.

Vertically the currents were in phase, but the correlation degrades with depth, going from characteristic values near $r = 0.9$ over the upper instrument separations of 33 m to as low as $r = 0.26$ for the 78 m separation between the top and intermediate instruments over the slope at MB1B. For the three moorings over the outer shelf, the degradation of the correlation at intermediate depths was less, ranging from $r = 0.53$–0.72 over 83 m.

Table 15 suggests that the cross-shelf correlation decreases considerably over fairly short distances. At MA2B and MA4B, separated by about 45 km, less than 10% of the variance was linearly related. However, between instrument pairs separated by about 10 km, such as MB1B and MB2B, the related portion was as much as 44% and as much as 34% between MB2B and MB4B.

Along the shelf, a significant fraction of the low-frequency current variance was linearly related over the entire length of the shelf, as much as 28% between MA2B and MC1B. The phase relations were such that the western records consistently led the eastern ones, corresponding to eastward-propagating disturbances, probably shelf waves. From the typical lags of 30 hr between MA2B and MB2B, and 18 hr between MB2B and MC1B, respectively separated by about 250 km and 100 km, the characteristic phase velocity was about 2 m s^{-1}. This is only slightly slower than suggested by Aagaard (1984), and it is close to the 1.1–1.6 m s^{-1} eastward phase velocity suggested by the 1986–87 upwelling events in Barrow Canyon and at the Beaufort Sea SeaCat sites.

We have also correlated the current records with the wind at three locations: Barter Island, Barrow, and Resolution Island. The results are summarized in Table 16. In general, the Barrow

TABLE 15. Linear Correlations of Beaufort Sea Current Meters. For 87119 to 88072, 1274 points, 6 hourly records(lag in hours), positive lag means column lags row.

	MA2B 79 m	MA2B 162 m	MB1B 64 m	MB2B 72 m	MC1B 108 m
MA2B 162 m	0.53 (6)	1.0	0.34 (42)	0.47 (30)	0.26 (60)
MA4B 45 m	0.31 (96)	0.18 (96)	0.22 (96)	0.22 (96)	0.14*(96)
MB1B 97 m	0.58 (–48)	0.36 (–48)	0.94	0.66 (–12)	0.62 (6)
MB1B 162 m	0.10*	–0.13* (42)	0.26	0.23	0.27
MB1B 994 m	–0.37 (–72)	0.31 (–78)	–0.35 (–36)	–0.31 (–54)	–0.37 (–36)
MB2B 105 m	0.43 (–24)	0.51 (–30)	0.47 (24)	0.85	0.48 (30)
MB2B 155 m	0.43 (–24)	0.58 (–36)	0.46 (12)	0.72 (–6)	0.48 (30)
MB4B 52 m	0.56	0.50 (–6)	0.43 (30)	0.58 (18)	0.39 (42)
MC1B 141 m	0.47 (–42)	0.29 (–60)	0.61	0.59 (–12)	0.95
MC1B 191 m	0.45 (–30)	0.42 (–60)	0.54 (–6)	0.59 (–12)	0.69
MA2B 79 m	1.0	0.53 (6)	0.64 (30)	0.63 (18)	0.53 (42)
MB1B 64 m	0.64 (–30)	0.34 (42)	1.0	0.64 (18)	0.63 (6)
MB2B 72 m	0.63 (–18)	0.47 (–30)	0.64 (–18)	1.0	0.61 (18)

* Not significant at the 95% level.

TABLE 16. Linear Correlations: Regional Winds vs. Beaufort Sea Current. For April 29, 1987 to March 13, 1988, 1274 pts, 6 hourly records (lag in hours), positive lag means current lags wind.

	Barrow (250T) $m\ s^{-1}$	Resolution Island (280T) $m\ s^{-1}$	Barter Island (280T) $m\ s^{-1}$
MA2B 79 m	0.52 (24)	0.35 (42)	0.29 (30)
MA2B 162 m	0.39 (24)	0.30 (30)	0.28 (24)
MA4B 45 m	0.14*	0.15*(18)	0.13*(12)
MB1B 64 m	0.40 (54)	0.32 (48)	0.24 (42)
MB1B 97 m	0.35 (54)	0.26 (54)	0.20 (54)
MB1B 162 m	–0.10*	–0.09*	–0.11*
MB1B 994 m	–0.17 (90)	–0.16 (96)	–0.11*
MB2B 72 m	0.48 (42)	0.38 (42)	0.32 (36)
MB2B 105 m	0.38 (42)	0.29 (54)	0.27 (42)
MB2B 155 m	0.35 (48)	0.25 (54)	0.23 (42)
MB4B 52 m	0.73 (24)	0.63 (30)	0.61 (24)
MC1B 108 m	0.37 (60)	0.34 (54)	0.26 (42)
MC1B 141 m	0.28 (66)	0.25 (48)	0.17 (42)
MC1B 191 m	0.26 (78)	0.22 (84)	0.17 (72)

* Not significant at the 95% level.

wind record was best correlated with the current and the Barter Island wind was the least well correlated. The latter is probably explainable by the proximity of the mountains to the coast in the vicinity of Barter Island, giving rise to both cyclostrophic and baroclinic effects. On the whole, the wind accounted for a relatively small fraction of the current variance, even at the uppermost current meters, ranging from 2–25% of the total variance (calculated as r^2, which corresponds to correlation coefficients of r = 0.14–0.50). Indeed, at MA4B, the shallow mooring closest to Barrow, the wind and current were effectively uncoupled. Only at MB4B, where the correlation coefficient is r = 0.73, did the wind account for more than half the current variance (r^2 = 53%). The wind generally led the current by 1–2 days, and there was some tendency for the lag to increase with increasing depth.

All our instruments were located below the surface mixed layer, which is typically 30-m thick in winter and much less during summer. Table 16 suggests that only about 15–25% of the fluctuating kinetic energy (which is proportional to their variance) in the currents deeper than 60–80 m was wind-driven. Note that Table 16 shows a further systematic decrease of the wind/current correlation with depth below the top current meter. On the average, this represents a decrease in the correlated variance (which we can interpret as a decrease in the wind-driven kinetic energy in the ocean) of 1.5×10^{-3} m^{-1}. We should therefore expect that an additional 15% of the wind energy is dissipated for every 100-m increase in depth. Effectively, on the open shelf and slope, the circulation below the mixed layer is primarily ocean-driven rather than wind-driven.

5. *Beaufort Sea Tidal Characteristics*

Tidal effects are small in the Beaufort Sea. Characteristic tidal heights are 10 cm or less, and the variance in the tidal bands of the sea surface elevation is typically less than 1% of total variance. Figure 25 shows the tidal elevation characteristics for the five largest constituents at MB2B near the shelf break at 147°W. The estimates are for consecutive 29-day periods. The largest semidiurnal constituent, M2, was close to 8 cm, and the two largest diurnal constituents, O1 and K1, were each about 3 cm. The amplitude estimates vary by as much as 5 cm over the year, and most of the phase estimates also show large variability.

Tidal currents were also small, typically 5 cm s^{-1} or less, and constituted only 1–2% of the total variance in the velocity field. Figure 26 shows the tidal current characteristics for the five largest constituents at 155 m at MB2B. In contrast to the tidal elevation constituents, the largest tidal current constituents were diurnal, and a variance analysis shows that some 80% of the total tidal variance in the current record was in the diurnal band. This was also true at 105 m depth at this mooring, but at the upper instrument at 72 m the variance in the diurnal band was nearly 40% less, suggesting vertical structure in the diurnal current field (but not in the semidiurnal, the

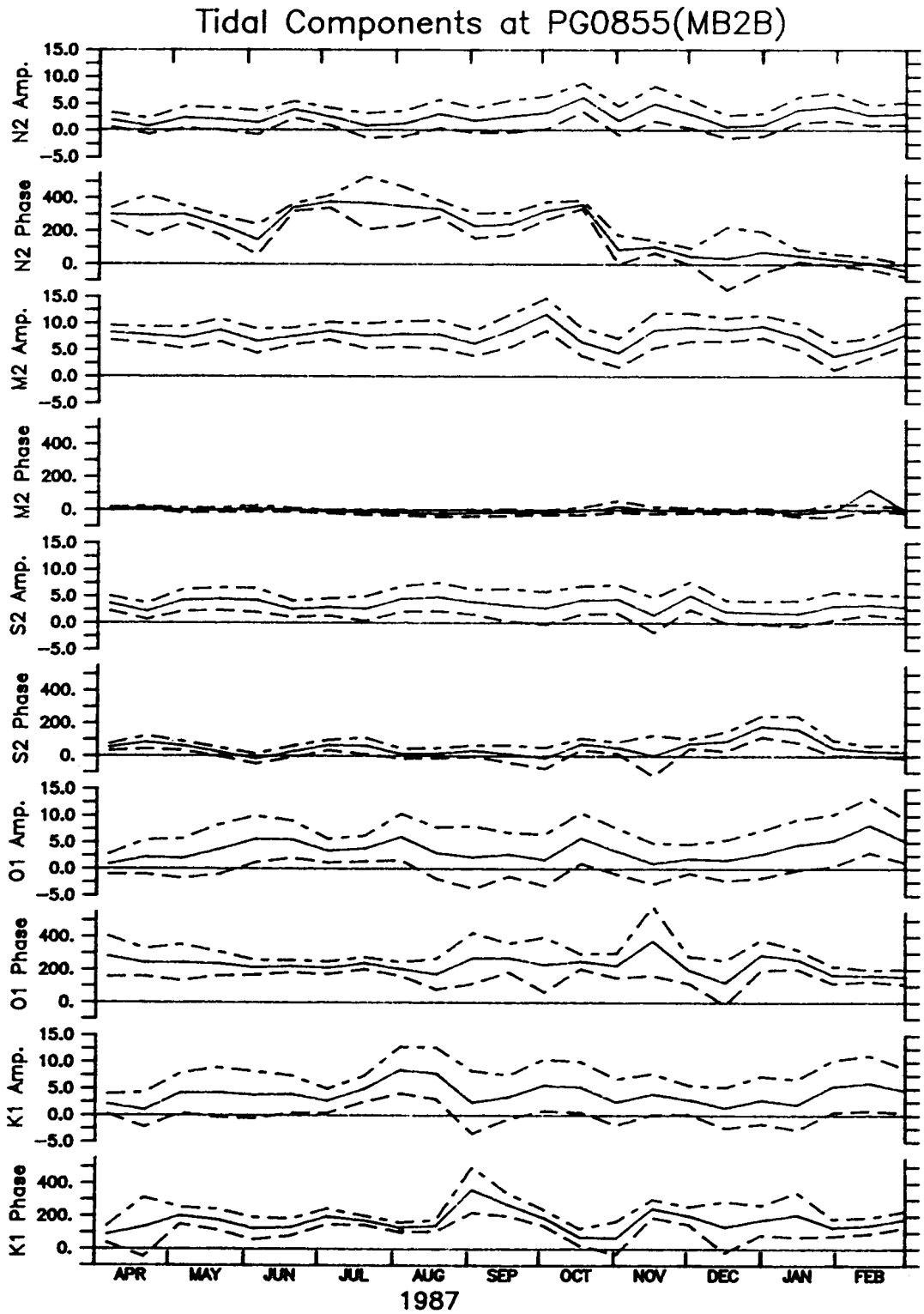

Figure 25. Elevations (cm) and phase (degrees) for the five largest tidal constituents at MB2B. Dashed lines show RMS error. Calculations are for 29-day segments.

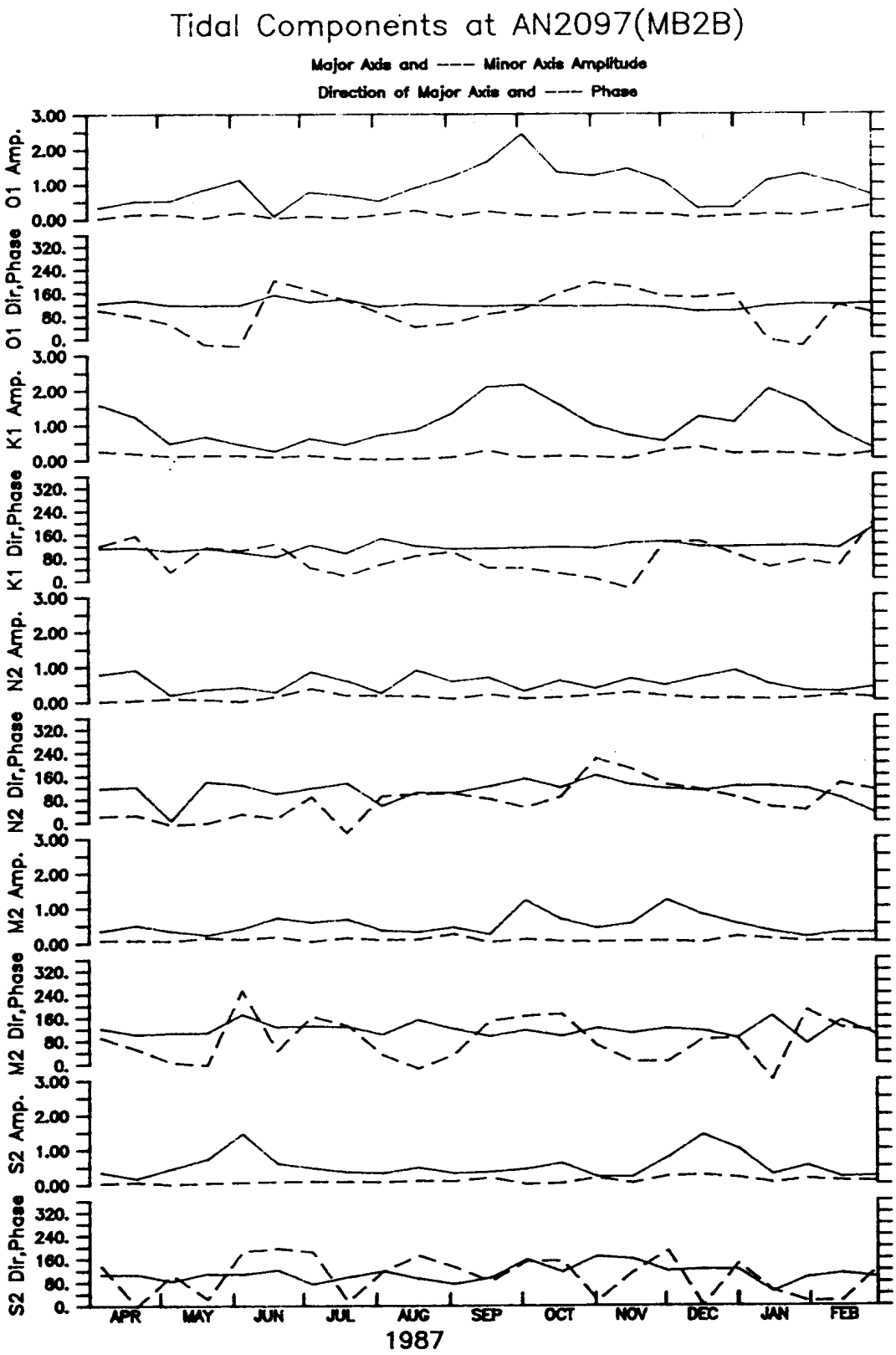

Figure 26. Tidal current characteristics for the five largest constituents at MB2B. Amplitudes are in cm s^{-1} and major axis directions and phases are in degrees. Calculations are for 29-day segments.

variance of which does not decrease at the upper instrument). Note that the estimated characteristics of most of the tidal ellipses vary considerably over the year.

D. Meteorological Results and Correlations

The results from the eight land-based meteorological stations are summarized from southwest to northeast along the coast in Table 17 and Figs. 27 to 34. Note that Cape Prince of Wales and Icy Cape stations had a different time base than the other stations, because the Wales station was setup later for an ONR project. The computer module at Icy Cape failed shortly after deployment and was replaced in March 1987. All the other records begin in September 1986. The most obvious results from visual inspection of the records are 1) that in all cases the pressures derived by METLIB from FNOC fields overlay the station pressures with the caveat that METLIB pressures were shifted some hours later in time; 2) that summer temperatures derived from FNOC fields reasonably match the station data, but throughout the winter, temperatures from FNOC were 10–20°C too warm during two or three week increments for all stations; 3) that autumn 1987 was even warmer than autumn 1986 (Appendix A); and 4) that the winds at a few stations were better modeled than others by the gradient wind generated by METLIB. Nome, Cape Prince of Wales, Icy Cape, and Barrow were fit well, while Kotzebue and Barter Island were not. The winds at Lonely were inaccurate since the anemometer had been nearly covered with snow in the winter of 1986–87 due to snow blower exhaust. Barter Island winds were strongly affected by the presence of the Brooks Range so that mountain barrier effects should be included for the nearshore zone (Kozo, 1980, 1984). The most inaccurate winds were at Kotzebue, but the reason has not been isolated.

The ice drifts for all ARGOS buoys are shown in Figs. 35 and 36. Table 17c gives record length statistics and Figs. 37–44 give time series results for eight of the longer lived ARGOS buoys. The overwhelming impression from the ice drift study is that 1) under most circumstances the Beaufort gyre extended onto the shelf and 2) there was little shear in the ice field outside the 20-m isobath and little coupling with the ocean below 60 m depth. This result is consistent with the relatively narrow fast ice zones along the Beaufort Shelf and with the general drift pattern seen by other investigators (Barry *et al.*, 1979; Campbell *et al.*, 1976; Campbell *et al.*, 1980; Carsey and Holt, 1987; Marko and Thompson, 1975; Pritchard, 1984; Weeks *et al.*, 1977).

For every Alaskan coastal station there is a lag of 6 to 12 hours from the observation time until that data is used by FNOC (or any other center) in the surface analysis (Table 18). These delays are usually caused by the time for the physical transmittal of the station data over the data collection network, the extensive error checking done at the NWS central site, and the artifice that a miss of the analysis cut-off time by a few minutes is effectively a miss of 6 hours. The consistent 12-hour lags for sea-level pressure of the METLIB data relative to the climate station

TABLE 17. Statistics on full-length records with RMS values.

a) Climate and METLIB data (First line climate, second line METLIB).

Barter I	Barrow	Kotzebue	Nome
Pressure			
1015.52 (0.95)	1016.10 (1.02)	1009.86 (0.98)	1007.27 (1.12)
1015.53 (1.00)	1015.82 (1.00)	1010.27 (0.96)	1007.74 (1.11)
Temperature			
–12.62 (6.20)	–13.10 (5.96)	–6.44 (5.45)	–3.57 (4.31)
–6.29 (4.25)	–8.25 (4.40)	–2.32 (4.34)	–0.92 (3.68)
Mean Speed			
5.57 (0.17)	5.39 (0.16)	5.25 (0.20)	4.17 (0.15)
4.52 (0.20)	5.79 (0.33)	6.46 (0.77)	6.73 (0.81)
Net Wind Speed			
1.36 (0.09)	2.70 (0.17)	1.28 (0.15)	1.64 (0.25)
2.65 (0.19)	3.58 (0.43)	3.84 (0.64)	3.78 (0.60)
Net Wind Direction			
276	252	255	230
250	235	222	223
Principal Axis (% Variance along that axis)			
280 (92.9%)	254 (76.0%)	284 (81.0%)	251 (58.8%)
247 (76.8%)	225 (83.7%)	196 (69.6%)	349 (61.0%)

TABLE 17. (continued)

b) GOES and METLIB data (First line GOES, second line METLIB)

Resolution I.	Lonely	Icy Cape	C.P. of Wales
Pressure			
1013.63 (1.15)	1013.48 (1.24)	1012.93 (1.00)	1008.24 (1.14)
1015.16 (1.15)	1015.36 (1.17)	1014.33 (1.01)	1009.27 (1.11)
Temperature			
−22.13 (6.83)	−15.09 (6.09)	−8.63 (5.67)	−0.89 (6.58)
−8.69 (3.95)	−9.79 (4.16)	−3.29 (3.88)	−2.34 (3.66)
Mean Speed			
4.73 (0.22)	2.89 (0.60)	5.50 (0.27)	6.75 (0.29)
4.88 (0.20)	5.67 (0.26)	5.96 (0.32)	7.31 (0.65)
Net Wind Speed			
1.92 (0.43)	1.61 (0.36)	3.28 (0.55)	2.70 (0.62)
2.98 (0.48)	3.48 (0.55)	3.66 (0.53)	4.59 (0.89)
Net Wind Direction			
248	249	262	233
245	240	226	209
Principal Axis			
253 (90.9%)	253 (83.2%)	260 (84.8%)	019 (82.5%)
234 (83.8%)	226 (85.7%)	217 (74.6%)	005 (68.0%)

c) ARGOS and METLIB pressure and temperature

	Pressure		Temperature	
	ARGOS	METLIB	ARGOS	METLIB
7013	1015.93 (1.92)	1016.32 (0.90)	−14.89 (6.73)	−8.75 (4.75)
7014	1014.97 (1.56)	1015.78 (0.54)	−12.55 (6.21)	−8.64 (4.87)
7015	1014.34 (2.67)	1015.77 (0.03)	−15.81 (4.92)	−13.66 (5.27)
7422	1010.69 (1.75)	1009.39 (0.74)	Bad Thermistor	
7426	1018.83 (2.44)	1018.67 (0.43)	−17.13 (4.55)	−6.70 (3.38)
7430	1016.85 (1.87)	1017.58 (0.87)	Bad Thermistor	
7431	1014.29 (1.60)	1014.91 (0.61)	−12.41 (7.14)	−6.14 (4.78)
7432	1017.28 (1.74)	1017.57 (0.73)	−14.21 (6.07)	−8.57 (3.59)

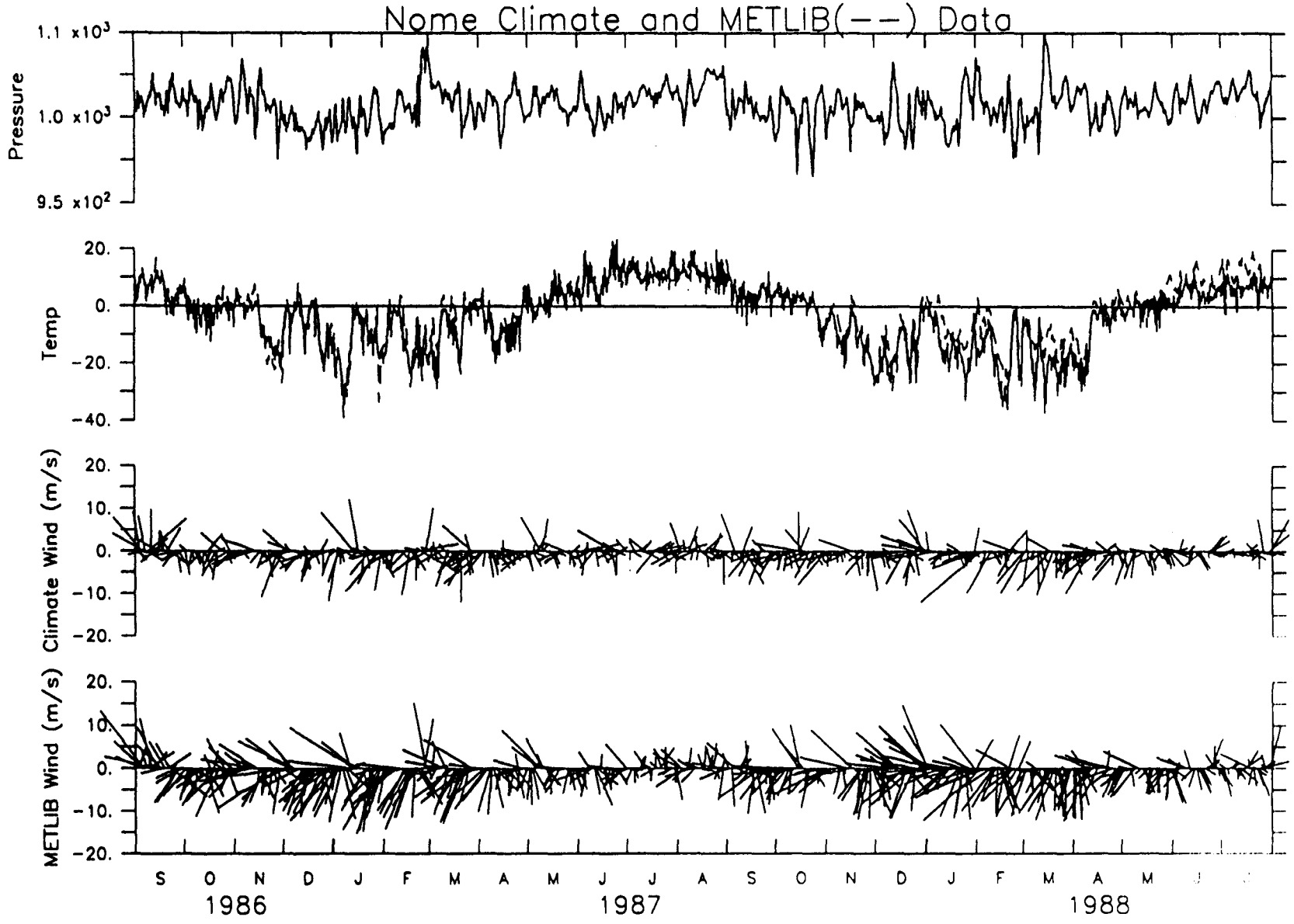

Figure 27. Comparison of National Weather Service and METLIB surface level pressure (mb), temperature (°C), and winds ($m\ s^{-1}$) at Nome. Pressure and temperature data are 6-hourly; one wind vector per day is plotted. In the pressure and temperature plots, METLIB values are plotted with a dashed line. Note that the METLIB pressure is indistinguishable from NWS pressure, and that the high end of the pressure scale (1050 mb) was labeled 1.1×10^3 by the plotting package.

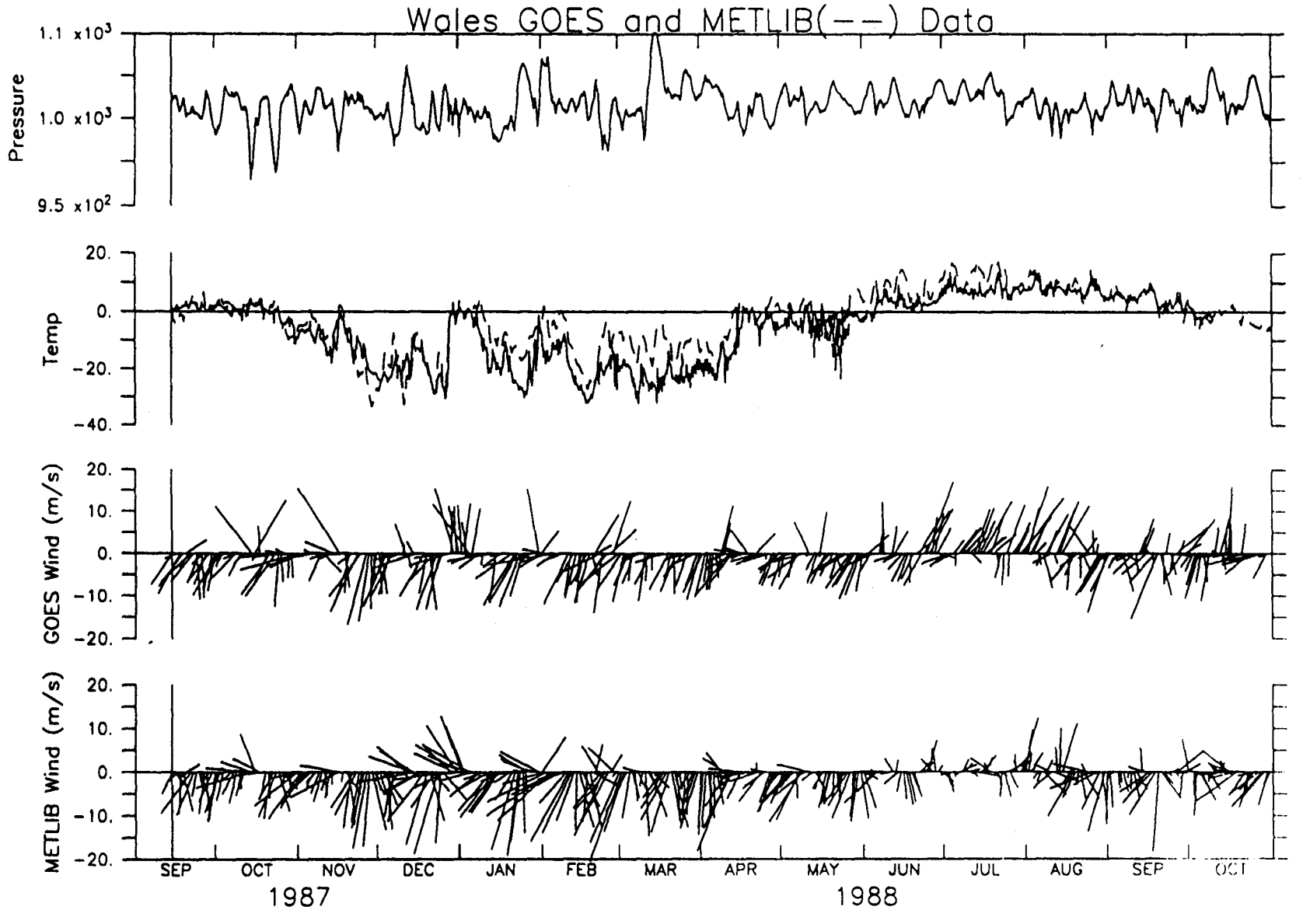

Figure 28. NWS and METLIB pressure, temperature, and winds at Cape Prince of Wales (Bering Strait). See Figure 27.

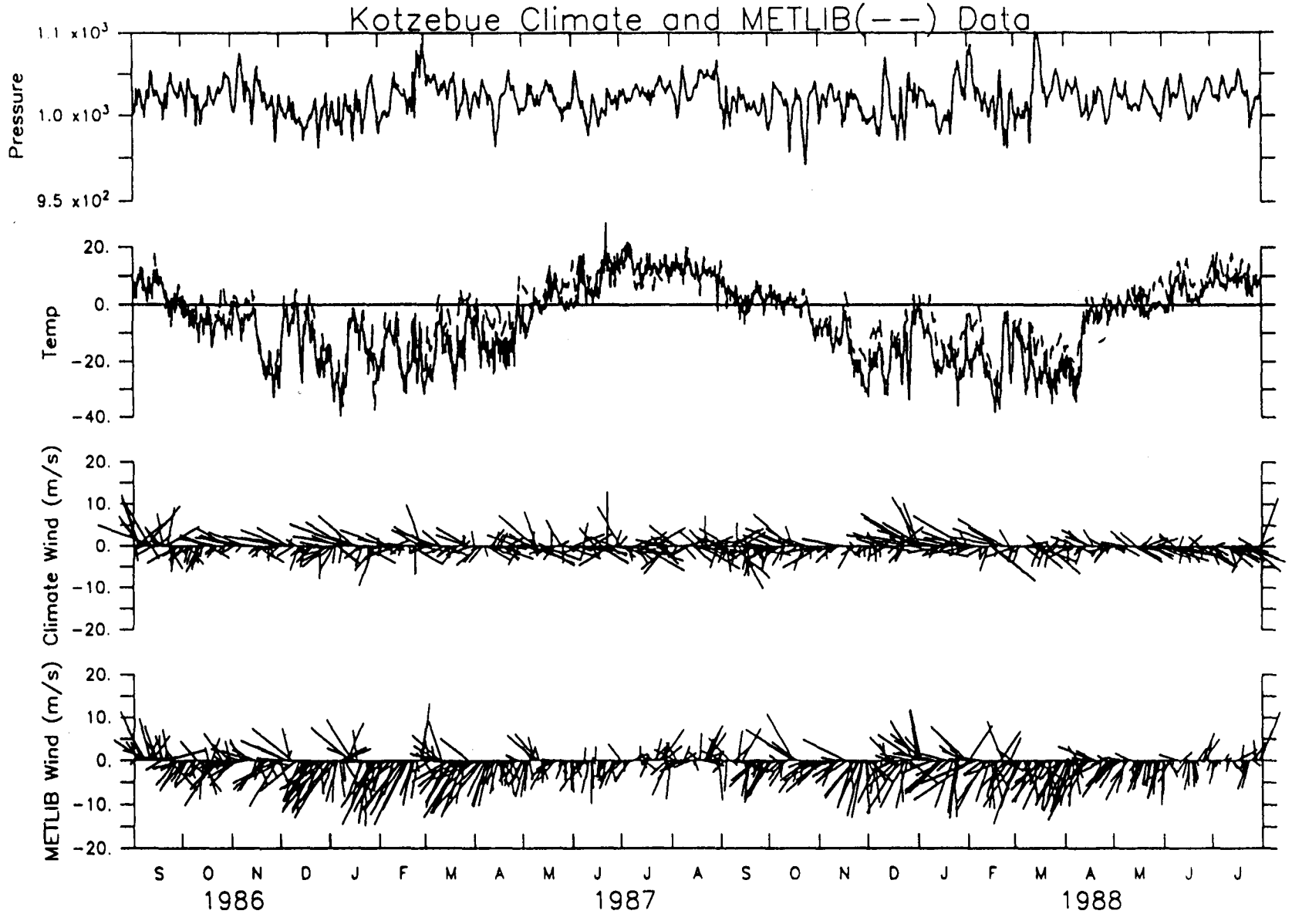

Figure 29. NWS and METLIB pressure, temperature, and winds at Kotzebue. See Figure 27.

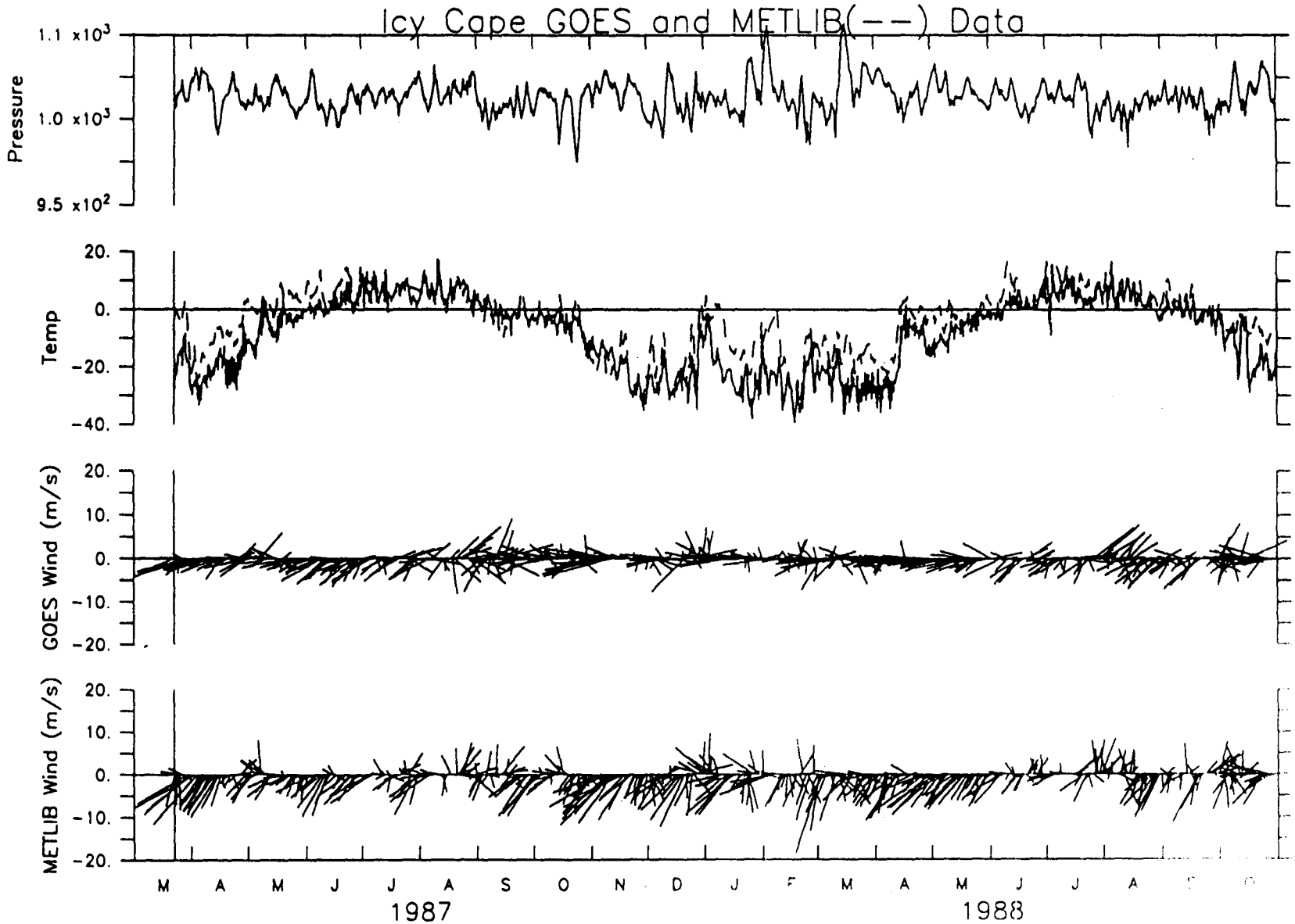

Figure 30. NWS and METLIB pressure, temperature, and winds at Icy Cape. See Figure 27.

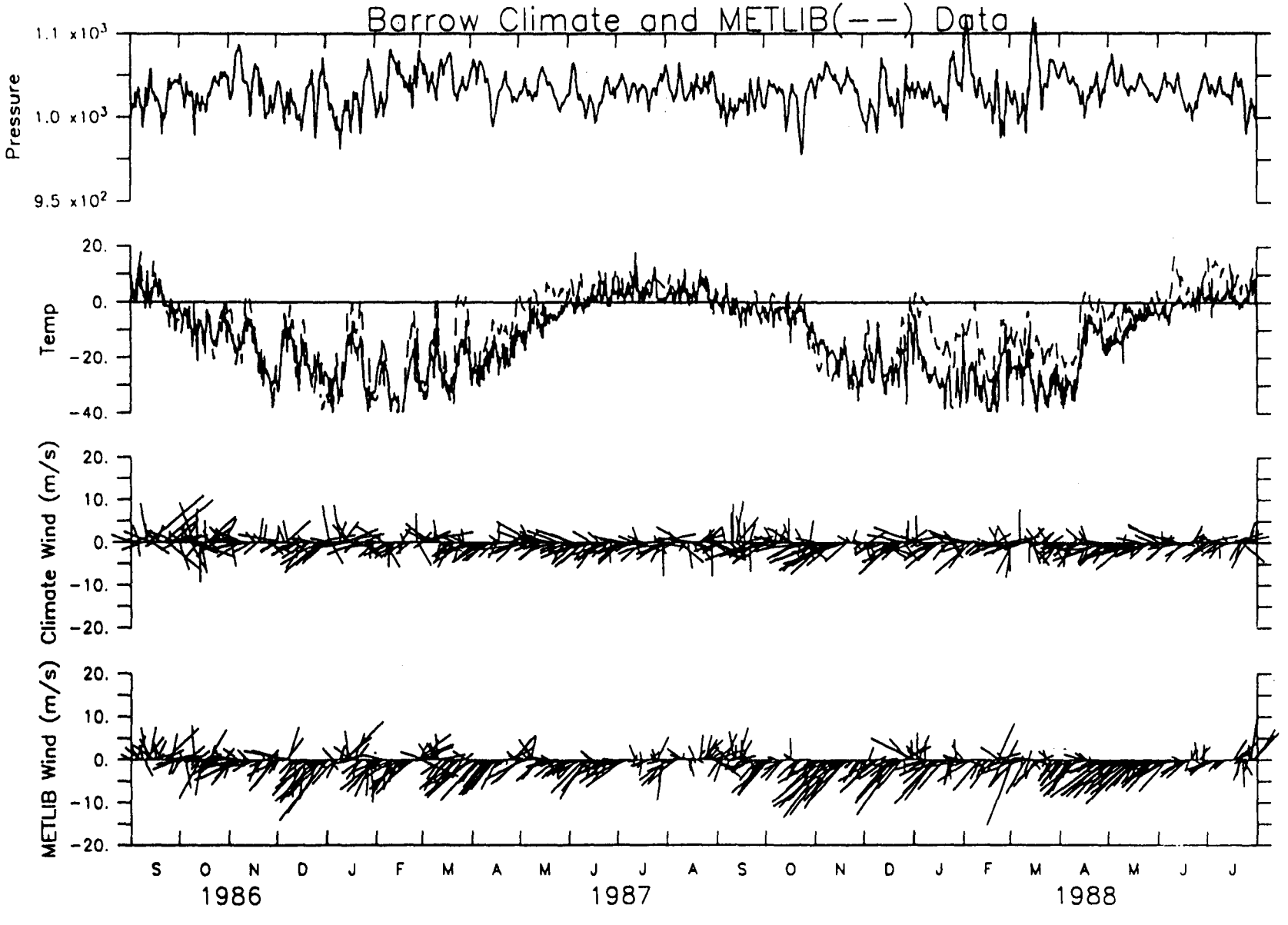

Figure 31. Comparison of surface level pressure (mb), air temperature (°C), and winds (m s^{-1}) measured at the shore station at Barrow with METLIB values. See Figure 27.

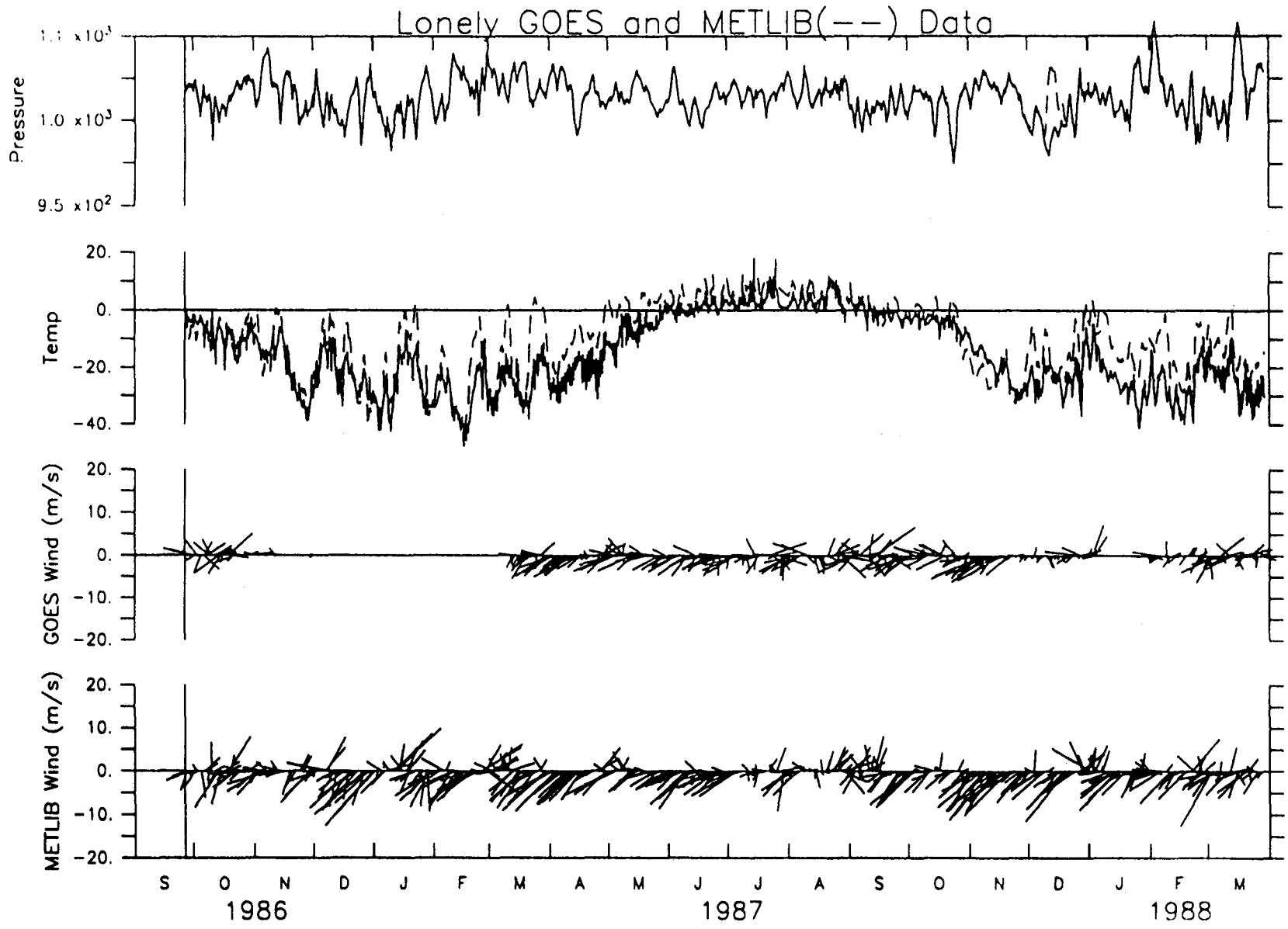

Figure 32. GOES and METLIB pressure, temperature, and winds at Lonely. See Figure 27.

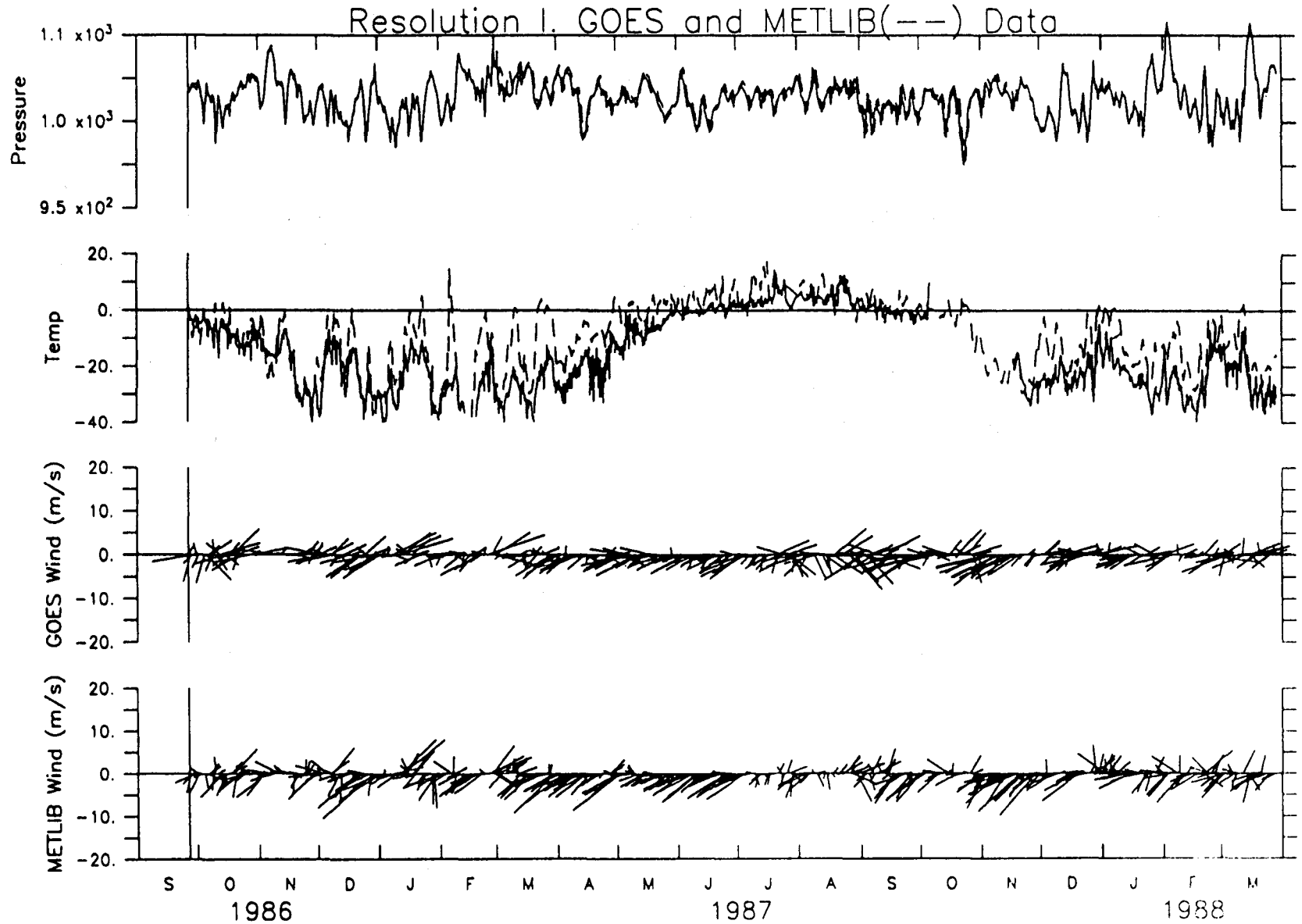

Figure 33. GOES and METLIB pressure, temperature, and winds at Resolution Island (Prudhoe Bay). See Figure 27.

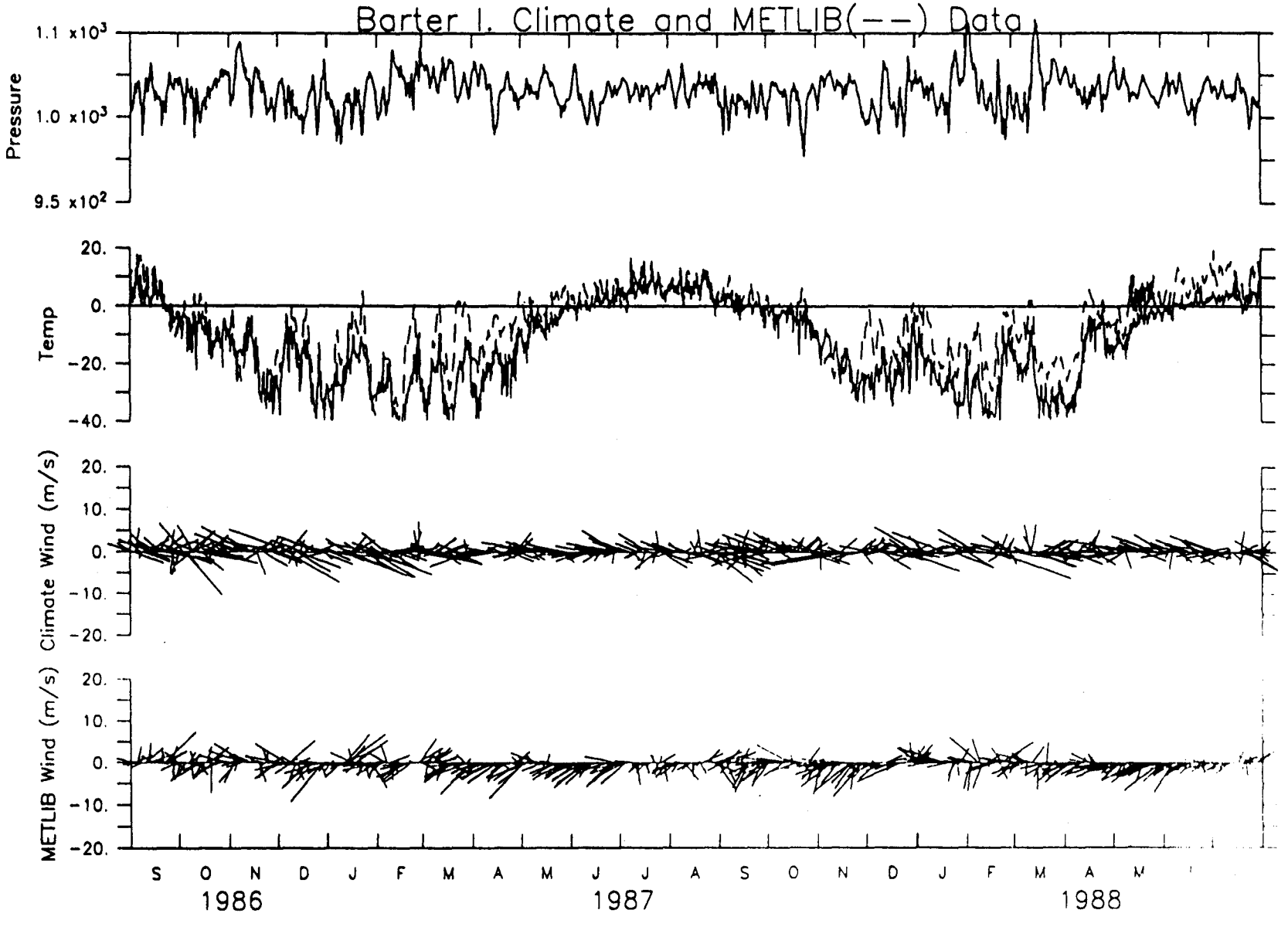

Figure 34. GOES and METLIB pressure, temperature, and winds at Barter Island. See Figure 27.

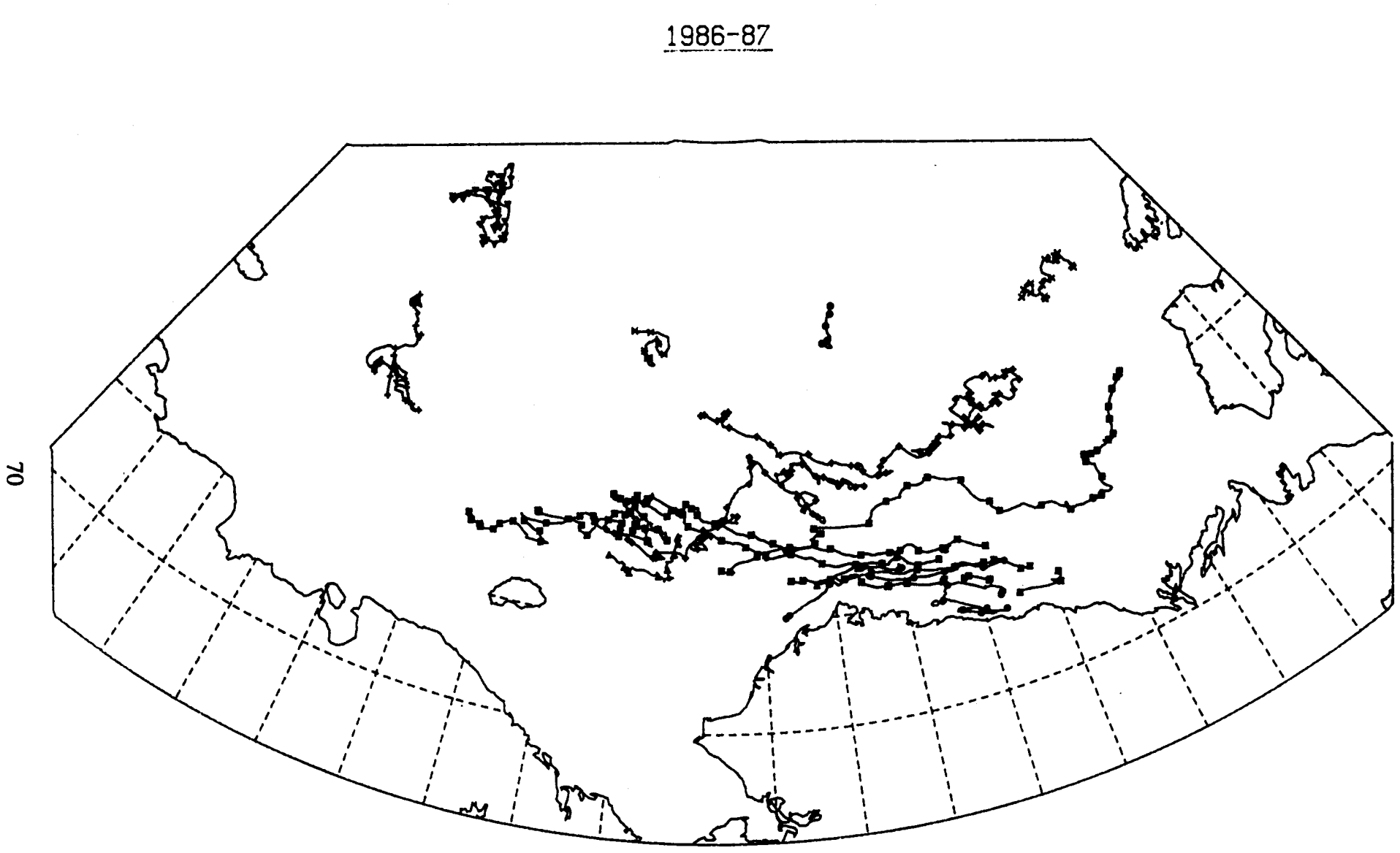

Figure 35. Plot of the 1986–1987 ARGOS buoy tracks.

1987-88

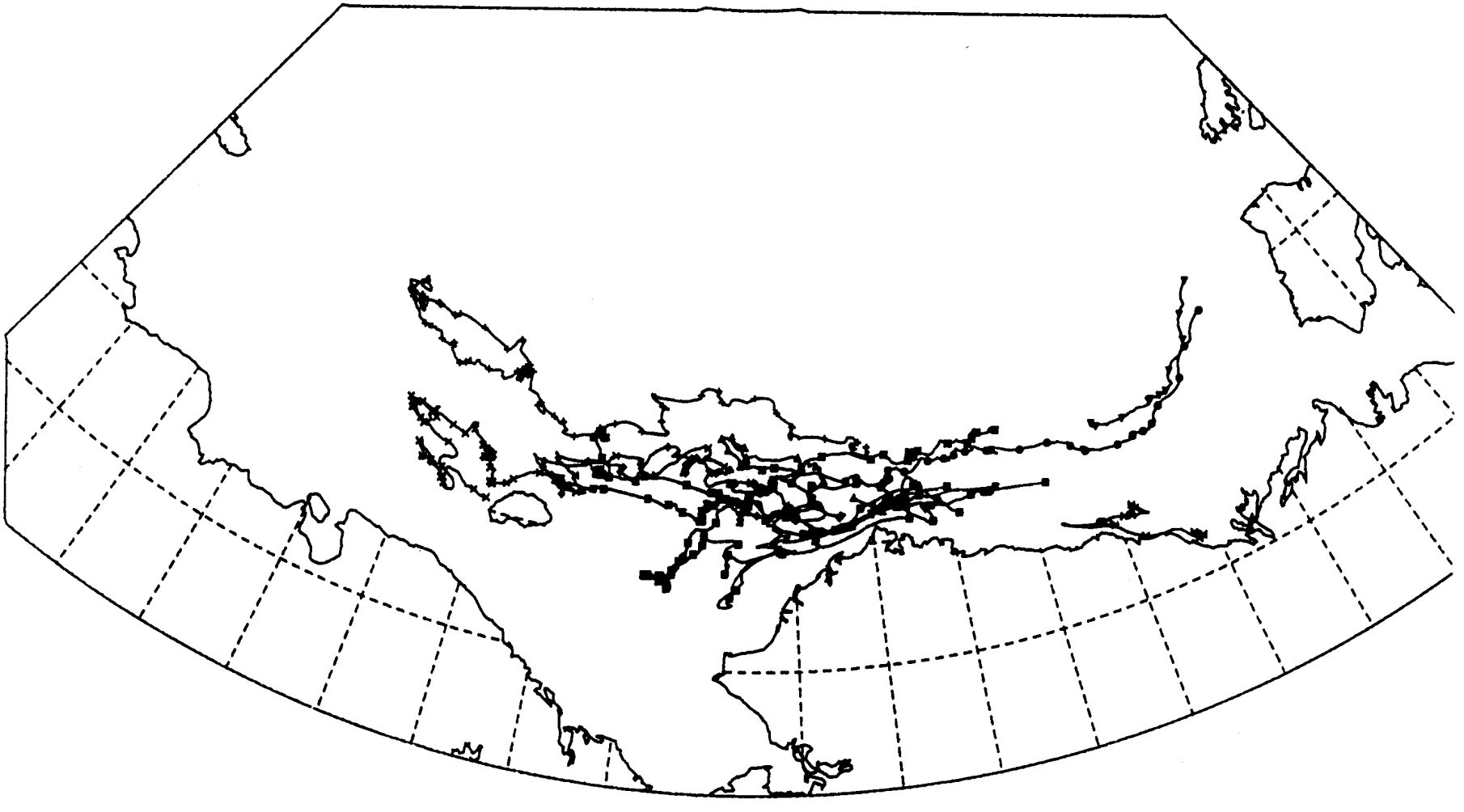

Figure 36. Plot of the 1988 ARGOS buoy tracks.

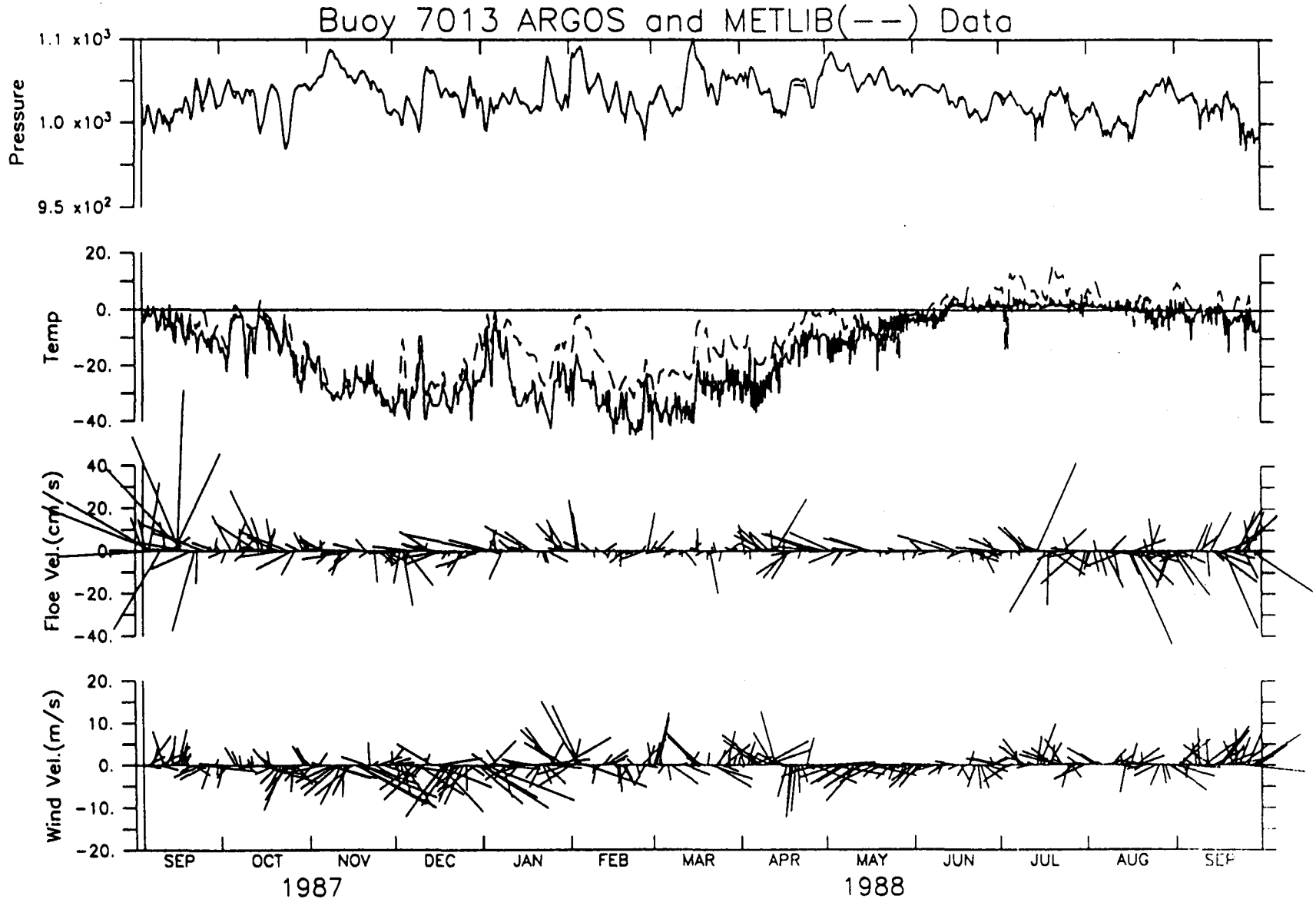

Figure 37. Comparison of surface level pressure (mb) and temperature (°C) measured by ARGOS buoy 7013 with METLIB pressure and temperature. METLIB winds and the velocity of the ice floe are also plotted; the buoy did not have an anemometer. See Figure 27.

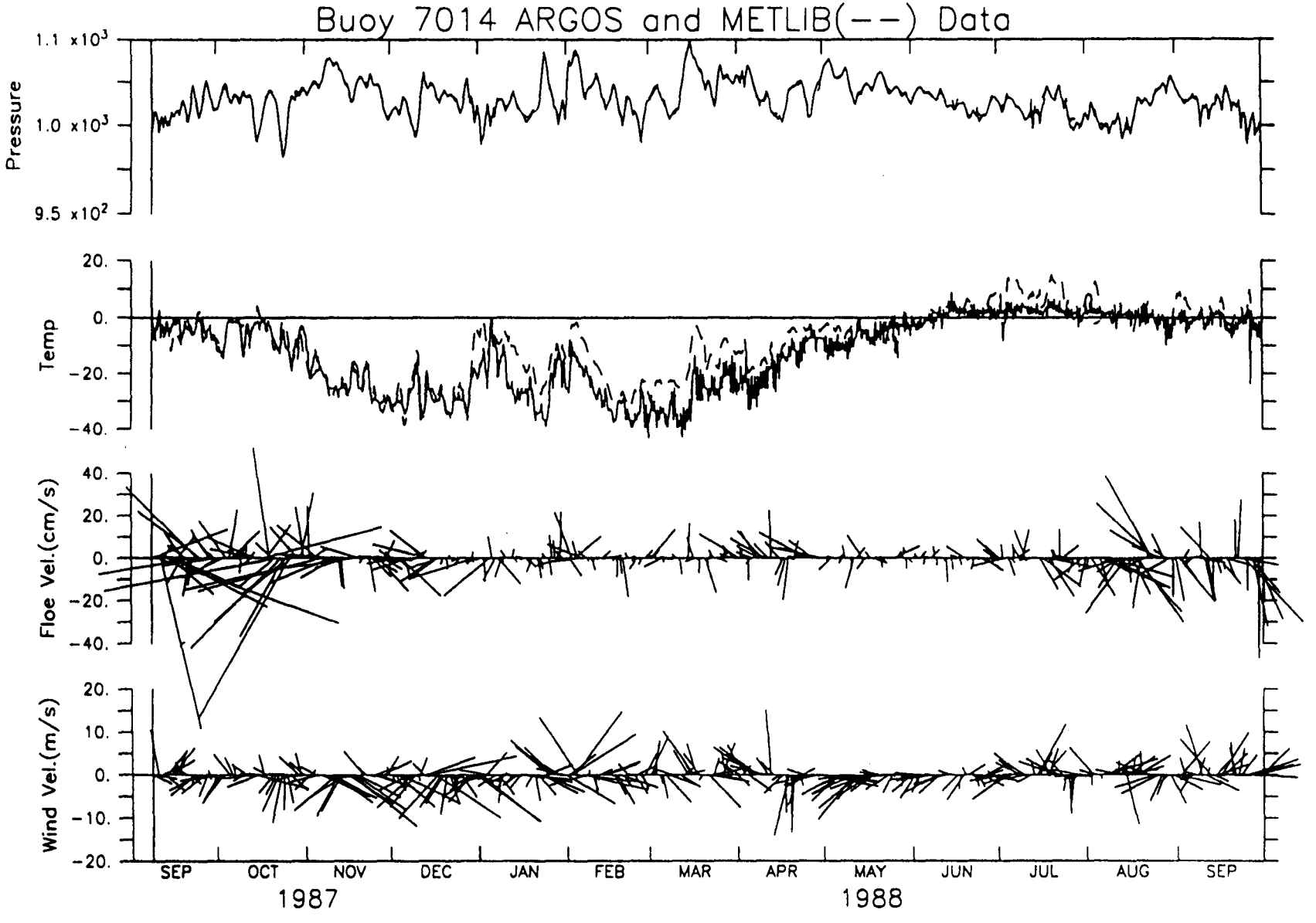

Figure 38. Pressure, temperature, floe velocity, and METLIB winds at ARGOS buoy 7014. See Figure 27.

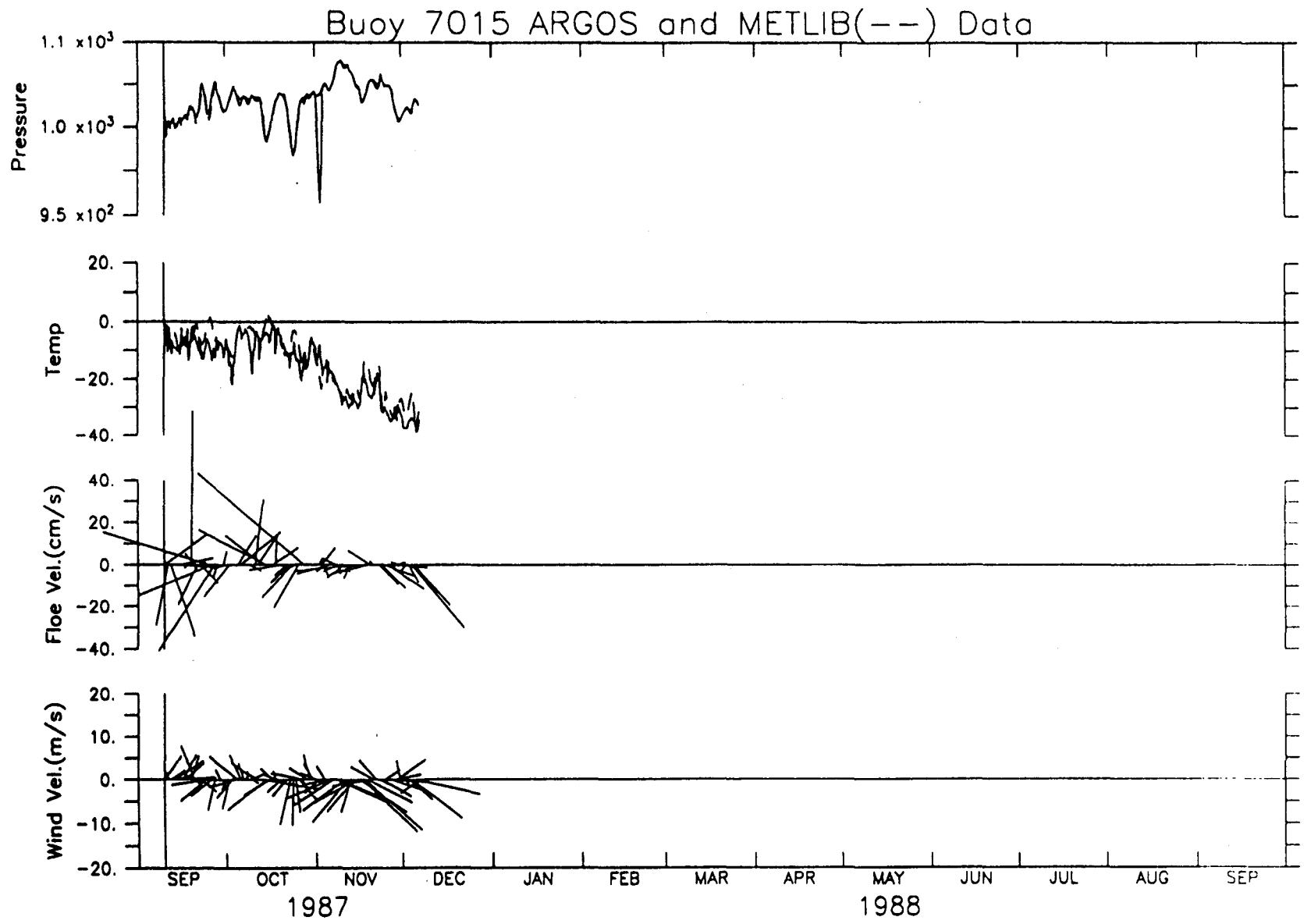

Figure 39. Pressure, temperature, floe velocity, and METLIB winds at ARGOS buoy 7015. See Figure 27.

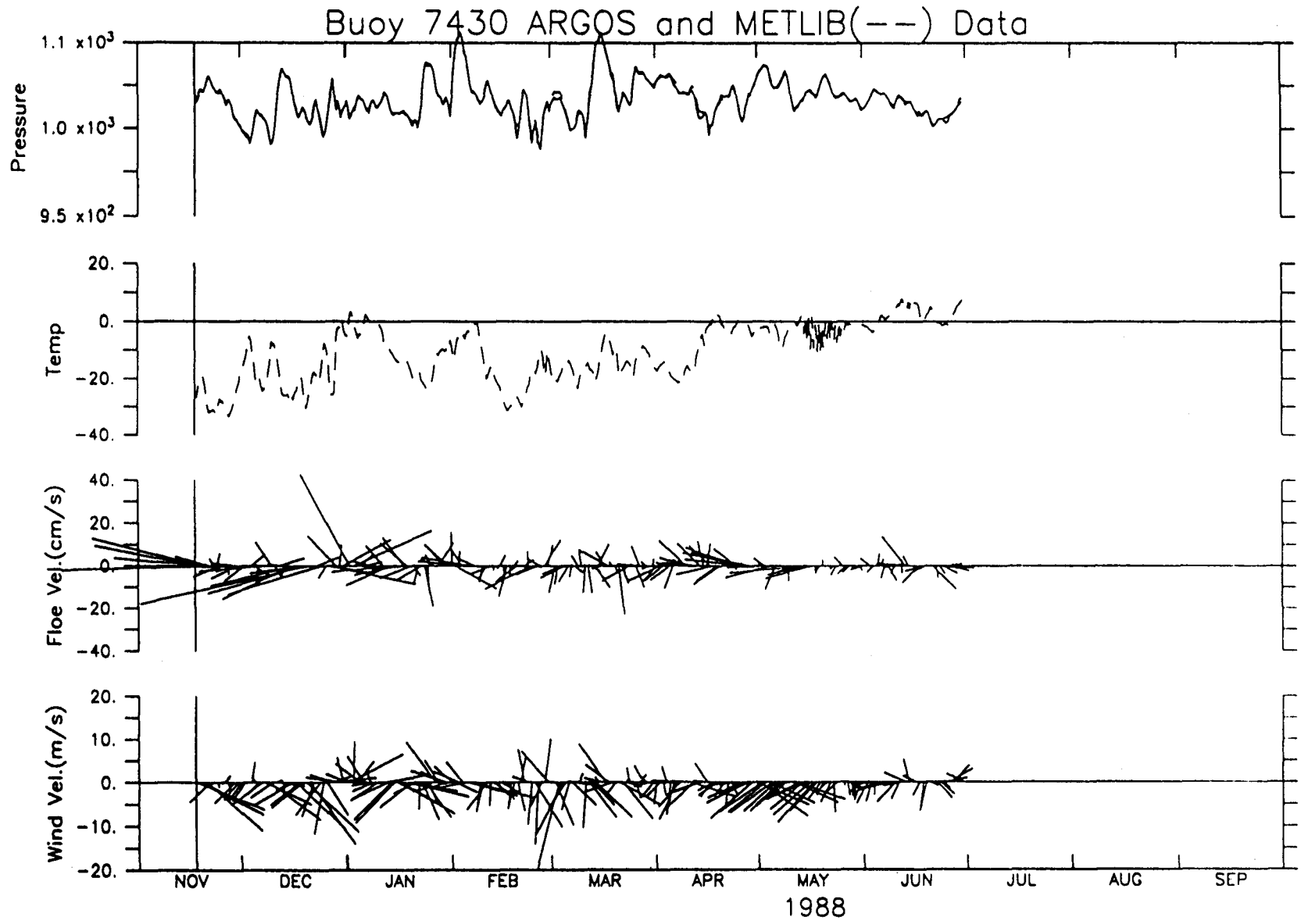

Figure 40. Pressure, temperature, floe velocity, and METLIB winds at ARGOS buoy 7430. See Figure 27.

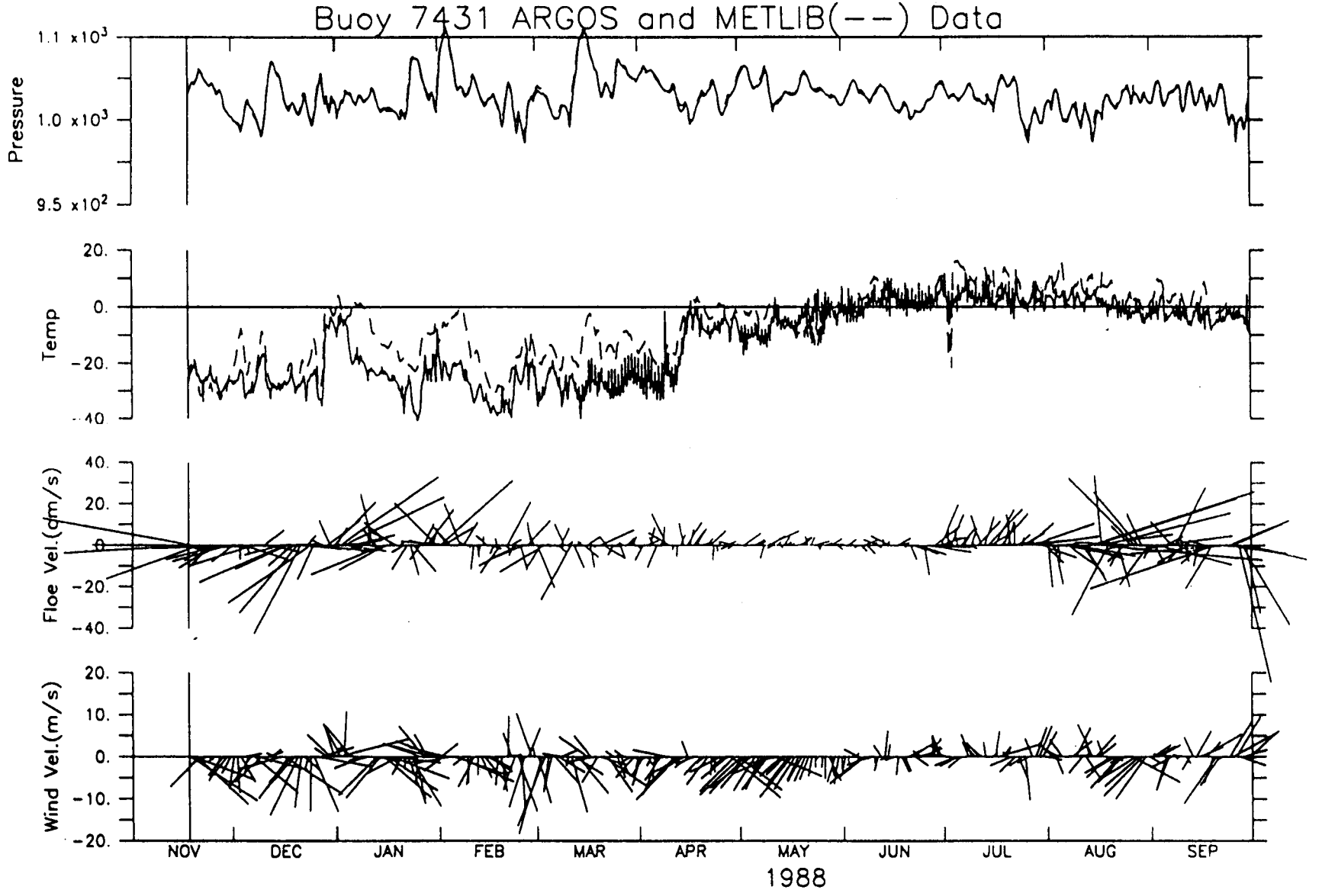

Figure 41. Pressure, temperature, floe velocity, and METLIB winds at ARGOS buoy 7431. See Figure 27.

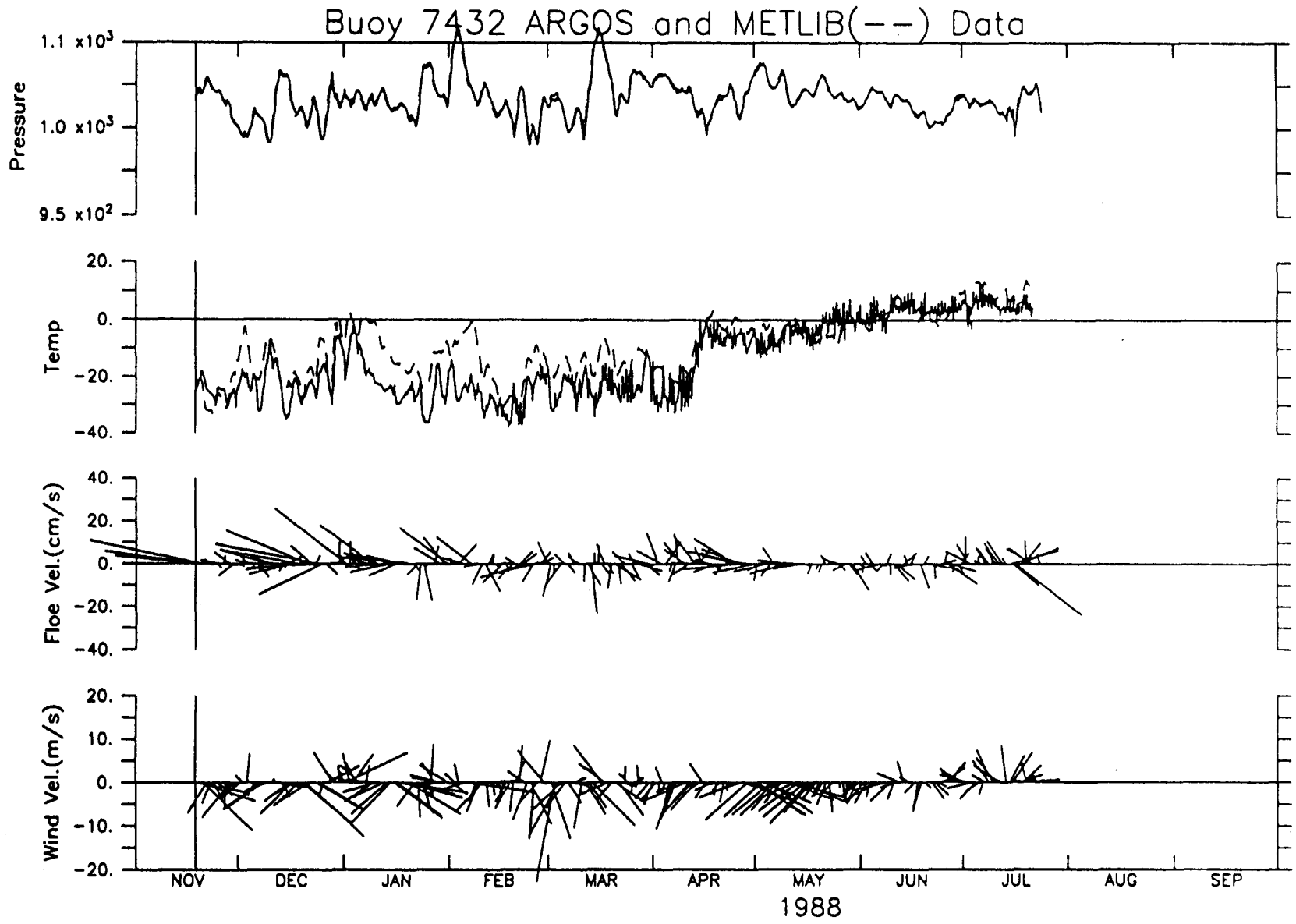

Figure 42. Pressure, temperature, floe velocity, and METLIB winds at ARGOS buoy 7432. See Figure 27.

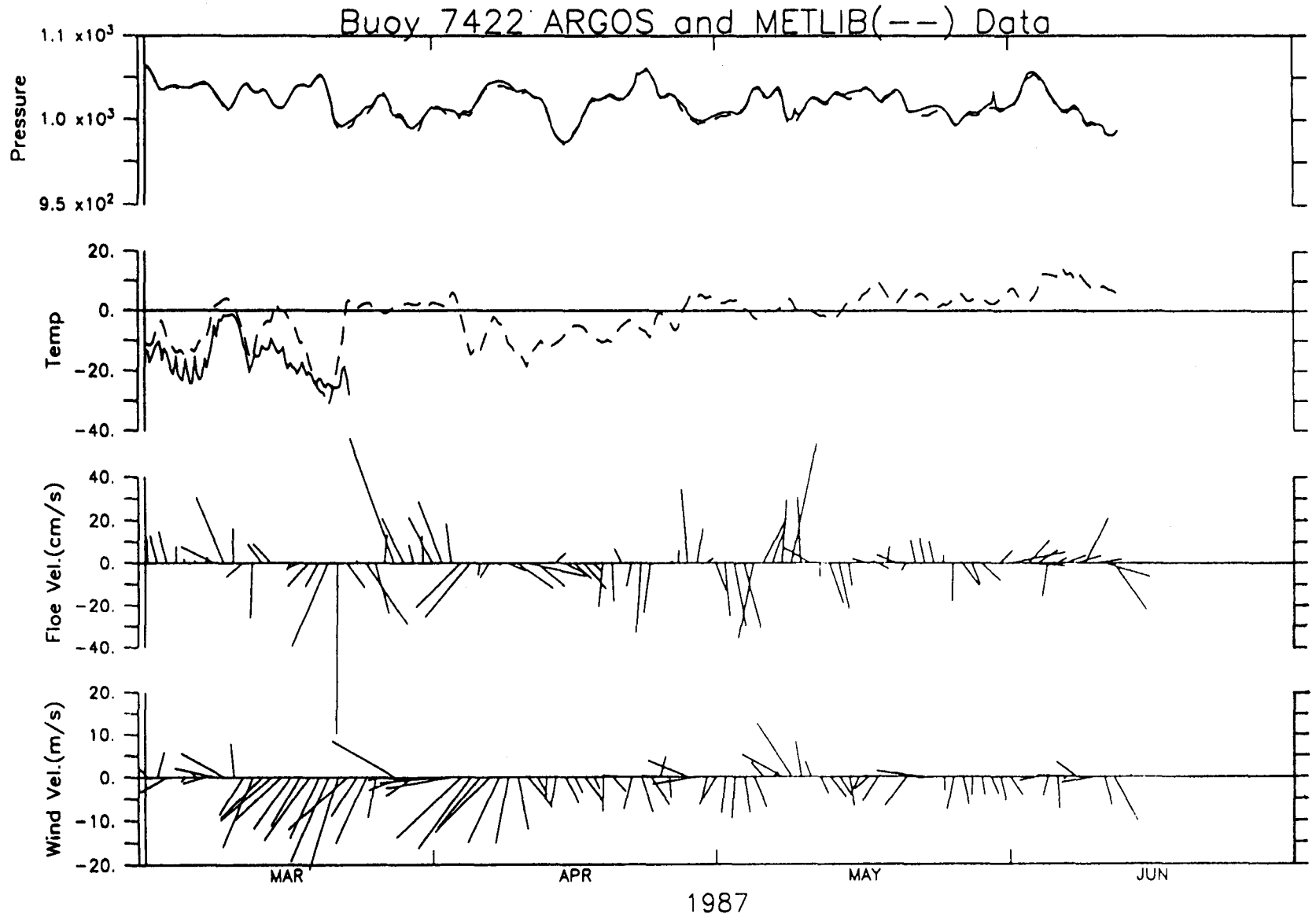

Figure 43. Pressure, temperature, floe velocity, and METLIB winds at ARGOS buoy 7422. See Figure 27.

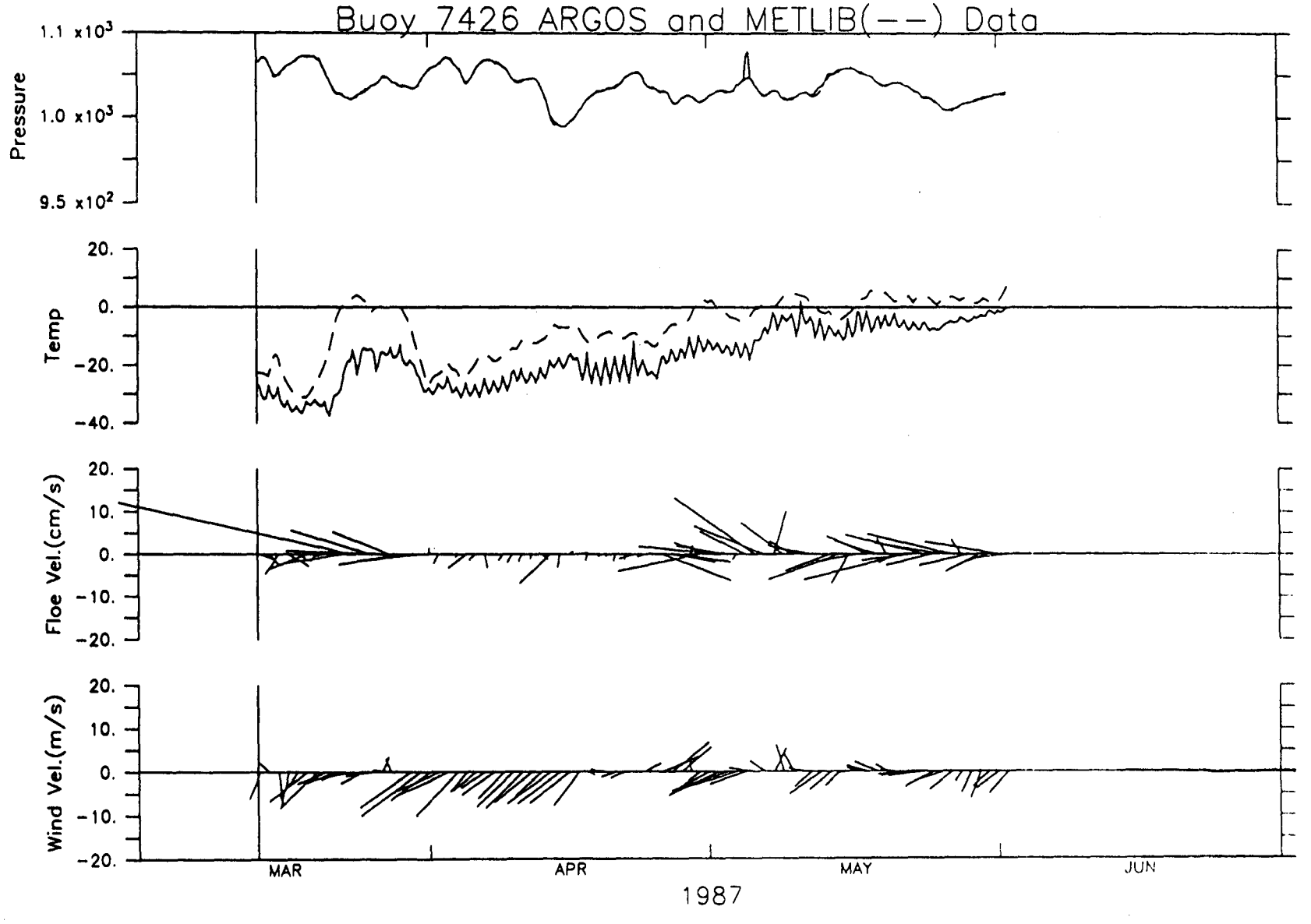

Figure 44. Pressure, temperature, floe velocity, and METLIB winds at ARGOS buoy 7426. See Figure 27.

TABLE 18. Sea-level pressure correlations. Data were 35-hr filtered and correlated for their full record lengths, as listed in Tables 14-16. Note that the climate data comparisons are made over a common time interval, but that the GOES and ARGOS comparisons are not. METLIB data always lagged Climate, GOES, or ARGOS data.

a) Climate and METLIB

	Barter I.	Barrow	Kotzebue	Nome
0 lag	.93	.94	.94	.94
6 hr lag	.97	.97	.97	.98
12 hr lag	.98	.98	.98	.98
18 hr lag	.95	.95	.94	.95
24 hr lag	.90	.90	.88	.88
30 hr lag	.82	.83	.80	.80
95% level	.18	.18	.18	.19

b) GOES and METLIB

	Resolution I.	Lonely	Icy Cape	C.P. of Wales
0 lag	.93	.94	1.00	1.00
6 hr lag	.94	.93	.98	.98
12 hr lag	.93	.89	.95	.93
18 hr lag	.90	.83	.89	.86
24 hr lag	.85	.75	.82	.78
30 hr lag	.79	.68	.74	.69
95% level	.20	.20	.20	.21

c) ARGOS and METLIB

	7013	7014	7015	7422	7426	7430	7431	7432
0 lag	.99	.99	.80	.99	.99	.99	.99	.99
6 hr lag	.98	.98	.79	.97	.99	.98	.98	.98
12 hr lag	.96	.95	.76	.95	.92	.96	.94	.95
18 hr lag	.92	.91	.72	.84	.92	.90	.89	.89
24 hr lag	.88	.85	.66	.74	.86	.84	.82	.83
30 hr lag	.83	.79	.60	.63	.80	.77	.75	.76
95% level	.32	.29	.45	.40	.53	.32	.29	.30

data is directly attributable to this process. This lag must be taken into account if gradient or geostrophic winds based on existing NMC or FNOC analyses are to be used to drive numerical models of sea ice drift and surface currents. Although it may seem like a small effect, this bias would introduce errors of about 10% into the estimates of wind stress, which is the same order of magnitude as the internal ice stress, geostrophic sea-surface tilt contribution, and the Coriolis term in the sea ice balance.

It is also important to note that it would be inappropriate to blend mesoscale surface meteorological observations with either the NWS or FNOC surface pressure fields without time-shifting the analysis fields backwards by 12 hours. The hidden time-shift is probably the major reason that the mesoscale network along the Alaska coast gave such an improved forecasting capability over using geostrophic or gradient winds calculated from standard analysis fields (Kozo, 1980, 1982a, 1982b, 1984; Kozo and Robe, 1986). With a continued adequate coverage by the Arctic Buoy Program and the input of those data into the international meteorological network, there is no further improvement to be gained by maintaining a separate sea-level pressure network along the North Slope. Other meteorological measurements, however, including the anemometer records, the drifting buoy positions, and all the mesoscale air temperature measurements were important to the study.

Temperatures at the four NWS coastal stations also seem to be shifted 6 to 12 hours, although the coefficients change little between 0 and 12 hours lag (Table 19). The temperature correlations overall are 10% lower than the pressure correlations. A disturbing aspect of the analyzed temperatures (METLIB from FNOC analyses) is that they are too warm in the winter and spring at all stations by 3° to 13°C (Table 17, Figs. 28–34, and Figs. 37, 38, 41, 42, and 44). Barrow (Climate) and Resolution Island (GOES) were both quite exposed to marine air and should have had minimal local continentality effects (due to the vastly different thermal characteristics of water and land), yet the FNOC temperatures generated by METLIB were too warm by 13° and 5°C, respectively, with the biggest errors in the coldest months (Table 17). These are huge errors and would be expected to drive an equilibrium thermodynamic ice model to ice-free conditions. Sverdrup (1933) stated that all land stations underpredict the polar marine winter temperatures (give winter air temperatures which are too cold) because of the cumulative effect of leads on the polar marine boundary layer air temperature. However, even the ARGOS buoys, which were riding modest sized floes, showed METLIB temperatures which were 2° to 6°C too warm in their respective record means with the same bias toward errors in winter and spring (Figs. 37, 38, 41, and 42).

One interpretation that could be given to the striking air temperature errors from the FNOC analysis fields is that these temperatures are representative of the mean boundary-layer temperature or the temperature near the top of the planetary boundary layer rather than the surface. Since outward long wave radiative cooling (Maykut and Church, 1973) and sensible heat fluxes

TABLE 19. Air temperature correlations.

a) Climate and METLIB

	Barter I.	Barrow	Kotzebue	Nome
0 lag	.89	.86	.92	.92
6 hr lag	.89	.86	.93	.92
12 hr lag	.88	.86	.92	.92
18 hr lag	.87	.85	.91	.92
24 hr lag	.86	.84	.90	.90
30 hr lag	.85	.82	.89	.89
95% level	.78	.77	.78	.73

b) GOES and METLIB

	Resolution I.	Lonely	Icy Cape	C.P. of Wales
0 lag	.44	.85	.89	.40
6 hr lag	.44	.84	.88	.40
12 hr lag	.44	.83	.87	.40
18 hr lag	.44	.82	.86	.40
24 hr lag	.43	.81	.85	.39
30 hr lag	.43	.79	.84	.39
95% level	.44	.76	.78	.56

c) ARGOS and METLIB (Buoys 7422 and 7430 had bad thermistors.)

	7013	7014	7015	7422	7426	7430	7431	7432
0 lag	.90	.91	.93	XX	.90	XX	.89	.88
6 hr lag	.90	.91	.93	XX	.89	XX	.89	.88
12 hr lag	.89	.90	.92	XX	.87	XX	.88	.87
18 hr lag	.89	.90	.90	XX	.85	XX	.88	.86
24 hr lag	.88	.89	.88	XX	.83	XX	.87	.85
30 hr lag	.87	.88	.87	XX	.81	XX	.86	.84
95% level	.86	.86	.96	XX	.87	XX	.91	.76

dominate the surface balance, there is strong cooling at the surface and a general subsidence in winter months (Sverdrup, 1933; Overland, 1985). Thus any thermodynamic sea ice model would need to be driven by a relatively complete boundary-layer model and should not use the FNOC analysis fields in the surface balance, as is typically done for longer model calculations.

The correlations between the gradient winds calculated by METLIB from FNOC fields with the measured winds have the same time delays as sea-level pressure and surface air temperature, but have lower absolute correlations compared to the scalar quantities (Table 20). The somewhat low correlations were caused by several factors: 1) the high-frequency variations had not been removed, so diurnal effects, such as the sea breeze were not deleted (Moritz, 1977; Kozo, 1982a, 1982b); 2) for certain stations, such as Barter Island, mountain barrier effects, especially enhanced in the winter by the stability of the lower boundary layer, were not included in the METLIB wind calculation (Dickey, 1961; Kozo, 1980, 1984; Kozo and Robe, 1986); and 3) seasonal variations in surface drag and radiation effects on boundary layer dynamics were not included in METLIB calculated winds (Banke and Smith, 1971; Banke *et al.*, 1976; Feldman *et al.*, 1979; Langleben, 1971; Maykut and Church, 1973; Smith and Banke, 1971; Wendler *et al.*, 1981).

There appear to be three regimes among the various weather stations. The Bering Strait region (Cape Prince of Wales, Nome and Kotzebue), the North Slope (Barrow, Lonely, Resolution, and Barter), and a transition zone represented by Icy Cape (Tables 21–24). More low pressure systems reach the southern stations than the North Slope stations; near the southern stations, the ocean is always ice free in summer, while near the northern stations there may be ice all year or only a short ice-free season. The seasonal air temperature maxima were in August in the south and shifted closer to the summer solstice along the North Slope (Pease, 1987).

Seasonally averaged values for temperature, pressure, and wind are given in Figs. 45–48; monthly averaged values are in Figs. 49–52; and monthly averaged wind variances are in Fig. 53 for all the land stations. Along the North Slope, there were sea-level pressure maxima in both years in December and February and pressure minima in September-October and January. The January minimum may seem odd because of the generally higher winter pressures than summer; however, this is seen in the Bering and Chukchi seas also, and is driven by blocking ridge activity over the eastern North Pacific each winter (Overland, 1981; Overland and Pease, 1982; Pease, 1987). Generally, Nome, Kotzebue, and Cape Prince of Wales are warmer, windier, and more randomly affected by winds from various directions than the North Slope, where summer mean maximum air temperatures are less than 10°C, winds are persistently northeasterly to easterly, and wind-direction variances are lower. Maximum wind variances were highest at all stations in the autumn and typically again in January.

A selection of weather maps for 1986–87 are presented in Figs. 143–150 in Appendix B. An added selection of maps for 1987–88 are given in Figs. 54–58. The October 1987 maps

TABLE 20. Wind speed correlations. Note that the correlations for Icy Cape and Cape Prince of Wales were on significantly shorter time series than for the other stations.

a) Linear Correlations along axes of maximum variance:

Climate and METLIB

	Barter I.	Barrow	Kotzebue	Nome
0 lag	.40	.57	.17	.55
6 hr lag	.46	.63	.19	.60
12 hr lag	.50	.64	.17	.59
18 hr lag	.48	.59	.11	.52
24 hr lag	.42	.51	.06	.43
30 hr lag	.35	.43	.02	.35
95% level	.09	.11	.11	.15

Complex Correlations (average angle of separation):

0 lags	0.53 (–2.8°)	0.72 (+1.2°)	0.53 (–10.4°)	.64 (–10.1°)

b) Linear Correlations along axes of maximum variance:

GOES and METLIB

	Resolution I.	Lonely	Icy Cape	C.P. of Wales
0 lags	.35	.30	.74	.64
6 hr lag	.37	.29	.71	.63
12 hr lag	.36	.25	.65	.57
18 hr lag	.35	.20	.57	.48
24 hr lag	.32	.16	.50	.39
30 hr lag	.29	.13	.45	.31
95% level	.11	.16	.15	.16

Complex Correlations (average angle of separation):

0 lags	0.56 (–8.5°)	0.59 (–7.7°)	0.79 (18.3°)	0.81 (22.1°)

TABLE 21. Correlations among climate stations. (Lag that gives the greatest correlation; 0 hours unless explicitly stated otherwise).

	Barter I.	Barrow	Kotzebue	Nome
Pressure				
Barter I.	1.0	0.96	0.84	0.69
Barrow	0.96	1.0	0.77	0.63
Kotzebue	0.86 (6)	0.80 (6)	1.0	0.96
Nome	0.75 (12)	0.68 (12)	0.96 (6)	1.0
Temperature				
Barter I.	1.0	0.96	0.90	0.84
Barrow	0.96 (6)	1.0	0.91	0.86
Kotzebue	0.90 (18)	0.91 (12)	1.0	0.95
Nome	0.85 (18)	0.86 (18)	0.95 (6)	1.0
Wind Speed				
Barter I.	1.0	0.53	***	–0.12(6)
Barrow	0.53	1.0	0.15	***
Kotzebue	0.09 (24)	0.21 (18)	1.0	0.43
Nome	–0.12	0.11 (30)	0.44 (6)	1.0

*** Correlation was not significant at the 95% level. Positive correlation means column lags row.

TABLE 22. Correlations among METLIB records at climate stations.

	Barter I.	Barrow	Kotzebue	Nome
Pressure				
Barter I.	1.0	0.96	0.84	0.68
Barrow	0.96	1.0	0.81	0.65
Kotzebue	0.86 (6)	0.82 (6)	1.0	0.95
Nome	0.73 (12)	0.69 (12)	0.96 (6)	1.0
Temperature				
Barter I.	1.0	0.93	0.82	0.74
Barrow	0.93 (6)	1.0	0.88	0.79
Kotzebue	0.83 (12)	0.88 (6)	1.0	0.95
Nome	0.73 (12)	0.79 (6)	0.95	1.0
Wind Speed				
Barter I.	1.0	0.68	0.23	***
Barrow	0.68	1.0	0.34	***
Kotzebue	0.25 (6)	0.37 (12)	1.0	0.83
Nome	0.14 (24)	0.20 (24)	0.85 (6)	1.0

TABLE 23. Correlations among Goes stations. Time interval is 28 March 1987 to 29 March 1988.

	Resolution I.	Lonely	Icy Cape
Pressure			
Resolution I.	1.0	0.87 (12)	0.91 (6)
Lonely	0.83	1.0	0.88
Icy Cape	0.90	0.88 (6)	1.0
Temperature			
Resolution I.	1.0	***	***
Lonely	***	1.0	0.96
Icy Cape	***	0.96 (6)	1.0
Wind Speed			
Resolution	1.0	0.68 (24)	0.52 (12)
Lonely	0.54	1.0	0.52
Icy Cape	0.51	0.54 (6)	1.0

TABLE 24. Correlations among METLIB records at GOES stations.

	Resolution I.	Lonely	Icy Cape
Pressure			
Resolution I.	1.0	0.99	0.96
Lonely	0.99	1.0	0.98
Icy Cape	0.96	0.98	1.0
Temperature			
Resolution I.	1.0	0.98	0.91
Lonely	0.98	1.0	0.96
Icy Cape	0.91(6)	0.96	1.0
Wind Speed			
Resolution	1.0	0.89	0.63
Lonely	0.89	1.0	0.82
Icy Cape	0.63	0.82	1.0

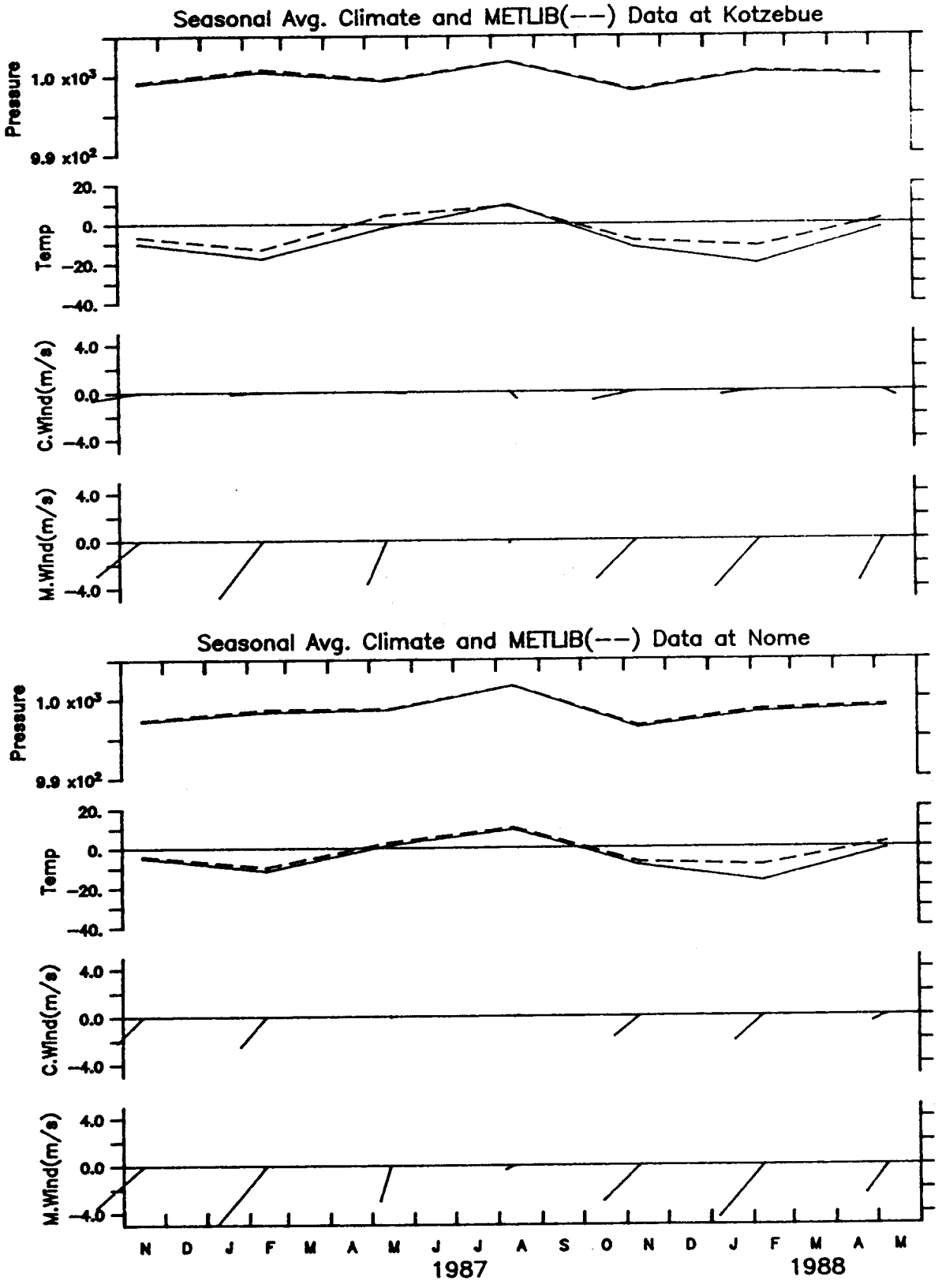

Figure 45. Seasonal average NWS and METLIB pressure (mb), temperature (°C), and winds (m s^{-1}) at Kotzebue and Nome. Data were averaged over January-March, April-June, July-September, and October-December and are plotted at the midpoint of the averaging interval.

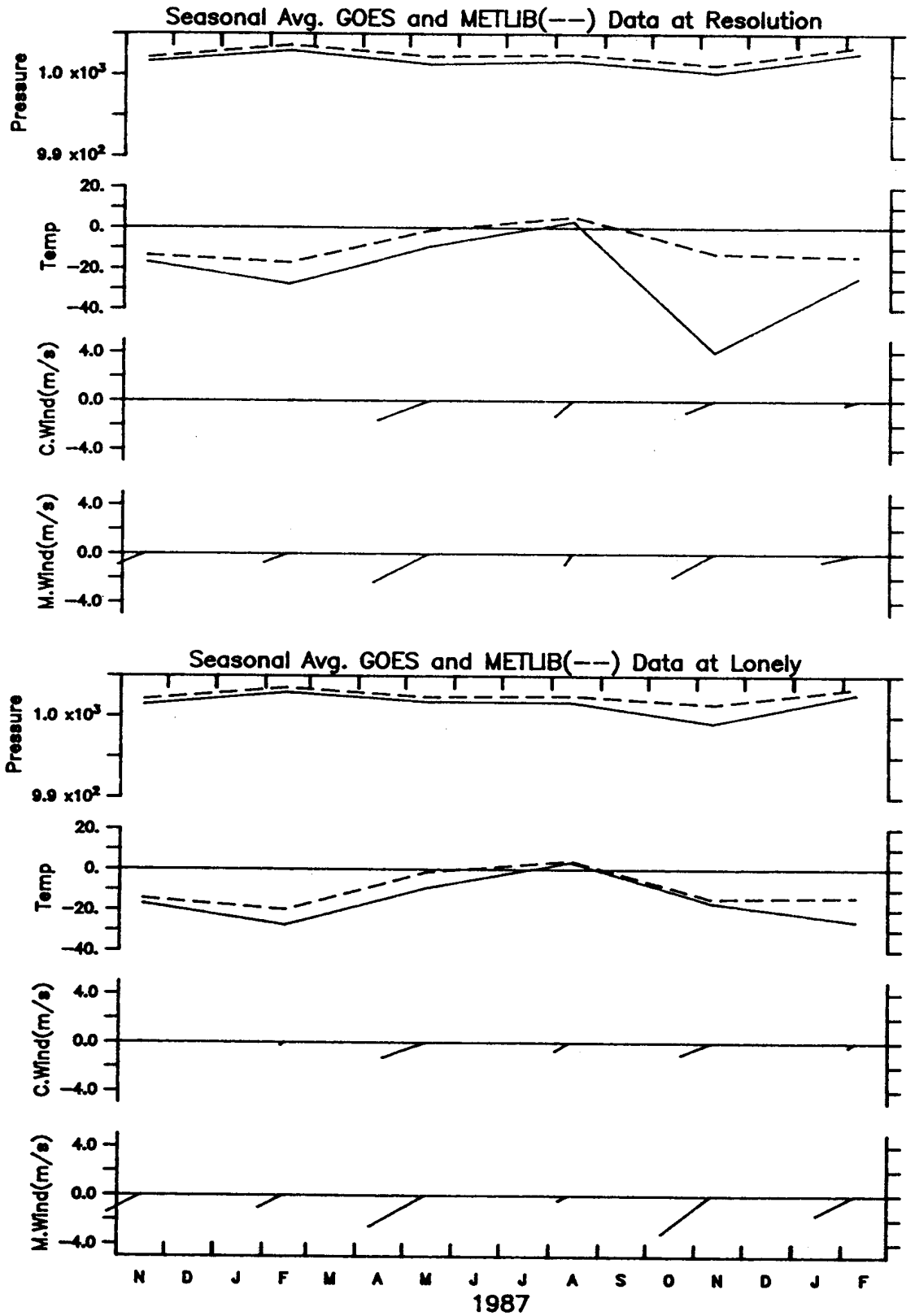

Figure 46. Seasonal average GOES station and METLIB pressure, temperature, and winds at Resolution Island and Lonely. See Figure 45.

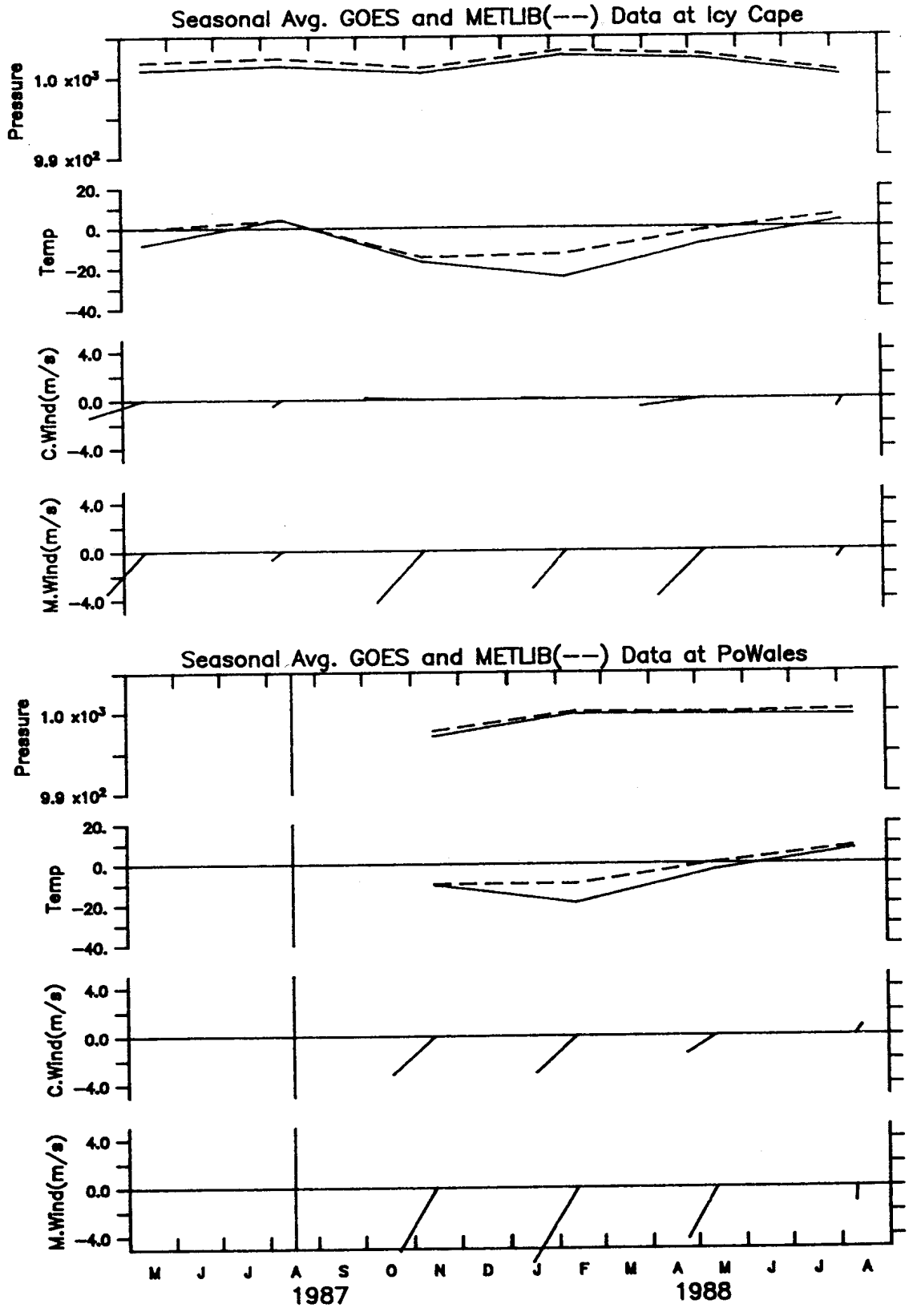

Figure 47. Seasonal average GOES station and METLIB pressure, temperature, and winds at Icy Cape and Wales. See Figure 45.

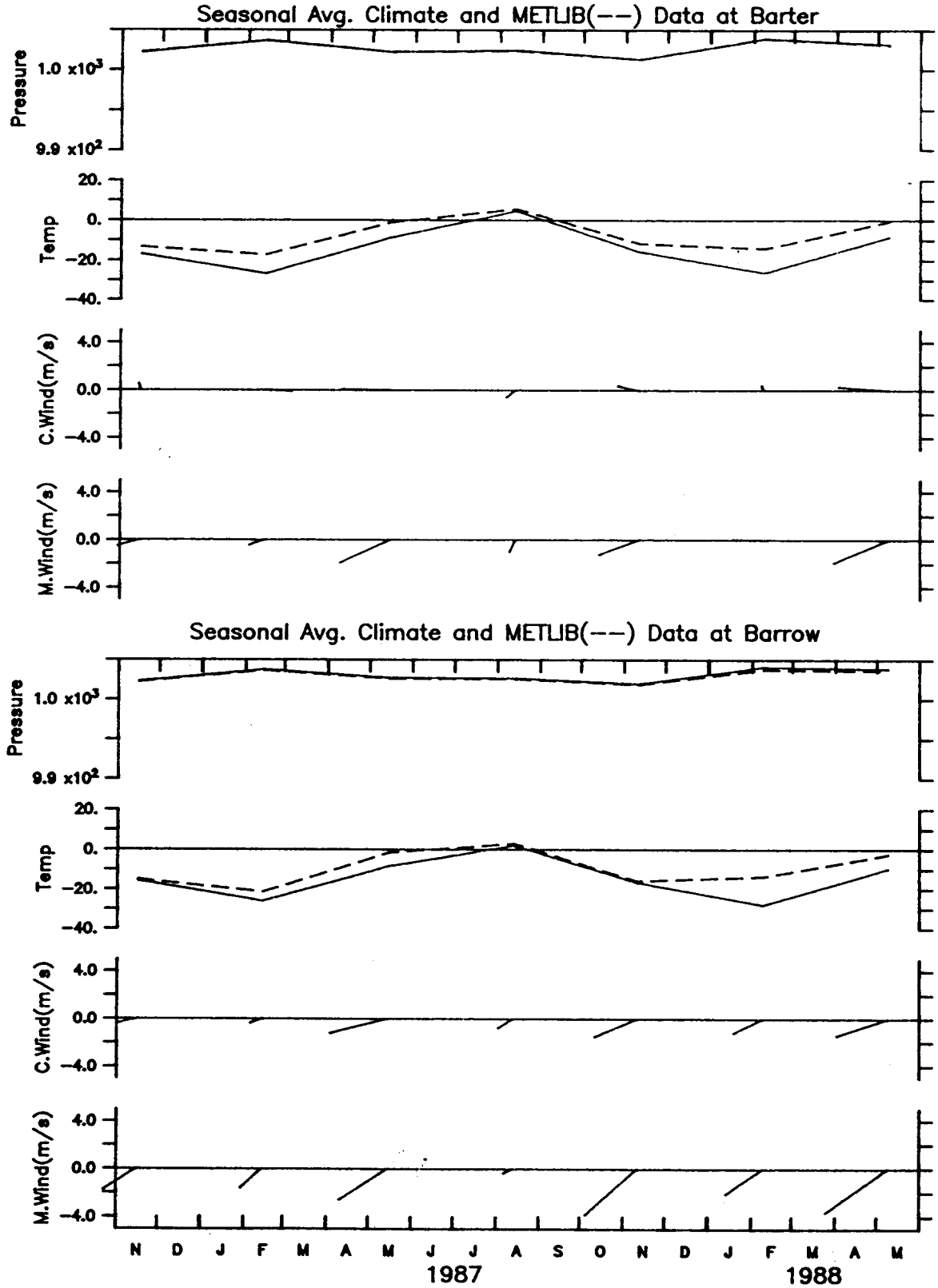

Figure 48. Seasonal average NWS and METLIB pressure (mb), temperature (°C), and winds (m s^{-1}) at Barter Island and Barrow.

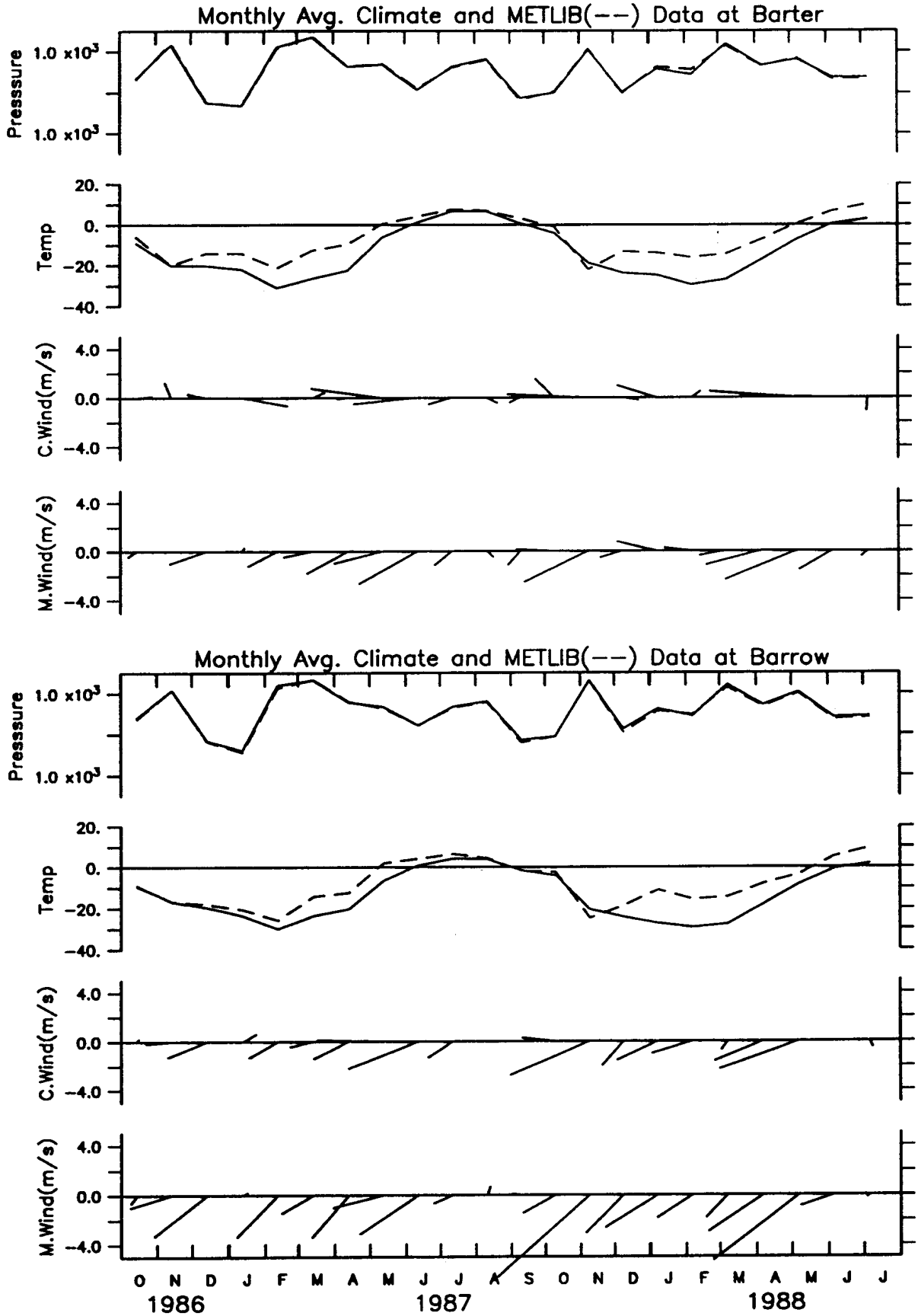

Figure 49. Monthly average NWS and METLIB pressure (mb), temperature (°C), and winds (m s^{-1}) at Barter Island and Barrow.

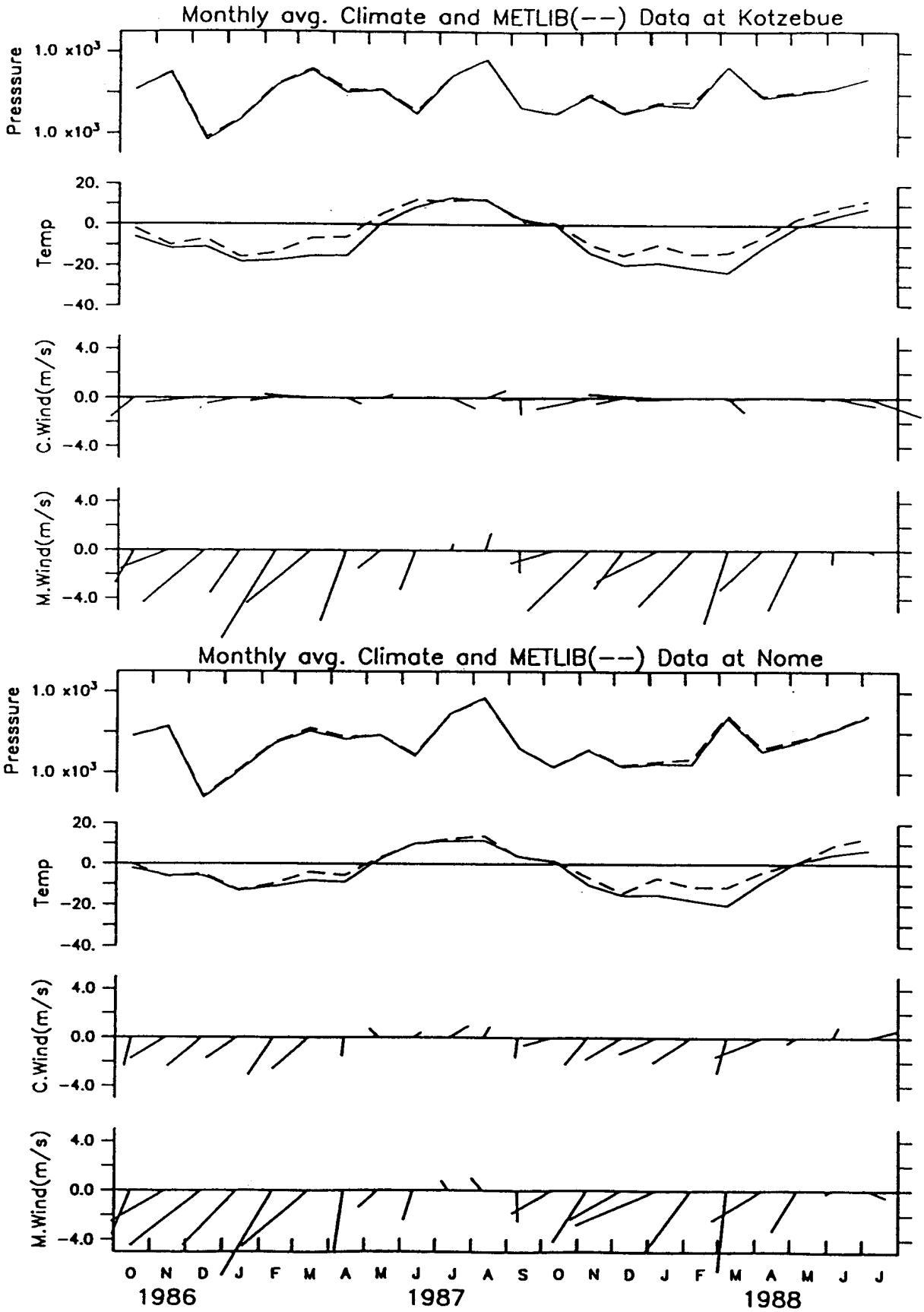

Figure 50. Monthly average NWS and METLIB pressure (mb), temperature (°C), and winds (m s^{-1}) at Kotzebue and Nome.

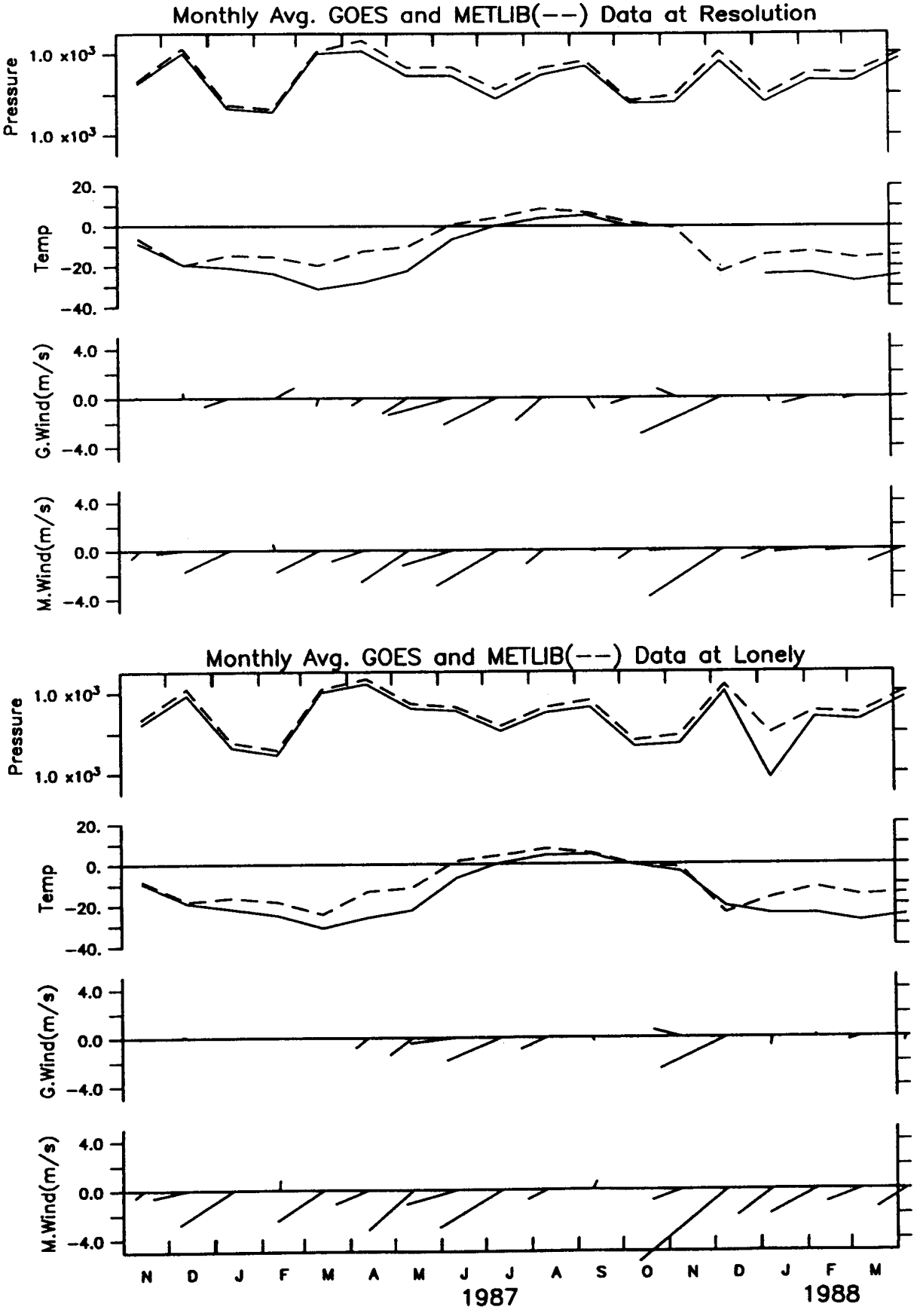

Figure 51. Monthly average GOES-station and METLIB pressure (mb), temperature (°C), and winds (m s^{-1}) at Resolution Island and Lonely.

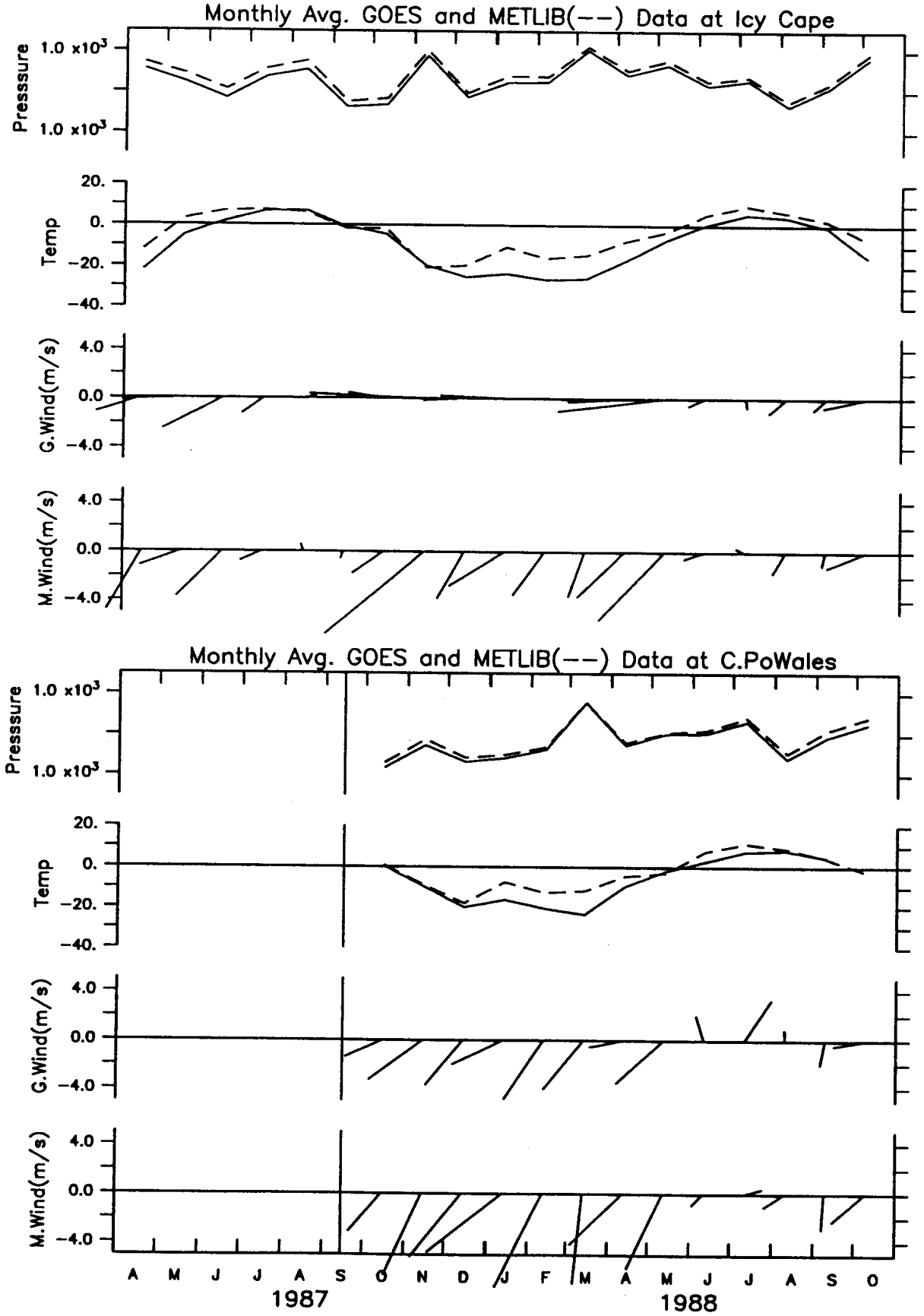

Figure 52. Monthly average GOES-station and METLIB pressure (mb), temperature (°C), and winds (m s^{-1}) at Icy Cape and Wales.

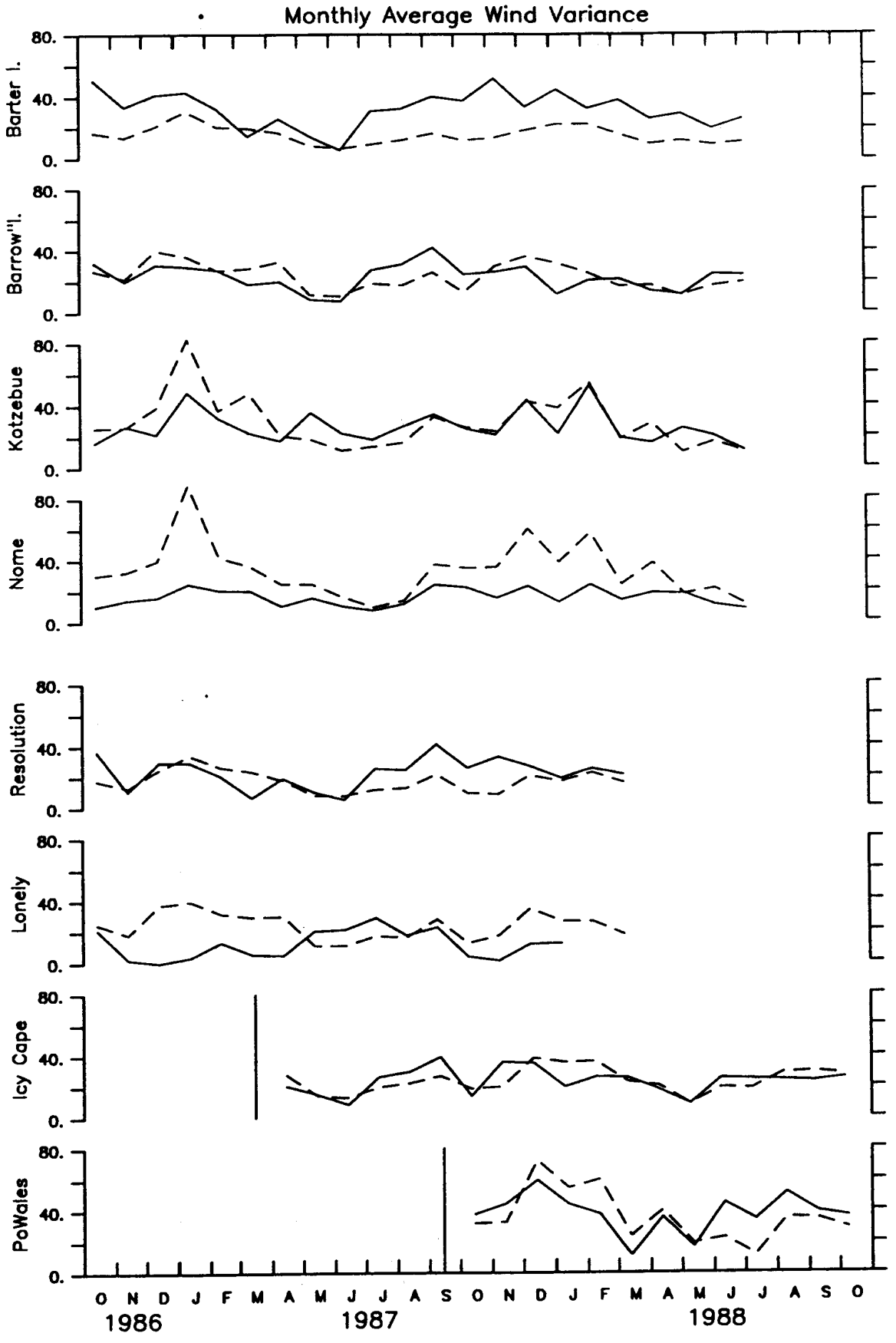

Figure 53. Monthly average wind variance ($m^2\ s^{-2}$) at the four National Weather Service Stations and four GOES stations.

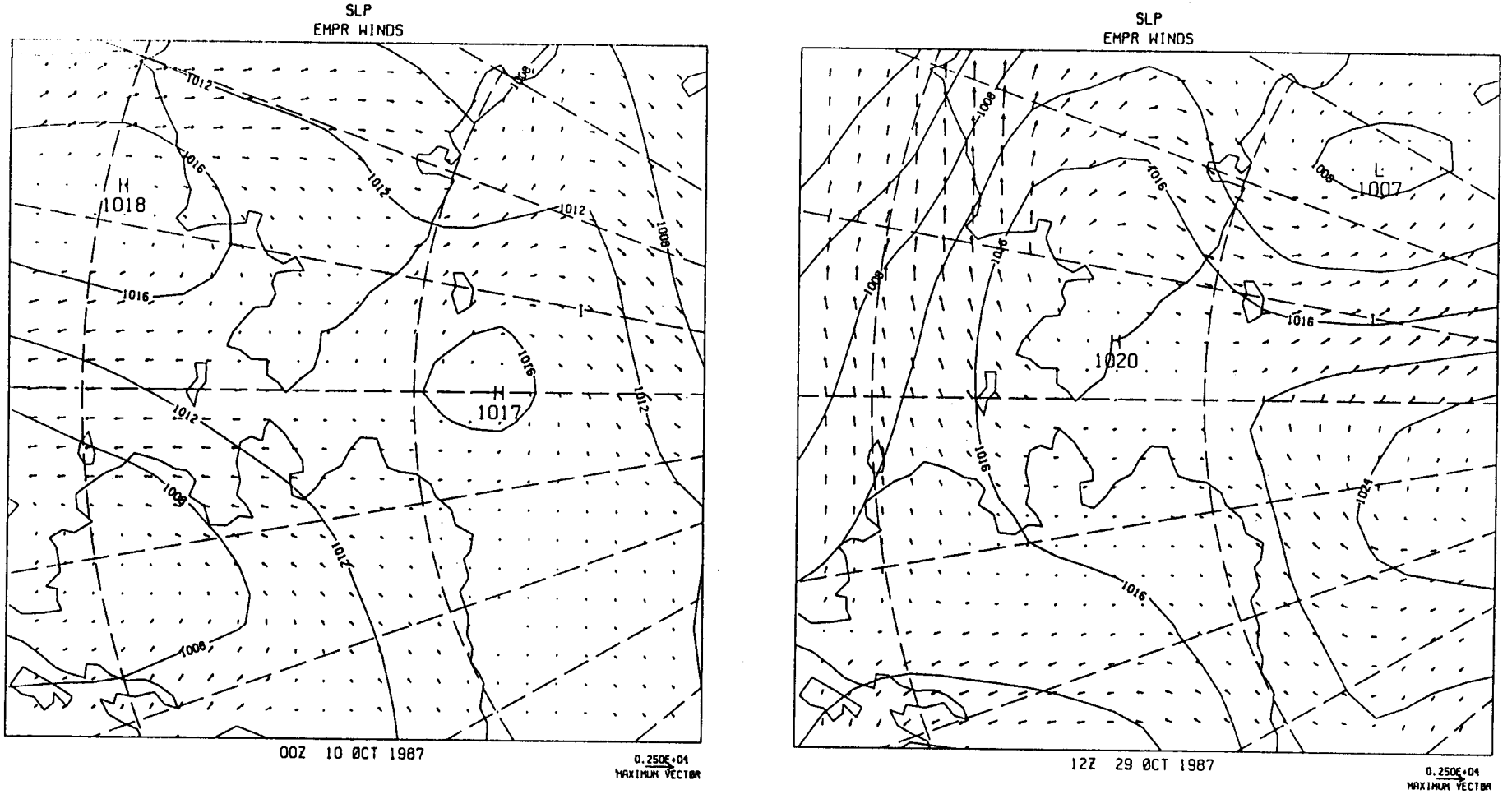

Figure 54. Pressure and wind fields over northern Alaska and eastern Siberia at 00Z 10 October 1987 and 12Z 29 October 1987.

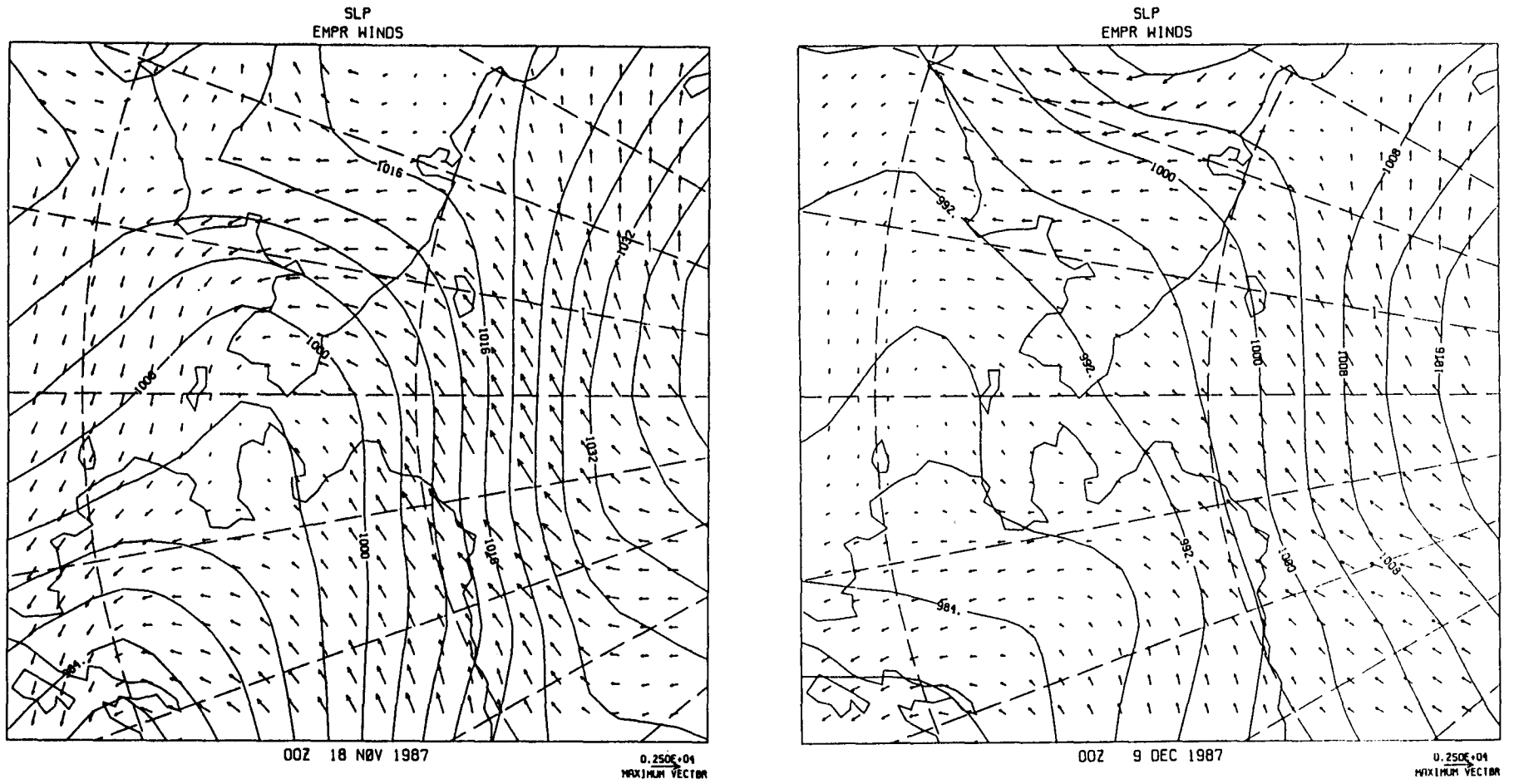

Figure 55. Pressure and wind fields over northern Alaska and eastern Siberia at 00Z 18 November 1987 and 00Z 9 December 1987. The absence of wind vectors northwest of Alaska in the first map indicates that the wind speed was greater than 25 m s^{-1}.

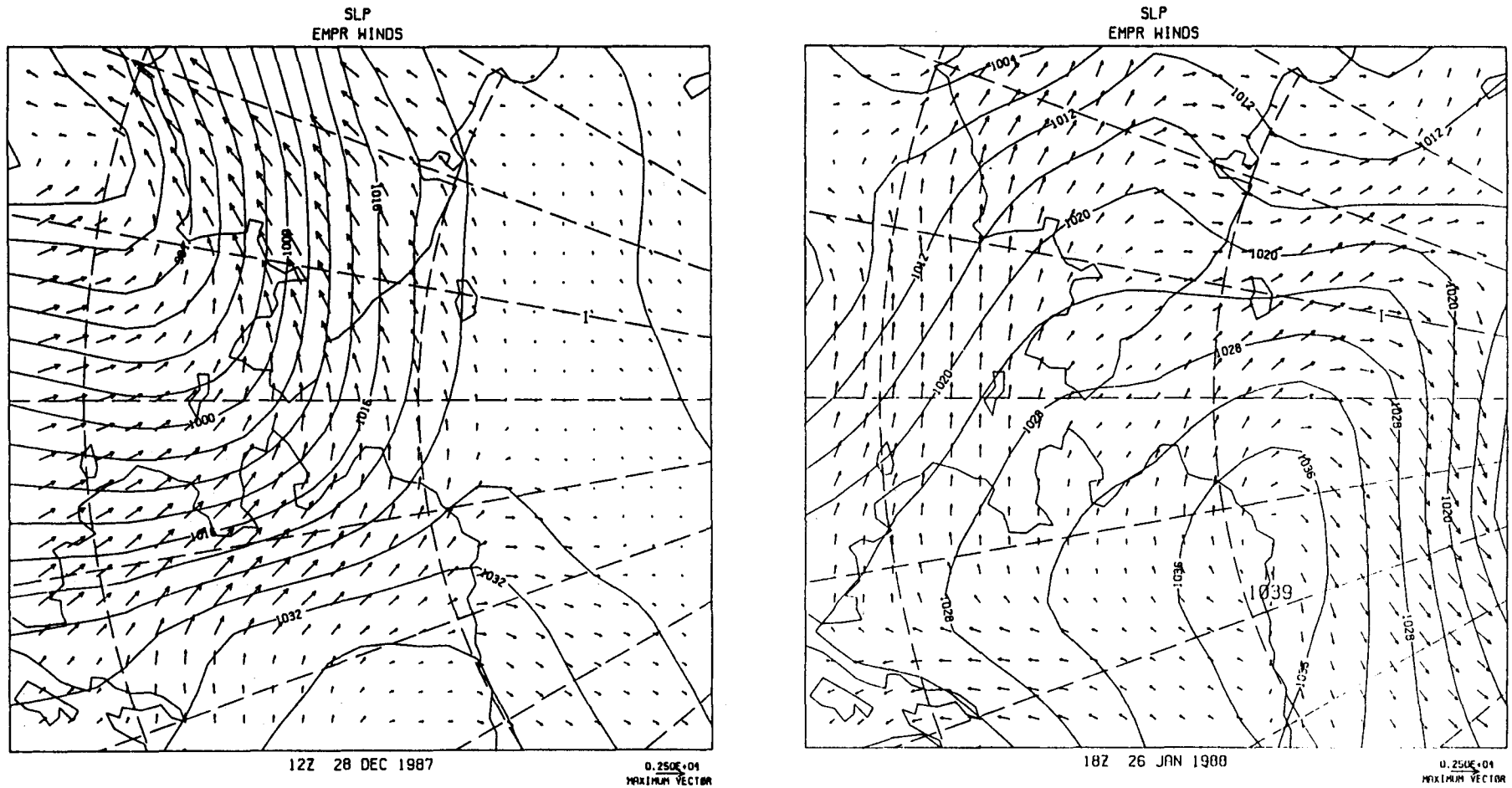

Figure 56. Pressure and wind fields over northern Alaska and eastern Siberia at 12Z 28 December 1987 and 18Z 26 January 1988.

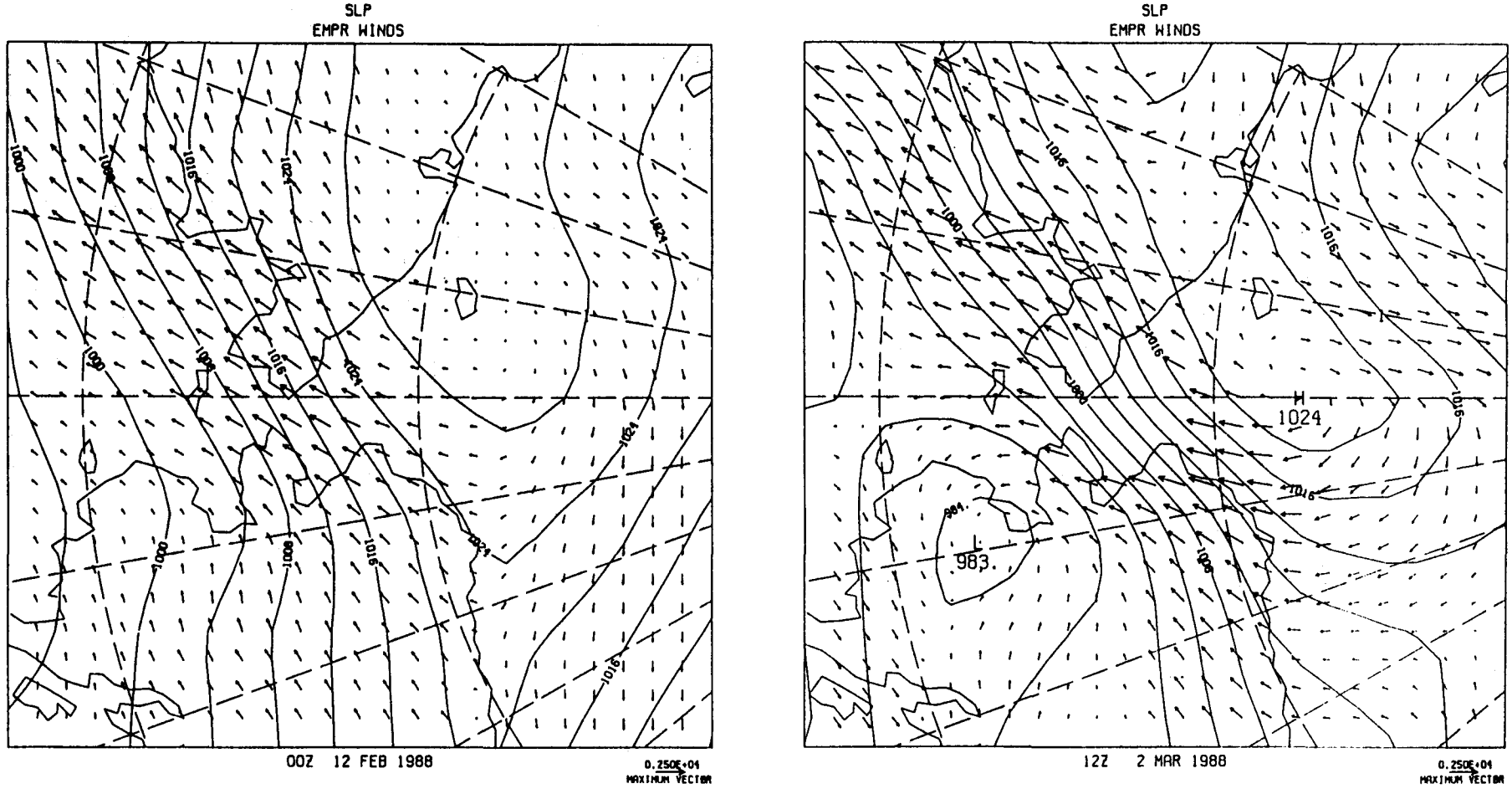

Figure 57. Pressure and wind fields over northern Alaska and eastern Siberia at 00Z 12 February 1988 and 12Z 2 March, 1988. In the latter chart, winds were greater than 25 m s^{-1} over much of the Chukchi Sea.

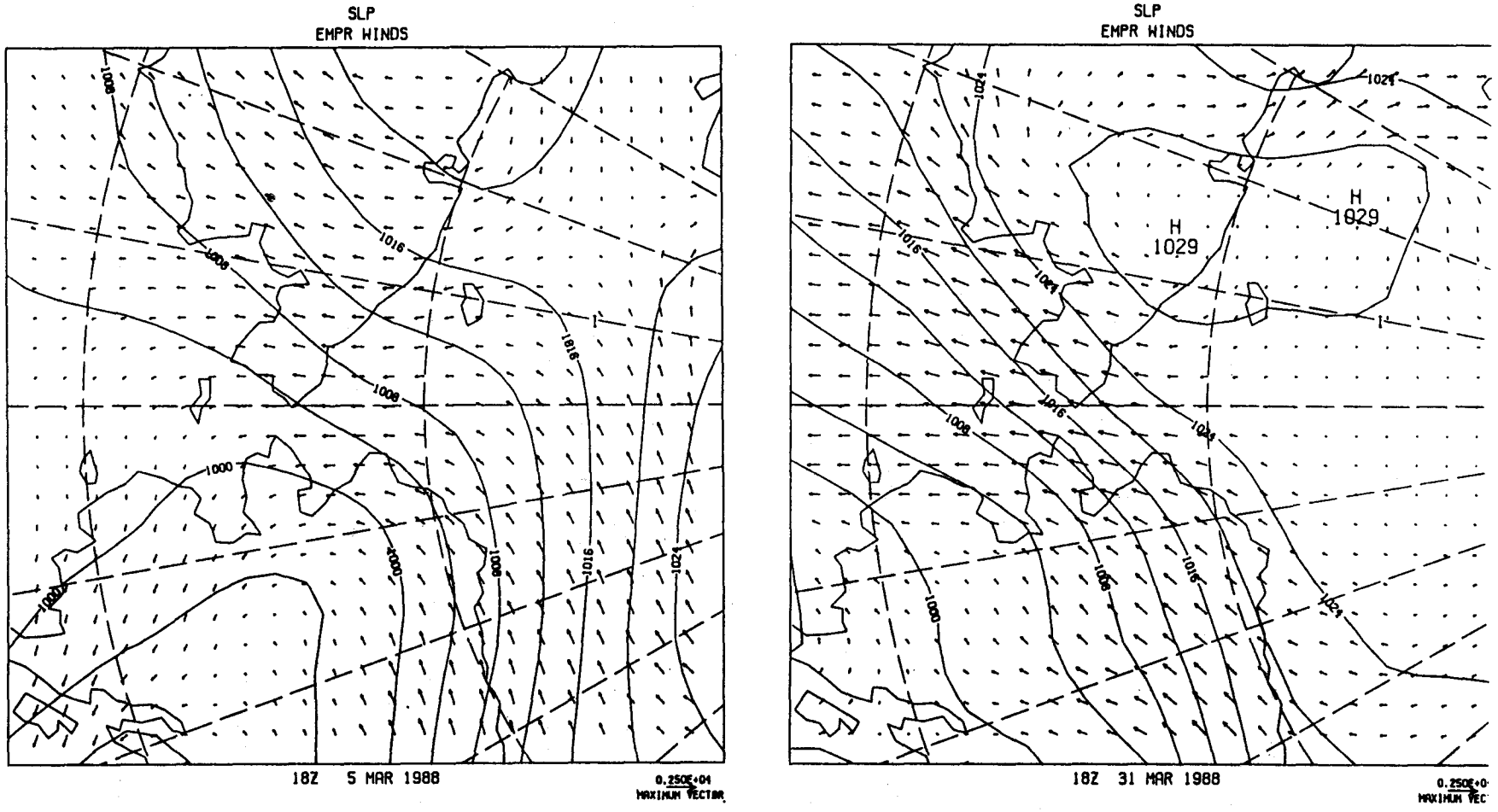

Figure 58. Pressure and wind fields over northern Alaska and eastern Siberia at 18Z 5 March 1988 and 18Z 31 March 1988.

show weak ridges over the northern areas retrograding to set-up of the Aleutian low-Siberian high with concomitant North Slope easterlies in November and December 1987. Late December and early January storms passed along the Alaskan west coast, driving some periods of southerly and southeasterly winds along the North Slope. Northeasterly to easterly flow resumed in February and March and continued through the end of the experiment.

One aspect of the 1986–1988 seasonal conditions which has not been satisfactorily explained by this analysis is whether the extreme minimum ice extents for this period were caused by atmospheric thermodynamic or circulation anomalies or by the advection of warm water from upstream sources, such as the Bering and Chukchi seas (Barry *et al.*, 1979; Bruno and Madsen, 1989; Henry and Heaps, 1976; Hufford, 1973; Mysak and Manak, 1989; Paquette and Bourke, 1974; Parker *et al.*, 1985; Reed and Kunkel, 1960; Rogers, 1978; Short and Wiseman, 1975; Walsh and Sater, 1981). It is thought that the analysis of the Chukchi Sea hydrographic data from the ONR-funded Freeze cruises may help us understand this important point.

IV. SYNOPSIS OF THE REGIONAL CIRCULATION

The northern Alaskan shelves, from the northern Bering Sea through the Chukchi and Beaufort seas to the Canadian border, extend over nearly 2000 km and include two substantially different oceanic regimes. The southern regime, covering about 70% of the total extent, is comprised of the northern Bering and Chukchi seas. It consists of a vast shallow shelf dominated by atmospheric forcing and by the great throughflow of Pacific waters into the Arctic Ocean. The circulation in the southern portion of this region, from the straits bordering St. Lawrence Island northward through Bering Strait, shows the effects of the constraining boundaries. On the other hand, the northern regime, comprised of the Alaskan Beaufort shelf, is narrow and is predominantly forced by the adjacent Arctic Ocean, to which it is completely open. It is in many ways simply an edge of the Arctic Ocean.

Bering Strait constitutes a choke point for the regional circulation and provides a convenient monitoring location for the Pacific inflow into the Arctic. That inflow is important not only to the northern Bering and Chukchi seas, but also to conditions in the upper several hundred meters of the Arctic Ocean (e.g., Killworth and Smith, 1984). We find that the transport through Bering Strait is predictable from the reduced geostrophic wind field according to the equation

$$T = 1.06–0.112\ W,$$

where T is the transport in sverdrups (1 Sv = 10^6 m^3 s^{-1}) and W is the component of the reduced geostrophic wind along 192°T in meters per second (cf. Coachman and Aagaard, 1988, for a complete discussion).

The reason for the strong control of the northward transport by the wind is that convergences and divergences are created by the interaction of the wind-driven Ekman layer with the restrictive and complex coastal geometry of the Alaskan and Siberian land masses. Such modifications alter the pressure field associated with the higher steric sea level of the Pacific Ocean relative to the Arctic Ocean. The northward mean flow driven by the latter pressure gradient is thereby considerably modified by the wind field on time scales ranging from the synoptic to the interannual. Our recent measurements suggest, however, that there is an asymmetry in the dynamical response of the Bering Strait flow to major changes in wind direction, with the flow responding readily to the northerly winds typical of winter, but that the effect of southerly winds is buffered. This differential response is probably associated with the different coastal geometry north and south of the strait.

With respect to the very low frequency variability of the Bering Strait flow, Figs. 59 and 60, from Coachman and Aagaard (1988), show the estimated seasonal and interannual variability of that transport. Note the marked annual cycle, with the maximum northerly flow in summer, but with a brief secondary maximum in January, which corresponds to a statistical decrease in the strength of the northerly winter winds. Note in Fig. 60 the large decrease in transport which occurred in the late 1960's. An extended analysis shows that, in fact, three of the four lowest-transport years of the century have occurred since 1969. It is therefore conceivable that significant aspects of the regional oceanography may not have been well sampled by the various observational programs of recent years.

Waters moving through Bering Strait show large temporal variability in their properties on all time scales and, in addition, there are, in general, pronounced property gradients across the strait at any given time. For example, the water passing through the western part of the strait is the most saline. This western water, which, south of the strait, is referred to as the Anadyr water mass, derives from water which has moved onto the shelf from the northwestern part of the deep Bering Sea and flowed northward through the Gulf of Anadyr and Anadyr Strait, west of St. Lawrence Island. The Anadyr Water, and its descendant north of Bering Strait, called the Bering Sea Water, are characterized by very high nutrient concentrations and in the northern Bering and southern Chukchi seas they support one of the world's most productive marine ecosystems. Within the Chukchi Sea, the Bering Sea Water appears to move principally northward following Hope Sea Valley, probably entering the Arctic Ocean east of Herald Island. The nutrient maximum within the Arctic Ocean derives from this inflow, as does the wide-spread secondary temperature minimum which is found at a salinity of about 33.1. The water which moves northward through eastern Bering Strait is marked by both lower salinity and much lower nutrient concentrations than waters to the west. It roughly follows the Alaskan coast line through the Chukchi Sea, primarily entering the Arctic Ocean through Barrow Canyon. Its contribution

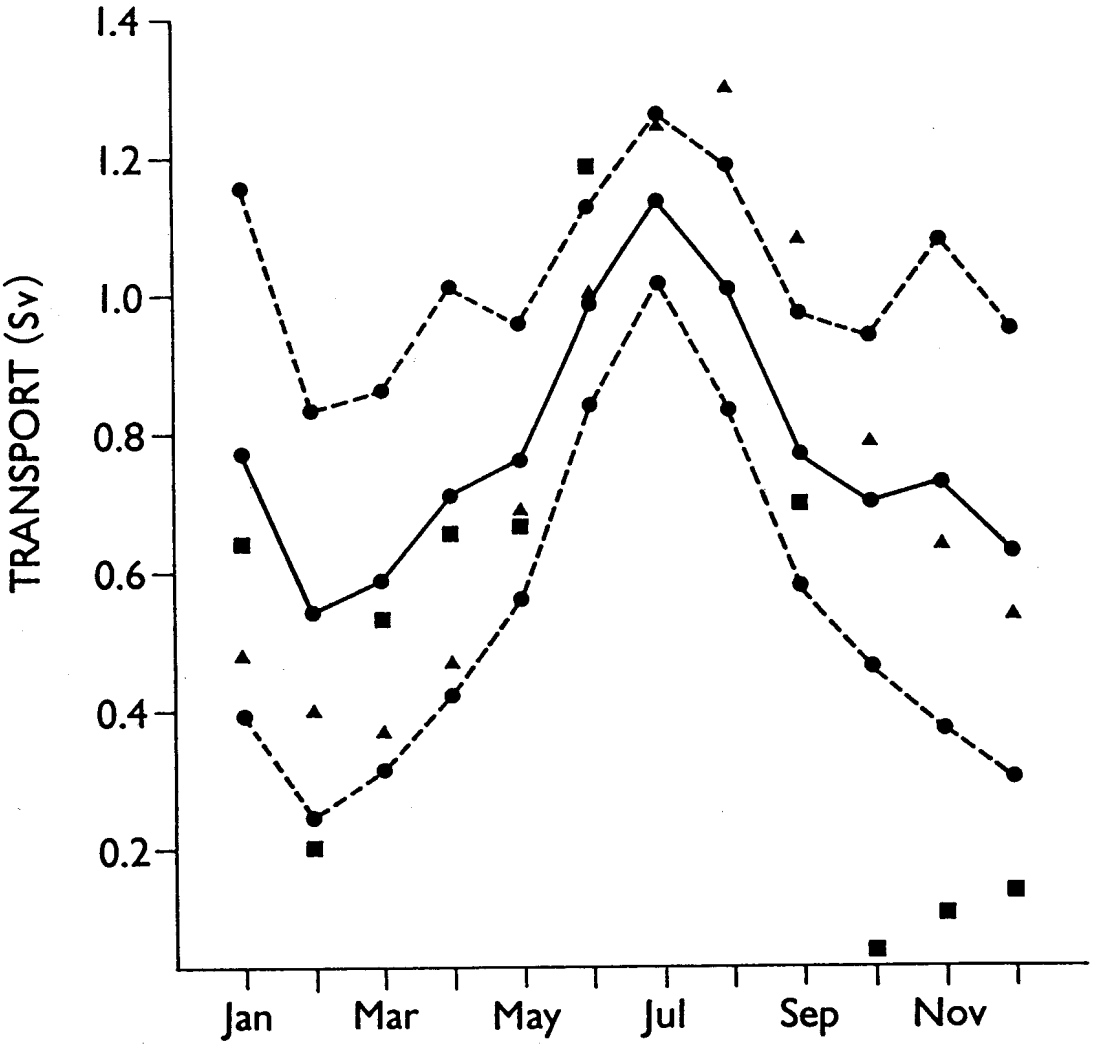

Figure 59. Annual Bering Strait transport signal.

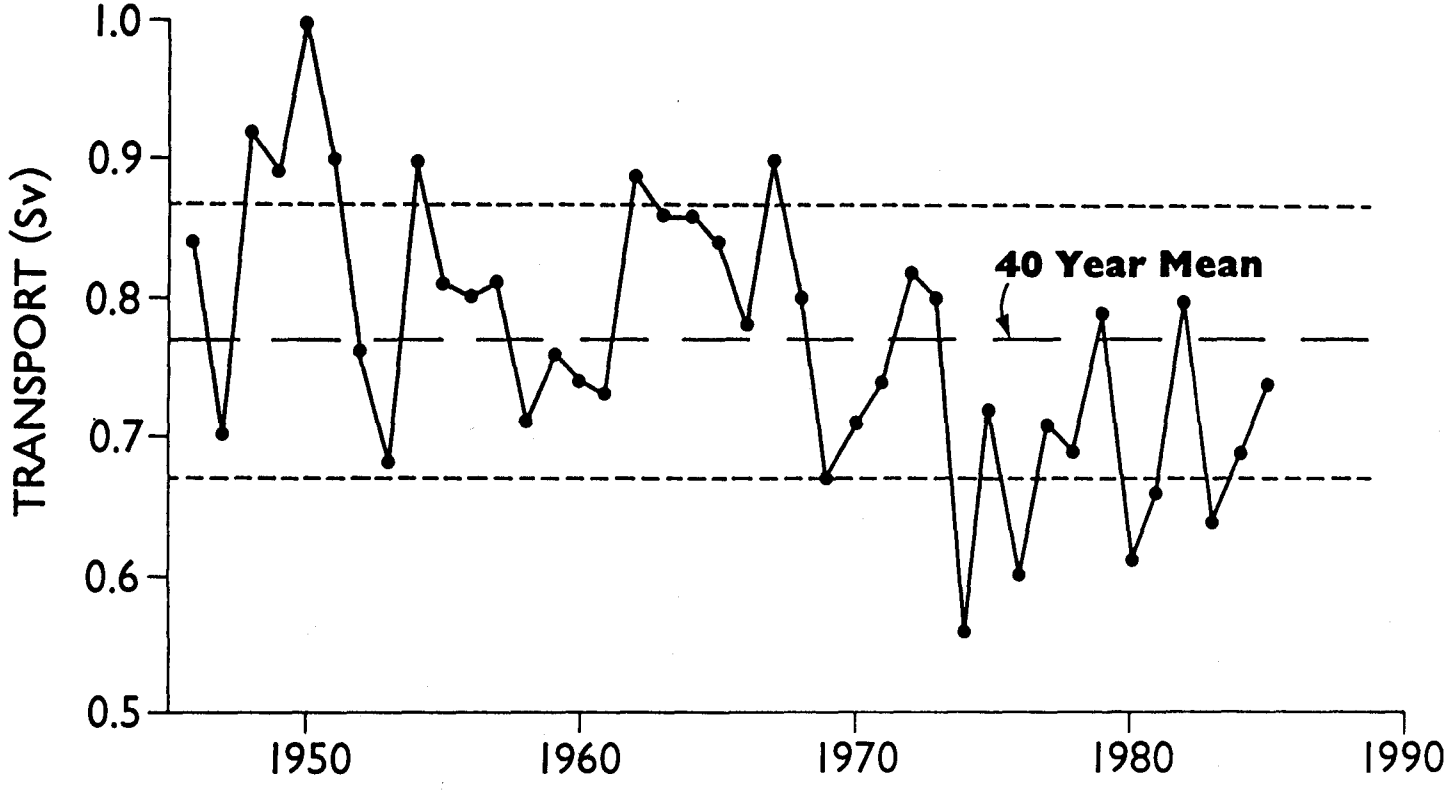

Figure 60. Forty years of annual transport estimates through Bering Strait.

to the Arctic Ocean is most easily seen in the secondary temperature maximum found at about 75 m depth throughout the Canadian Basin.

Another important contribution to the characteristics of the water on the shelf comes during winter, when both the northern Bering and the Chukchi seas are marked by numerous large coastal polynyas. These are maintained by the prevailing offshore winds over the south- and west-facing coasts, which transport new ice seaward. Because of the high formation rates of new ice in the polynyas, they salinize the underlying water through brine rejection. The cold and saline waters thus formed over the shelves give rise to much of the density structure of the Arctic Ocean and are therefore of major climatic significance. Cold brines have previously been seen draining from the Chukchi Sea through Barrow Canyon, but during 1986–87 they were absent. While the reason for this absence is unknown, it points toward the need to take interannual variability into account both in observational and modeling efforts.

While most of the Chukchi Sea is characterized by a general northward flow, in the Beaufort Sea the motion of the surface waters as deduced from the ice drift is nominally westward, manifesting the southern limb of the clockwise Beaufort gyre. However, the ice can undergo prolonged periods of eastward drift as well. Deeper in the water column over the inner shelf (landward of about the 40–50 m isobath) there is also a mean westward set, and the circulation appears strongly wind-driven. There is, however, some evidence for mean eastward motion east of 146°W, possibly corresponding to the different wind regime in the eastern Beaufort Sea.

Over the outer shelf and slope, the circulation is characterized by a strong subsurface flow which in the mean is eastward, i.e., contrary to the mean ice motion, but which experiences frequent reversals toward the west. This current dominates the outer Alaskan Beaufort shelf and it appears to be part of the large-scale circulation of the Arctic Ocean, an important component of which is a deep and relatively narrow boundary current circulating in a counterclockwise sense in each of the two major Arctic Ocean basins. In the Beaufort Sea this flow is referred to as the Beaufort Undercurrent, where it has characteristic long-term mean speeds in the neighborhood of 5–10 cm s^{-1}, while daily mean values are typically ten times as great. In the mean sense, the undercurrent is probably typically found below about 40 m, but its depth appears to vary markedly. While the undercurrent shows a wind influence, the correlations are small, so that effectively the circulation over the outer shelf and slope is primarily ocean-driven rather than locally wind-driven, both in its mean and variable components. The ocean-driven variability includes both eddies and shelf waves, the latter commonly having eastward phase velocities of about 1.5 m s^{-1}.

Upwelling along the outer shelf of the Beaufort Sea is a frequent occurrence and appears to be connected with the eastward-traveling wave-like disturbances observed in the velocity records. Vertical displacements may be as much as 150 m, but there is no indication of a significant net onshore flux associated with these events, except in Barrow Canyon, where the resultant

turbulent salt and heat fluxes are sufficiently large to potentially be of local importance. Temporarily, of course, water with deep offshore properties can be found on the Beaufort shelf, even though it apparently does not remain there in large quantities.

V. SUMMARY OF THE PRINCIPAL CONCLUSIONS

1. Below the upper 40–50 m of the ocean, the principal circulation feature of the outer shelf and slope of the Beaufort Sea is the Beaufort Undercurrent, a strong flow which in the mean is directed eastward, but which is subject to frequent reversals toward the west. The reversals are normally associated with upwelling onto the outer shelf. The undercurrent is very likely part of a basin-scale circulation within the Arctic Ocean.

2. While we find statistically significant wind influence on the subsurface flow in the southern Beaufort Sea, it is generally of secondary importance, accounting for less than 25% of the flow variance below 60 m. An important implication is that at least below the mixed layer, the circulation on the narrow Beaufort shelf is primarily forced by the ocean rather than by the local wind. Therefore, to the extent that a localized problem or process study requires consideration of the shelf circulation, such as would be the case for oil-spill trajectory modeling, a larger-scale framework must be provided, within which the more local problem may be nested.

3. There were large changes in wind variance with season, with the largest variances occurring in the late-summer/early autumn and again in January because of blocking ridges in the North Pacific shifting the storm track westward over the west coast of Alaska and across the North Slope.

4. Despite the seasonally varying wind field, as well as the large seasonal differences in the upper-ocean temperature and salinity fields, we find no evidence for a seasonal variability in the subsurface circulation in the Beaufort Sea. This situation contrasts with that in Bering Strait, and probably also in much of the Chukchi Sea, where a seasonal cycle in the transport is apparent. Therefore, while the northward flow of water from the Pacific is of major significance to the structure and chemistry of the upper ocean in the Arctic (including the Beaufort Sea), as well as its ice cover and biota, the dynamic significance of that flow to the Beaufort Sea appears minimal.

5. In contrast to the lack of a seasonal oceanographic signal at depth, the interannual variability in the flow characteristics can be considerable. For example, during the period fall 1986-spring 1987, the Beaufort Undercurrent appears to have been anomalously deep compared with both earlier and ensuing measurements, perhaps by 30–40 m. The consequences of such anomalies for the upper-ocean velocity structure and transport are likely significant.

6. During much of the experiment the meteorological conditions were milder than normal, consistent with less coastal ice in the summer and autumn, the passage of more storms up the west coast of Alaska and across the North Slope, and generally higher air temperatures

along the North Slope. These climatological near-minimum ice years were followed in 1988 by the heaviest summer ice along the Chukchi coast since 1975.

7. The atmospheric sea-level pressure field is well represented at all buoys and stations by the METLIB products from the FNOC surface analysis, if the 12-hour lag of the FNOC pressures is taken into account. Unfortunately the surface air temperature field from FNOC is not representative of the station data from either land-based stations or drifting ice buoys. The errors in the temperature field are characterized by a systematic over-prediction during winter and spring of some 10–20°C, leading to an annual average over-prediction for air temperature of 3–13°C at all measuring sites. Although we recommend that gradient winds be used for modeling purposes and that these be calculated from the time-shifted surface analysis, the surface temperature analysis should not be used for any model calculations, except perhaps as an upper boundary condition for a rather complete planetary boundary layer model.

VI. ACKNOWLEDGMENTS

The Beaufort Sea Mesoscale Circulation Study is a contribution to the Marine Services Project of the Pacific Marine Environmental Laboratory. This study was funded in part by the Minerals Management Service, Department of the Interior, through and Ineragency Agreement with the National Oceanic and Atmospheric Administration, Department of Commerce, as part of the Alaska Outer Continental Shelf Environmental Assessment Program. A portion of the meteorological measurements were funded by the Office of Naval Research, Arctic Programs. The Barrow Canyon moorings were funded by the National Science Foundation, Division of Polar Programs.

C.H. Darnall was chief engineer for the project. G.A. Galasso and W.J. Blake were engineers for the meteorological portion. K. Krogslund of the University of Washington completed the oceanic chemical analyses for the Beaufort Sea. V.L. Long, N. Jenkins, and P. Turet contributed to the data analyses. We also acknowledge the numerous other NOAA, Coast Guard, and civilian personnel who contributed to the successful completion of the experiment in a hostile physical environment.

R. Colony from the Polar Science Center, Applied Physics Laboratory, University of Washington, Seattle, WA, provided all the buoy records as listed in Table 7 and cooperated in the buoy deployments. J.H. Swift, Scripps Institution of Oceanography, La Jolla, CA, supplied data from the AIWEX (Arctic Internal Wave Experiment). L.K. Coachman and R.B. Tripp, School of Oceanography, University of Washington, contributed hydrographic data from ISHTAR (Inner Shelf Transport and Resources).

VII. REFERENCES

Aagaard, K. (1989): A synthesis of the Arctic Ocean circulation. *Rapp. P.-v. Reun. Cons. Int. Explor. Mer, 188*, 11–22.

Aagaard, K. (1984): The Beaufort Undercurrent. In *The Alaskan Beaufort Sea: Ecosystems and Environments*, P.W. Barnes, D.M. Schell, and E. Reimnitz (eds.), Academic Press, Orlando, FL, 47–71.

Aagaard, K. (1988): Current, CTD, and pressure measurements in possible dispersal regions of the Chukchi Sea, Outer Continental Shelf Environmental Assessment Program. Final Reports of the Principal Investigators, 57, 255–333, Department of Commerce/Department of Interior, Anchorage.

Aagaard, K., L.K. Coachman, and E.C. Carmack (1981): On the halocline of the Arctic Ocean. *Deep-Sea Research, 28*, 529–545.

Aagaard, K., C.H. Pease, and S.A. Salo (1988a): Beaufort Sea Mesoscale Circulation Study – Preliminary Results. NOAA Technical Memorandum ERL PMEL-82, 171 pp.

Aagaard, K., S. Salo, and K. Krogslund (1987): Beaufort Sea Mesoscale Circulation Study: Hydrography, USCGC *Polar Star* Cruise, October, 1986. NOAA Data Report ERL PMEL-19, 83 pp.

Aagaard, K., S. Salo, and K. Krogslund (1988b): Beaufort Sea Mesoscale Circulation Study: Hydrography, Helicopter Operations, April, 1987. NOAA Data Report ERL PMEL-22, 25 pp.

Aagaard, K., J.H. Swift, and E.C. Carmack (1985a): Thermohaline circulation in the arctic mediterranean seas. *J. Geophys. Res., 90*, 4833–4846.

Aagaard, K., A.T. Roach, and J.D. Schumacher (1985b): On the wind-driven variability of the flow through Bering Strait. *J. Geophys. Res., 90*, 7213–7221.

Albright, M. (1980): Geostrophic wind calculations for AIDJEX, Sea Ice Processes and Models. R.S. Pritchard (ed.), University of Washington Press, Seattle, WA, 402–409.

Anderson, N.O. (1974): A short note on the calculation of filter coefficients. *Geophysics, 39* (1), 69–72.

Banke, E.G., and S.D. Smith (1971): Wind stress over ice and over water in the Beaufort Sea. *J. Geophys. Res., 76*, 7368–7374.

Banke, E.G., S.D. Smith, and R.J. Anderson (1976): Recent measurements of wind stress on Arctic sea ice. *J. Fish. Res. Board Canada, 33*, 2307–2317.

Barry, R.G., R.E. Moritz, and J.C. Rogers (1979): The fast ice regimes of the Beaufort and Chukchi Sea coasts, Alaska. *Cold Regions Sci. Tech., 1*(2), 129–152.

Bruno, M.S., and O.S. Madsen (1989): Coupled circulation and ice floe movement model for partially ice-covered continental shelves. *J. Geophys. Res., 94*(C2), 2065–2077.

Campbell, W.J., P. Gloersen, W.J. Webster, T.T. Wilheit, and R.O. Ramseier (1976): Beaufort Sea ice zones as delineated by microwave imagery. *J. Geophys. Res., 81*, 1103–1110.

Campbell, W.J., P. Gloersen, H.J. Zwally, R.O. Ramseier, and C. Elachi (1980): Simultaneous passive and active microwave observations of near-shore Beaufort Sea ice. *J. Petrol. Tech., 21*, 1105–1112.

Carsey, F., and B. Holt (1987): Beaufort-Chukchi ice margin data from Seasat: Ice motion. *J. Geophys. Res., 92*(C7), 7163–7172.

Coachman, L.K., and K. Aagaard (1981): Re-evaluation of water transports in the vicinity of Bering Strait. In: *The Eastern Bering Sea Shelf: Oceanography and Resources, Vol. 1*, D.W. Hood and J.A. Calder (eds.), University of Washington Press, Seattle, WA, 95–110.

Coachman, L.K., and K. Aagaard (1988): Transports through Bering Strait: Annual and interannual variability. *J. Geophys. Res., 93*, 15535–15539.

Coachman, L.K., and C.A. Barnes (1961): The contribution of Bering Sea water to the Arctic Ocean. *Arctic, 14*, 147–161.

Coachman, L.K., K. Aagaard, and R.B. Tripp (1975): Bering Strait: The Regional Physical Oceanography. University of Washington Press, Seattle, 172 pp.

Coachman, L.K., and D.A. Rankin (1968): Currents in Long Strait, Arctic Ocean. *Arctic, 21*, 27–38.

Codispoti, L.A. (1979): Arctic Ocean processes in relation to the dissolved silicon content of the Atlantic. *Mar. Sci. Comm., 5*, 361–381.

Codispoti, L.A., and F.A. Richards (1968): Micronutrient distributions in the East Siberian and Laptev seas during summer 1963. *Arctic, 21*, 67–83.

D'Asaro, E.A. (1988): Generation of sub-mesoscale vortices: A new mechanism. *J. Geophys. Res., 93*, 6685–6693.

Dickey, W.W. (1961): A study of a topographic effect on wind in the Arctic. *J. Meteorol., 18*, 790–803.

Feldman, U., P.J. Howarth, and J.A. Davies (1979): Estimating the surface wind speed over drifting pack ice from surface weather charts. *Boundary-Layer Meteorol., 16*, 421–429.

Foldvik, A., K. Aagaard, and T. Torresen (1988): On the velocity field of the East Greenland Current. *Deep-Sea Res., 35A*, 1335–1354.

Garrison, G.R., and P. Becker (1976): The Barrow Submarine Canyon: A drain for the Chukchi Sea. *J. Geophys. Res., 81*, 4445–4453.

Garrison, G.R., and R.G. Paquette (1982): Warm water interactions in the Barrow Canyon in winter. *J. Geophys. Res., 87*, 5853–5859.

Hart, J.E., and P.D. Killworth (1976): On open ocean baroclinic instability in the Arctic. *Deep-Sea Res., 23*, 637–645.

Henry, R.F., and N.S. Heaps (1976): Storm surges in the southern Beaufort Sea. *J. Fish. Res. Board Canada, 33*, 2362–2376.

Hufford, G.L. (1973): Warm water advection in the southern Beaufort Sea, August-September 1971. *J. Geophys. Res., 78*, 2702–2707.

Hufford, G.L., On apparent upwelling in the southern Beaufort Sea. *J. Geophys. Res., 79*, 1305–1306.

Johnson, M.W. (1956): The plankton of the Beaufort and Chukchi Sea Areas of the Arctic and its Relation to the Hydrography. Arctic Institute of North America Technical Paper No. 1, Montreal, P.Q.

Jones, E.P., and L.G. Anderson (1986): On the origin of the chemical properties of the Arctic Ocean halocline. *J. Geophys. Res., 91*, 10759–10767.

Killworth, P.D., and J.M. Smith (1984): A one-and-a-half dimensional model for the Arctic halocline. *Deep-Sea Res., 31A*, 271–293.

Kinder, T.H., D.C. Chapman, and J.A. Whitehead, Jr. (1986): Westward intensification of the mean circulation on the Bering Sea shelf. *J. Phys. Oceanogr., 16*(7), 1217–1229.

Kinney, P., M.E. Arhelger, and D.C. Burrell (1970): Chemical characteristics of water masses in the Amerasian Basin of the Arctic Ocean. *J. Geophys. Res., 75*, 4097–4104.

Kozo, T.L. (1980): Mountain barrier baroclinicity effects on surface winds along the Alaskan Arctic coast. *Geophys. Res. Lett., 7*, 377–380.

Kozo, T.L. (1982a): An observational study of sea breezes along the Alaskan Beaufort Sea coast: Part I. *J. Appl. Meteorol., 21*, 891–905.

Kozo, T.L. (1982b): An observational study of sea breezes along the Alaskan Beaufort Sea coast: Part II. *J. Appl. Meteorol., 21*, 906–924.

Kozo, T.L. (1984): Mesoscale wind phenomena along the Alaskan Beaufort Sea coast. In: *The Alaskan Beaufort Sea: Ecosystem and Environment*, P. Barnes, D. Schell, and E. Reimnitz (eds.), Academic Press, Orlando, FL., 23–45.

Kozo, T.L., and R.Q. Robe (1986): Modeling winds and open water buoy drift along the eastern Beaufort Sea coast, including the effects of the Brooks Range. *J. Geophys. Res., 91*, 13011–13032.

Langleben, M.P. (1971): Albedo of melting sea ice in the southern Beaufort Sea. *J. Glaciology, 10*(58), 101–104.

Macklin, S.A., R.L. Brown, J. Gray, and R.W. Lindsay (1984): METLIB-II – A Program Library for Calculating and Plotting Atmospheric and Oceanic Fields. NOAA Technical Memorandum ERL PMEL-54, 53 pp.

Manley, T.O., and K. Hunkins (1985): Mesoscale eddies of the Arctic Ocean. *J. Geophys. Res., 90*, 4911–4930.

Marko, J.R. and R.E. Thomson (1975): Spatially periodic lead patterns in the Canadian Basin sea ice: A possible relationship to planetary waves. *Geophys. Res. Lett., 2*(10), 431–434.

Maykut, G.A., and P.E. Church (1973): Radiation climate of Barrow, Alaska, 1962–1966. *J. Appl. Meteorol., 12*, 620–628, 1973.

Melling, H., and E.L. Lewis (1982): Shelf drainage flows in the Beaufort Sea and their effect on the Arctic Ocean pycnocline. *Deep-Sea Res., 29*, 967–986.

Moore, R.M. (1981): Oceanographic distributions of zinc, cadmium, copper and aluminum in waters of the central Arctic. *Geochim. Cosmochim. Acta, 45*, 2475–2482.

Moore, R.M., and J.N. Smith (1986): Disequilibria between ^{226}Ra, ^{210}Pb and ^{210}Po in the Arctic Ocean and the implications for chemical modification of the Pacific water inflow. *Earth Planet. Sci. Lett., 77*, 285–292.

Moore, R.M., M.G. Lowings, and F.C. Tan (1983): Geochemical profiles in the central Arctic Ocean: Their relation to freezing and shallow circulation. *J. Geophys. Res., 88*, 2667–2674.

Moritz, R.E. (1977): On a possible sea-breeze circulation near Barrow, Alaska. *Arctic and Alpine Research, 9*(4), 427–431.

Mountain, D.G., L.K. Coachman, and K. Aagaard (1976): On the flow through Barrow Canyon. *J. Phys. Oceanogr., 6*, 461–470.

Mysak, L.A., and D.K. Manak (1989): Arctic sea ice extent and anomalies, 1953–1984. *Atmos.-Ocean*, in press.

Overland, J.E. (1981): Marine climatology of the Bering Sea. In: *The Eastern Bering Sea Shelf: Oceanography and Resources, Vol. 1*, D.W. Hood and J.A. Calder (eds.), University of Washington Press, Seattle, WA, 15–22.

Overland, J.E. (1985): Atmospheric boundary layer structure and drag coefficients over sea ice. *J. Geophys. Res., 90*, 9029–9049.

Overland, J.E., R.A. Brown, and C.D. Mobley (1980): METLIB – A Program Library for Calculating and Plotting Marine Boundary Layer Wind Fields, NOAA Technical Memorandum ERL PMEL-20, 53 pp.

Overland, J.E., and C.H. Pease (1982): Cyclone climatology of the Bering Sea and its relation to sea ice extent. *Mon. Weather Rev., 110*, 5–13.

Overland, J.E., and A.T. Roach (1987): Northward flow in the Bering and Chukchi seas. *J. Geophys. Res., 92*, 7097–7105.

Paquette, R.G. and R.H. Bourke (1974): Observation on the coastal current of Arctic Alaska. *J. Mar. Res., 32*, 195–207.

Parker, N., B. Thomson, J. Bullas, and W. Hume (1985): September 1985 Beaufort Sea storm. Report 85–7, Scientific Services, AES Western Region, Edmonton, Alberta, 24 pp.

Pease, C.H. (1987): Meteorology of the Chukchi Sea: An overview. In: *Chukchi Sea Information Update*, D.A. Hale (ed.), NOAA/NOS Ocean Assessments Division – Alaska Office, Anchorage, AK, 11–19.

Pritchard, R.S. (1984): Beaufort Sea ice motions. *The Alaskan Beaufort Sea Ecosystems and Environments*, P.W. Barnes, D.M. Schell, and E. Reimnitz (eds.) Academic Press, Orlando, FL, 95–113.

Reed, R.J. and B.A. Kunkel (1960): The Arctic circulation in summer. *J. Meteorol., 17*, 489–506.

Rogers, J.C. (1978): Meteorological factors affecting interannual variability of summertime ice extent in the Beaufort Sea. *Mon. Weather Rev., 106*(6), 890–897.

Short, A.D. and W.M.J. Wiseman, Jr. (1975): Coastal breakup in the Alaskan Arctic. *Geol. Soc. Amer. Bull., 86*, 199–202.

Smith, S.D., and E.G. Banke (1971): Wind stress over ice and over water in the Beaufort Sea. *J. Geophys. Res., 76*, 7368–7374.

Spaulding, M., T. Isaji, D. Mendelsohn, and A.C. Turner (1987): Numerical simulation of wind-driven flow through the Bering Strait. *J. Phys. Oceanogr., 7*, 1799–1816.

Sverdrup, H.U. (1933): Meteorology, Part 1, Discussion. The Norwegian North Polar Expedition with the "Maud", 1918–1925. *Scientific Results, 2*(1), Geofysik Institut, Bergen, 331 pp.

Tripp, R.B. (1987): ISHTAR cruise report: R/V *Thomas G. Thompson* Cruise TT-212, 29 June-19 July 1987. School of Oceanography, University of Washington, Seattle, unpublished data report.

Wallace, D.W.R., R.M. Moore, and E.P. Jones (1987): Ventilation of the Arctic Ocean cold halocline: Rates of diapycnal and isopycnal transport, oxygen utilization and primary production inferred using chlorofluoromethane distributions. *Deep-Sea Res., 34A*, 1957–1979.

Walsh, J.J., C.P. McRoy, L.K. Coachman, and 18 other authors (1989): Carbon and nitrogen cycling within the Bering/Chukchi seas: Source regions for organic matter affecting AOU demands of the Arctic Ocean. *Prog. Oceanogr.*, in press.

Walsh, J.E., and J.E. Sater (1981): Monthly and seasonal variability in the ocean-ice-atmosphere systems of the North Pacific and the North Atlantic. *J. Geophys. Res., 86*(C8), 7425–7445.

Weatherly, G.L., and P.J. Martin (1978): On the structure and dynamics of the oceanic bottom boundary layer. *J. Phys. Oceanogr., 8*, 557–570.

Weeks, W.F., A. Kovacs, S.J. Mock, W.B. Tucker, W.D. Hibler III, and A.J. Gow (1977): Studies of the movement of coastal sea ice near Prudhoe Bay, Alaska. *J. Glaciology, 19*(81), 533–546.

Wendler, G., F.D. Eaton, and T. Ohtake (1981): Multiple reflection effects on irradiance in the presence of Arctic stratus clouds. *J. Geophys. Res., 86*(C3), 2049–2057.

Yeats, P.A. (1988): Manganese, nickel, zinc and cadmium distributions at the Fram 3 and Cesar ice camps in the Arctic Ocean. *Oceanolog. Acta, 11*, 383–388.

☆ U.S. GOVERNMENT PRINTING OFFICE: 1989—773-002/11,012 REGION NO. 8